Long Distance Exploding Wires

Rowan Peter William Sinton

A thesis presented for the degree of
Doctor of Philosophy
in
Electrical and Computer Engineering
at the
University of Canterbury,
Christchurch, New Zealand.

2011

ABSTRACT

Electrical arcs are usually created with the breakdown of air, requiring an average electric field (AEF) of at least 100 kV/m in long spark gaps. This thesis explores a novel method of creating long electrical arcs using exploding wires (EWs). Arcs up to 60 m long have been produced with AEFs of just 4.5 kV/m. Extensive observations of the EW process are presented, which demonstrate that the arcs, which are a type of 'restrike', form via the seldom-reported 'plasma bead' restrike mechanism. Beads of plasma appear to form at sites of wire fragmentation, and can expand and coalesce into a continuous plasma column.

There are strict conditions under which the plasma beads, and hence restrike channels, are produced. A restrike prediction model has been developed to provide a reliable method of producing restrike. The model was derived from the improved understanding of the restrike mechanism, and uses the wire's length and the energy supply voltage and characteristics as inputs. Capability diagrams are then constructed, which allow researchers to easily design experiments that will produce restrike.

Extensive descriptions are provided of the experimental environments that were designed and constructed to facilitate long distance EW experiments. Experiments have been performed inside a high voltage laboratory, in the laboratory's outdoor compound, off the laboratory's earth grid and completely off-site. The off-site location allowed vertical experiments, suspended by a weather balloon, to be performed. This led to a theory on artificially triggered lightning, which is one of many exciting future applications that are suggested. It is also predicted that other research groups will be able to create arcs of several hundred metres long.

ACKNOWLEDGEMENTS

I would like to give my sincerest thanks the following people, who were instrumental to this research and my continuing education.

I am forever indebted to Dr. Wade Enright, my primary supervisor, for the countless hours we spent together, discussing exploding wires, engineering, politics, nature and just about everything else. He has taught me so much more than the degree requirements, and I am sure the knowledge will prove useful in every aspect of my life.

I would also like to thank my secondary supervisor Prof. Pat Bodger for our 'weakly' meetings, many of which were on mountains or rivers. His academic experience was invaluable in guiding my research to a satisfying conclusion.

Ryan van Herel, my colleague and partner-in-crime, thanks for everything. While Ryan completed a great Master's thesis titled 'Wire Explosion via Induction', he was present for almost every experiment and discussion of my research, and so has contributed immeasurably to its success.

A huge amount of technical expertise was needed to construct equipment for this research. I would like to thank Jac Woudberg, Dave Healy, and Ken Smart for their technical support. I would also like to thank Stephen Beuzenberg for his generous laboratory assistance and Debbie Dick for her administrative support.

To my fellow postgraduates, including Dave Smith, Andrew Lapthorn, Irvin Chew, Lance Frater and Shreejan Pandey to name just a few, and also the undergraduates Yanosh Irani and Bevan Gray who were involved in this research, thank you for all your inspirations, help and the good times.

Lastly, I would like to thank my beautiful partner Sylvia Nissen, who has been with me for as long as this thesis has. Thank you for all of your support, love and lunches.

LIST OF PUBLICATIONS

The following publications have resulted from the research presented in this thesis. The journal and conference papers are peer-reviewed; the magazine articles are not.

JOURNAL PAPERS

Sinton, R., van Herel, R., Enright, W. and Bodger, P. (2010), 'Investigating long-distance exploding-wire restrike', Plasma Science, IEEE Transactions on, Vol. 38, No. 4, Apr, pp. 1015-1018.

Sinton, R., van Herel, R., Enright, W. and Bodger, P. (2010), 'Observations of the long distance exploding wire restrike mechanism', Journal of Applied Physics, Vol. 108, No. 5, p. 053304.

Sinton, R., van Herel, R., Enright, W. and Bodger, P. (2011), 'Generating Extra Long Arcs Using Exploding Wires', Journal of Applied Physics, accepted 9 Oct 2011.

CONFERENCE PAPERS

Sinton, R., Hammond, C., Enright, W. and Bodger, P. (2009), 'Generating high voltages with a plasma coil transformer', In Techcon Asia-Pacific, Sydney, Australia, pp. 211-219.

Sinton, R., van Herel, R., Enright, W. and Bodger, P. (2010), 'Design and construction of a triggered spark gap for long distance exploding wire experiments', In Australasian Universities Power Engineering Conference, Christchurch, New Zealand.

Sinton, R., van Herel, R., Enright, W. and Bodger, P. (2011), 'A Marx generator for exploding wire experiments', In Asia-Pacific Power and Energy Engineering Conference, Wuhan, China.

van Herel, R., Sinton, R., Enright, W. and Bodger, P. (2011), 'Formation of a plasma conductor by induction', In Asia-Pacific Power and Energy Engineering Conference, Wuhan, China.

MAGAZINE ARTICLES

Sinton, R., van Herel, R., Enright, W. and Bodger, P. (2009), 'Plasma conductors and windings', Australasian Transmission and Distribution Magazine, 2009, Issue 5 (Oct/Nov), pp. 22-23.

Sinton, R., van Herel, R., Enright, W. and Bodger, P. (2010), 'Exploding wire', The Shed Magazine, 2010, Oct/Nov, pp. 60-62.

Sinton, R., van Herel, R., Enright, W. and Bodger, P. (2011), 'Atmospheric partial discharge experiments', Australasian Transmission and Distribution Magazine, 2011, Issue 1 (Feb/Mar), pp. 78-79.

CONTENTS

LIST OF FIGURES

LIST OF TABLES

Chapter 1

INTRODUCTION

1.1 OVERVIEW

High voltage arcs have fascinated scientists and captivated the attention of the public for centuries. The most widely known electrical arc phenomenon is natural lightning. An energetic thunderstorm may strike awe and fear, for good reason, into the hearts of observers, with its dramatic display of speed, enormity and power. Bolts of lightning kilometres long can flash overhead and the resulting thunder rattles windows. It causes one to wonder about the immensely strong forces of nature that drive the display. So, its not surprising that when members of the public view a display at a high voltage laboratory, the most popular exhibit is often the artificial lightning – a large spark gap flash-over using an impulse generator or high voltage transformer.

The electrical breakdown strength of air is approximately 3 MV/m [Whitehead 1920], implying at an elementary level that billions of Volts would be required to break down the gap between the clouds and the earth, or that arcs only a metre or two long could be created artificially. However, nature has a tendency of accomplishing huge tasks via simple mechanisms, as can be observed where water has carved a canyon into rock. Arcs can bridge long gaps by incrementally ionising short sections of the gap. The electric field is intensified at the tip of the channel, focusing the action of the electric field on the adjacent section of air. In the laboratory, these tendrils of ionisation are called streamers, and allow spark gaps to break down with an average electric field as low as 100 kV/m [Gallet *et al.* 1975]. In natural lightning, the incremental breakdowns are called stepped leaders, and can cause the gap between the clouds and the earth to break down with an average electric field of just 10 kV/m [Uman 2000]. Long distance exploding wires (EWs), which also have an incremental breakdown mechanism, provide a method for the production of arcs using as little as 4.5 kV/m.

Previous research at the University of Canterbury has uncovered a mechanism in which long distance EWs could create long arcs using relatively low voltages. The arcs, known in the study of EWs as 'restrike', were created up to 10 m long using a capacitor bank charged to 60 kV. However, they could not be created reliably; there was no obvious method to select a

wire diameter, wire length and capacitor voltage to produce an arc. This research was largely phenomenological[1], and set out to create a model that could predict whether or not restrike would be created, and to concurrently improve understanding of the long distance EW restrike mechanism.

1.2 THESIS OUTLINE

First, a literature review is presented (Chapter 2), which explains the fundamental processes that can occur in short EWs, including fragmentation and restrike. The longest documented EW experiments and previous research at the University of Canterbury are summarised. The literature review highlights that the long distance EW research field is largely unexplored and so there is substantial room for original contributions. However, this also means that making headway into the field relies heavily on gathering new experimental data, which required the development of a complete experimental environment (Chapter 3).

The phenomenological study consisted of observation of EW experiments (Chapter 4) and the development of a mathematical restrike prediction model (Chapter 5). In reality, these two tasks progressed concurrently, with each guiding the other, but the findings have been divided into two chapters for clarity. The main conclusions from the observational study are used to justify assumptions in the later stages of the model development.

Detail is then given on the practicalities of producing long arcs (Chapter 6). Experiments were performed in several environments, including inside the laboratory, outside the laboratory and completely off-site. A technique for performing vertical EW experiments is then presented, which uses a thin, lightweight wire to return the EW current, allowing the experiment to be supported by a weather balloon. Lastly, potential future research topics are suggested (Chapter 7), with the aim of inspiring further research at the University of Canterbury and by other research groups. The future applications include even longer arc lengths, triggering natural lightning and forming plasma conductors into useful shapes. Lastly, the main conclusions of this research are presented (Chapter 8).

[1] A phenomenological model is one that expresses the observations of a phenomenon in a way that is consistent with, but does not derive directly from, a fundamental theory.

Chapter 2

BACKGROUND

2.1 INTRODUCTION

The exploding wire (EW) phenomenon has been studied for decades but it is not yet properly understood. This is partially due to the large variation in experimental results between studies; few authors report the same observations. The EW phenomenon is also intrinsically difficult to observe, because it is extremely fast, violent and condensed.

This chapter is a review of the literature that contained observations of EW mechanisms or techniques for analysing EW experiments. The chapter has been subdivided into the core concepts required to understand long distance EW, beginning with a description of the processes that will be later shown to constitute the long distance EW restrike mechanism. Chronologically, these are: the fragmentation of the wire in the solid and/or liquid state, the formation of plasma beads at fracture points, and the initiation of the restrike channel. The average electric field (AEF) quantity is introduced, which forms the basis for the mathematical restrike prediction model that is developed later in this thesis. The effect of enamel coating on a wire is reviewed, since all experiments performed in this thesis used enamelled wire. The previous research conducted at the University of Canterbury is then summarised.

2.2 EARLY WORK

Modern research into the EW phenomenon began in the 1950s. A series of conferences were held, the proceedings of which were compiled into four volumes that have formed the founding literature of EW and defined many new terms. They are still referred to by almost every researcher. The summary of the EW process by the proceedings editor Chace in [Chace and Moore 1959] is still mostly valid today.

The description given by Chace was that the wire first underwent Ohmic heating and melted. Further heating then took the liquid metal to boiling point, at which time a violent phase

change to gas occurred. This left the metal as a colloidal foam, which is a liquid with gas bubbles. After a period of microseconds or milliseconds, the colloidal foam transposed to a gas with liquid particles, which was called a colloidal reversal. The conductivity of the wire then dropped by several orders of magnitude, creating what was termed the 'dwell time'. Very little current flowed during this period, which could last for several milliseconds. During the dwell time, the metal gas density was too high to allow for ionisation because the mean free path of the electrons was too short. This density was maintained by inertia and atmospheric pressure. Once the gas had expanded sufficiently, 'restrike' could occur, which was the ionisation of the metal vapour path and consequent dramatic rise in conductivity and current. The form of the current flow through the restrike channel depended upon the experimental configuration, but was usually either under-damped oscillations or a single over-damped pulse.

2.3 THE EXPLODING WIRE PROCESS

2.3.1 Fragmentation

One of the first processes that may occur in EW is fragmentation. This can happen when the wire is in either the solid or liquid state, but fragmentation in the solid state generally happens at lower current densities [Molokov and Allen 1997]. Theories on the mechanism causing fragmentation were hotly debated, and none have been fully confirmed. [Ternan 1986] proposed that stress waves, instigated by rapid thermal expansion, were responsible for fracturing the wire. [Graneau 1987a] proposed that a longitudinal electromagnetic force was present, and could be predicted by Ampère's force law, which led to much controversy and a debate about fundamental electromagnetic forces. The existence of such a force was challenged by [Robson and Sethian 1992] and [Carpenter and Graneau 1984]. Relativistic electromagnetic longitudinal forces have also been suggested as an explanation for fragmentation [Ivezic 1991, Graneau 1987b]. [Molokov and Allen 1997] showed that thermal expansion combined with the electromagnetic pinch force may overcome the ultimate strength of the material. This was developed further by [Lukyanov and Molokov 2001], who used the aforementioned magneto-thermo-elastic model to study wires with clamped ends.

For higher-energy EWs, such as 130 mm long, 0.05 mm diameter copper wires exploded at 5 kV, [Vlastos 1973b] found that the wires can develop sausage and helical instabilities in the liquid state, which in turn lead to fragmentation.

The importance of the occurrence of fragmentation was highlighted in [Taylor 2002b], where it was observed that plasma beads, which will be discussed next, formed at the sites of fracturing. Taylor used a series of X-radiological photographs to show the wire fragmenting (fig. 2.1a). The wire first broke into sections several centimetres long, with breaks at the kinks caused by the

initial buckling of the wire. The buckling was said to be consistent with thermal expansion of the wire by estimating the wire's expanded length and noting an increase from the initial length. Confinement by the wire's own inertia, rather than constraint from the electrodes, had previously been shown to be sufficient to allow buckling to occur. Excess heating at the kink locations then led to premature vaporisation, which effectively causes fragmentation, at those sites.

In an attempt to better understand fragmentation, a thyristor was used in parallel with the EW to divert the current at a specific time partway through the explosion process [Taylor 2004]. Analysis of the results was complicated because significant current continued to flow through the wire while it was in a low resistance, solid state. With precise timing, the wire could be taken to a temperature very close to the melting point without fracturing. When energy dissipation was increased, signs of melting were seen with a band-like structure appearing at intervals along the wire. With slightly more energy dissipation, the wire fragmented in the solid state. In subsequent tests with the thyristor triggered later, the wire became molten before it fragmented. This seemingly contradictory and confusing result at least shows that fragmentation in both the solid and liquid states are possible with this type of EW, and neither can be easily ruled out. Taylor also photographed the remains of wires that had shattered in the solid state (fig. 2.1c), and in [Taylor 2002a], captured an X-radiograph image of a spinning liquid copper droplet that was ejected from a wire (fig. 2.1b).

A description and photograph of the fragmentation of EWs up to 1 m long is given in [Nagaoka *et al.* 1926]. The current was not sufficient to explode 0.24 and 0.8 mm diameter wires, but instead the wire was 'torn into fragments'. The ejected particles followed parabolic paths and dropped to the floor (fig. 2.2).

2.3.2 Plasma Beads

An important mechanism in this research is the formation of 'beads' of plasma along the axis of the wire prior to restrike. Very few authors have observed and reported plasma beads. A very early report of plasma beads was presented in [Nagaoka *et al.* 1926]. Using a 40 kV, 1.7 μF capacitor stack, wires of up to 1 m in length were exploded. 'Beads of light', appearing as small discoids, were observed to form throughout the whole length of wire, but especially near the centre (fig. 2.3). Experiments using aluminium, copper and manganin[1] wires produced similar results. Plasma beads can also be seen in their photograph depicting fragmentation of a manganin wire (fig. 2.2).

In [Taylor 2002b], plasma beads were reported as being a precursor to restrike. They were found to form at the wire kink locations, which had become sites of premature vaporisation (fig. 2.4).

[1] Manganin is an alloy of copper, manganese and nickel.

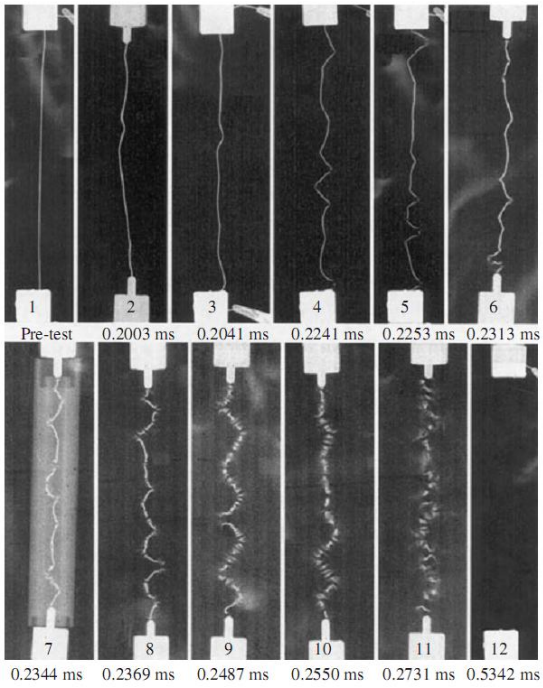

(a) A series of 150 mm long wires fragmenting.

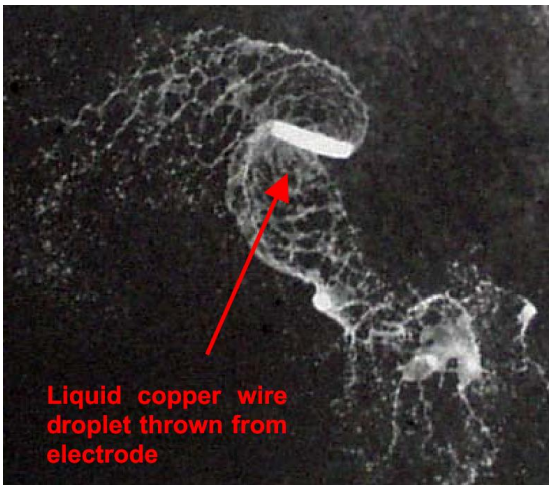

(b) A liquid copper droplet that was ejected from a wire near the electrode.

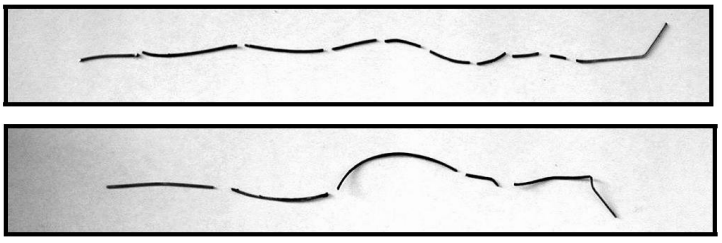

(c) Photographs of solid, fragmented wire remains.

Figure 2.1 Reproduced images from [Taylor 2002b] and [Taylor 2004].

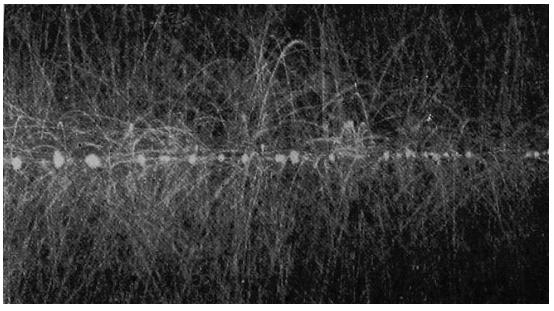

Figure 2.2 A 1 m long, 0.12 mm diameter manganin wire ejecting wire fragments[Nagaoka *et al.* 1926].

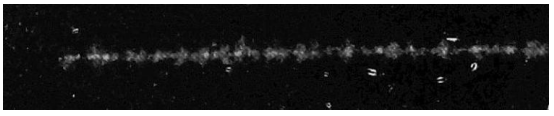

Figure 2.3 A 1 m long, 0.12 mm diameter copper wire producing plasma beads [Nagaoka *et al.* 1926].

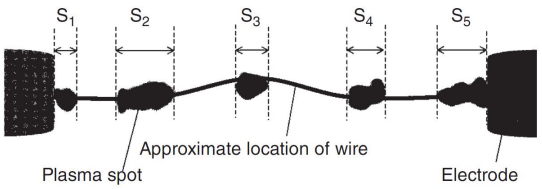

Figure 2.4 A negative image of plasma beads on a 185 mm length of wire [Taylor 2002b].

Taylor used 150 to 185 mm lengths of 1 mm diameter copper wire, exploded using a unique power supply that included an inductor that was varied from 26 to 800 μH in series with a 800 μF capacitor bank. The radial expansion rate of the plasma beads was measured, and found to be up to 1200 ms^{-1} for high-powered discharges. Taylor also calculated the total length of wire that was shrouded by the plasma beads, and plotted this as a function of time alongside the time-varying resistance. It was then shown that Taylor's version of restrike occurred when the shroud length equalled the wire length.

A key finding from Taylor's investigations of plasma beads was that the wire's total resistance increased with the plasma shroud length [Taylor 2003]. The peak of the resistance occurred just prior to the occurrence of restrike. It was hypothesised that a thin layer of poorly conducting metal vapour existed in the boundary between the molten wire and the plasma shroud.

Plasma beads were also reported in [Baksht *et al.* 2004], although thin aluminium foil was used rather than wire. The study used 5 cm long, 10 mm diameter tubes of 10 μm thick foil. Using the voltage and current waveforms to calculate the energy dissipation and the foil's resistance, they suggested that only part of the foil vaporised and created plasma beads, which then conducted the current around the remaining liquid material.

2.3.3 Restrike and Plasma

The characteristic of the restrike plasma has been the most studied feature of EW, but is not so important to this research. Unfortunately, most of the previous work focuses on much higher energy EWs and so has limited direct applicability to long distance EW experiments. A method of calculating the temperature, electron density and thermal conductivity of the restrike channel using a measurement of the electrical conductivity is presented in [Lundquist and Vlastos 1970]. Calculation results were presented for 13 cm long, 0.05 mm diameter wires, exploded using both 5 and 23 kV. Although the study used constantan[2] wires, it still provides some indication of the restrike channel temperature of copper wires. Channel currents of 0.6 and 4.15 kA produced respective plasma temperatures of 16.1 and 20.4×10^3 K.

[2]Constantan is a copper-nickel alloy.

2.4 AVERAGE ELECTRIC FIELD

The metric of average electric field (AEF), usually defined as the initial capacitor bank voltage divided by wire length, has been used by several authors as a means of quantifying EW experiments. The most detailed use was by Vlastós, who categorised the outcomes of EW experiments by their AEFs, noting that different AEFs produced three distinct restrike mechanism types [Vlastos 1973a]. The first type was an ionised channel that formed at or near the wire surface, called a peripheral arc, which did not have a dwell time. The second type, which occurred when the AEF was too low for a peripheral arc, was through ionisation of the wire vapour, called an axial arc. This did have a dwell time, the length of which could be explained by the expansion of the metal vapour until a low enough pressure was reached to allow for ionisation. A third type, the exterior arc, occurred at a much lower AEF, when the conditions allowed for ionisation of the rarefied vapour medium surrounding the wire.

The occurrence of restrike on EWs up to 116 inches long were reported in [Dannenberg and Silva 1969]. It was also found that 54 and 116 inch long wires would not produce restrike using less than 18 and 36 kV respectively. The authors concluded that the minimum voltage required for a given length of wire, i.e. the AEF, was 3.5 kV/ft (11.5 kV/m), with more reliable results obtained at 3.8 kV/ft (12.5 kV/m). The highest AEF presented was with a 54 inch wire at 40 kV (29.2 kV/m). Restrike was initiated using non-enamelled wires of various metals, including tungsten, aluminium and nickel, but none of the copper wire experiments initiated restrike.

A graphical version of AEF was presented in [Bhat and Jordan 1971], where the outcomes of EW experiments were plotted on a plane of voltage versus length for experiments using bare copper wires of gauge AWG #37, #39 and #42 (0.064, 0.089 and 0.114 mm) (fig. 2.5). The planes were divided into four zones, representing: (I) restrike without a dwell time; (II) restrike with a dwell time; (III) no restrike and incomplete discharge of capacitor bank; and (IV) no restrike and complete discharge of the capacitor bank. The slopes of the boundary lines between zones have values of approximately 27 and 200 kV/m.

2.5 BARE VS. ENAMELED WIRES

EW research is usually conducted using bare metallic wires. Where coated wires have been compared to bare wires, authors report significantly different outcomes. Bare and enamelled copper wires of gauges AWG #39 (0.089 mm) and #42 (0.064 mm) were studied in [Bhat and Jordan 1971]. The energy supply was a 551 μF capacitor bank. Voltages up to 20 kV and wire lengths up to 50 cm were used. It was shown that for both gauges of wire, enamelled wires would initiate restrike at much longer lengths than bare wires (Table 2.1).

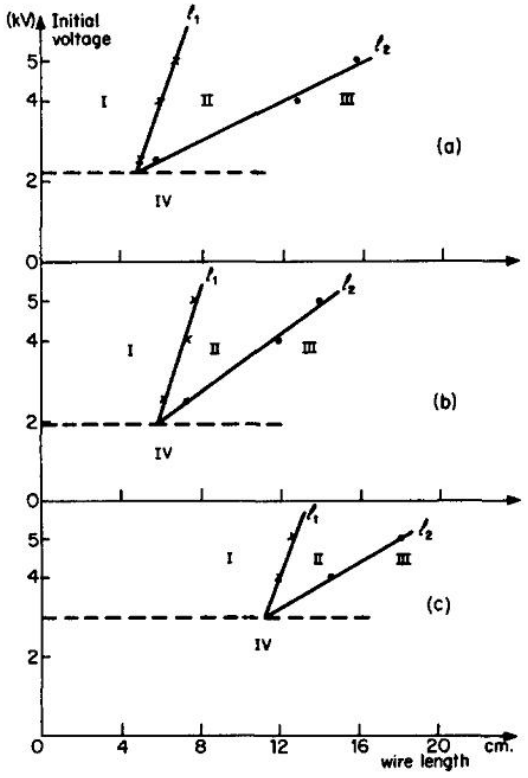

Figure 2.5 Division of the voltage versus length plane into four zones of experimental outcome [Bhat and Jordan 1971]. (a) AWG #42; (b) AWG #39; (c) AWG #37.

Wire	Bare	Enameled
AWG #39	13 cm (26 kV/m)	38 cm (9.2 kV/m)
AWG #42	16 cm (22 kV/m)	51 cm (6.8 kV/m)

Table 2.1 The longest length that produced restrike using bare and enamelled wires with an initial voltage of 3.5 kV [Bhat and Jordan 1971].

A comparison of bare and coated wires was also made in [Sinars *et al.* 2000], where it was observed that the wire expansion rate was higher when using coated wires. Results were presented of untreated, polyimide-insulated and oil-coated 25 μm tungsten wires, and untreated, polyester-insulated and oil-coated 25 μm silver wires. It was suggested that the coating allowed further heating of the metal by delaying the formation of plasma around the wire. This is perhaps more plausible than the explanation given in [Bhat and Jordan 1971], where it was suggested that the coating traps thermionic emission electrons, creating a build up of charge, a radially-directed negative electric field, and ionisation of the air surrounding the wire that facilitates restrike.

Coating was used to enhance restrike on EWs in a vacuum in [Sarkisov *et al.* 2005]. The coating allowed corona-free discharge, and subsequently anomalously high energy deposition in the wire. Results were presented using 2 cm long, 12 μm tungsten wires, and compared uncoated wires to wires coated with 2 μm of polyimide. The energy supply was a 7 nF capacitor bank charged to 60 kV.

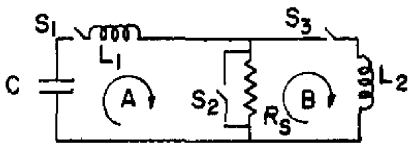

Figure 2.6 The simplified circuit diagram of the magnetic energy storage system presented in [DiMarco and Burkhardt 1970]. C is the capacitor bank, switch S_2 is the exploding foil fuse, and R_S is the load.

2.6 LONG DISTANCE EW

The longest documented case of restrike EW prior to this thesis, other than previous work at the University of Canterbury, was in [Dannenberg and Silva 1969], where restrike was produced on EWs up to 2.95 m long. The apparatus consists of a 40 kV capacitor bank with 1 MJ of energy storage and a 10 foot long shock tunnel. The machine was introduced as being beyond the capabilities of most existing facilities at the time. The study used various metals such as tungsten, aluminium, nickel and copper, and diameters from 0.076 to 0.64 mm. They did not manage to induce restrike using copper wire. Two lengths were studied, 54 inches (1.37 m) and 116 inches (2.95 m), for which the minimum voltages to produce restrike were 18 and 36 kV (13.1 and 12.2 kV/m), respectively. Dwell times of 100 to 150 μs for 54 inch arcs and 400 to 500 μs for 116 inch arcs were recorded, but no explanation for the relatively long times was given.

2.7 EXISTING APPLICATIONS

2.7.1 Pulsed Power Systems

A magnetic energy storage system, presented in [DiMarco and Burkhardt 1970], uses exploding foils as an opening switch device (fig. 2.6). The system used an exploding foil fuse made of folded copper foil with Mylar, polyethylene and fibreglass cloth as insulation between the layers. The fuse was inserted in series with a capacitor bank and was designed to open at the peak current, causing a large inductively-driven voltage to be developed across a parallel-connected load. Load voltages as high as 90 kV were achieved, which caused a rate of current rise of 10^{13} A/s in a 19 nH load. The fuse was proven to withstand 600 kV/m upon becoming open-circuit.

A pulsed power generator presented in [Shimomura *et al.* 2000] used a Marx circuit, storage inductor and an EW fuse. The circuit was able to generate output voltages of up to 800 kV with a rise-time of 15 ns, using a 75 kV output from the Marx circuit. The fuses were 30 cm lengths of copper wire, with diameters of 0.03, 0.05 and 0.1 mm.

2.7.2 Generation of X-rays

High-power EWs and X-pinches can produce x-rays, such as in [Burkhalter *et al.* 1977]. Multi-wire arrays of EWs were investigated as an x-ray back-light source in [Shelkovenko *et al.* 1999]. The X-pinch creates a point source of x-rays to cast a shadow image of an object directly onto a film. Spatial resolution of 1 to 5 μm and a temporal resolution of 0.7 to 2 ns was achieved. Fast Z-pinch implosions of EWs were used in [Matzen 1997] to convert electrical energy into x-rays, where currents of 6 to 8 MA were driven through cylindrically symmetrical loads, producing x-ray energies exceeding 400 kJ.

2.7.3 Production of Shock Waves

EWs are known to produce strong cylindrical shock waves [Bennett 1958]. In several studies, the shock waves have been intensified by submerging the EW in water. The efficiency of energy transfer from the electrical circuit into the mechanical energy of the compressed water flow was calculated in [Grinenko *et al.* 2006]. A 6 GW, nanosecond time-scale EW had a transfer efficiency of 15%. In a similar study by [Grinenko *et al.* 2005], the maximum pressure at the boundary was found to be 60 MPa.

An experimental investigation into the use of EW shock waves for the destruction of solid materials was presented in [Lisitsyn *et al.* 1997]. A 14.9 μF, 25 kV capacitor bank was discharged into copper and aluminium wires, 0.2 mm in diameter and 1.5 to 9 cm long. Shock wave velocities of 1500 m/s were measured.

A method of shattering the canopy of a jet aircraft to aid the safe ejection of the pilot has been investigated [Novac *et al.* 2005]. EWs of various materials were embedded into plates of acrylic, Tufnol and polycarbonate (fig. 2.7). It was found that the most effective cuts were made when strong shock waves were created, which was correlated to the peak electrical power absorbed in the EW.

2.8 RESEARCH AT THE UNIVERSITY OF CANTERBURY

2.8.1 Watson and Hiscock: Wire Fragmentation

The first interest in EW at the University of Canterbury was from Watson and Hiscock, who wrote an unpublished paper titled ‘An explanation of the fragmentation of copper wire by high electric current’ in 1999, which is included in the appendix of [Mulholland 2004]. Watson and Hiscock calculated that an axial, compressive component of the Maxwell stress can be sufficient

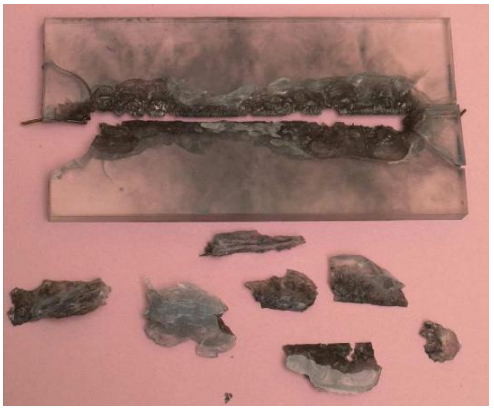

Figure 2.7 A stretched acrylic plate cut with an EW [Novac *et al.* 2005].

to overcome the tensile strength of copper at high temperatures. The calculated fragmentation currents were very close to the experimentally obtained values.

2.8.2 Mulholland: A Plasma Canon

Watson and Hiscock's work was continued by [Mulholland 2004], who found during fragmentation experiments that some of the long wires would erupt into plasma channels at higher voltages. Restrike was produced using 5 m lengths of 0.3 mm diameter enamelled copper wire at voltages of 30 and 40 kV (6 and 8 kV/m), but not at 5, 10 or 20 kV (1, 2 and 5 kV/m). Restrike was not produced using 0.6 and 1 mm diameter wires.

Mulholland then created a 'plasma cannon' by using a simple combustion cannon to fire a projectile at a metal target that was connected to a high voltage capacitor bank. The projectile trailed a 10 m copper wire with one end earthed. Later, full plasma lengths of up to 20 m were initiated by doubling the capacitor voltage to 120 kV (6 kV/m). Wires of diameter 0.2, 0.22, 0.27 and 0.3 mm produced restrike, but wires of diameter 0.125 and 0.375 mm did not.

2.8.3 Smith: Long Distance Plasma Discharges

In 2005, long distance EW as a means of creating directional ionisation paths in air was investigated by [Smith 2005]. A test setup was created, including a 22.8 μF capacitor bank capable of being charged to 60 kV. Restrike was produced using 0.3 mm diameter enamel coated copper wires up to 10 m long. Outdoor experiments were also performed, attempting to create a 100 m plasma path. Only a 10 m restrike was initiated, but a 70 m experiment produced plasma beads (fig. 2.8).

During Smith's continuing research [Smith 2008], an experimental setup was constructed to investigate long distance EW in more detail. The equipment included a capacitor bank rated

Figure 2.8 A 70 m long EW producing plasma beads [Smith 2005].

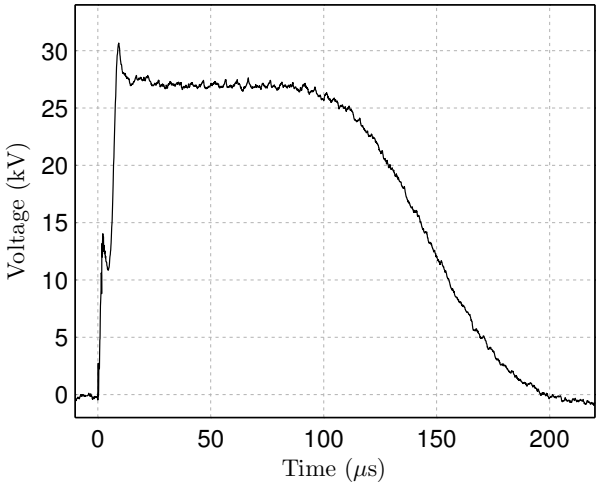

Figure 2.9 The voltage waveform from a 3 m long, 0.2 mm diameter wire exploded using 30 kV [Smith 2008].

to 60 kV, 21.4 μF and a mechanically triggered spark gap [Smith *et al.* 2007]. The main experimental set was a series of 100 EWs with voltages of 15, 30, 45 and 60 kV, wire diameters of 0.2, 0.27, 0.375 and 0.63 mm, and wire lengths of 1, 3, 5, 7 and 9 m. Enamelled copper wire was used for all experiments. Voltage and current waveforms and the final capacitor bank voltage were recorded. Smith identified that some of the voltage and current waveforms exhibited a dwell time and restrike, for example in Figure 2.9, where the restrike occurred after a dwell time of about 100 μs.

Analysis of the data included comparison of the total energy dissipated in each experiment, W_T, which was calculated as

$$W_T = \frac{1}{2} C \left(V_i^2 - V_f^2 \right) \tag{2.1}$$

where C is the capacitor bank capacitance and V_i and V_f are the initial and final capacitor voltages respectively. For each of the four initial capacitor voltages, the energy dissipation was plotted in three dimensions as a function of both diameter and length (fig. 2.10). These were then divided up into areas that represented apparently similar outcomes, based on visual observations, energy dissipation, waveforms and photographs.

Using an initial capacitor bank charge voltage of 15 kV and longer and thicker wires, experiments

resulted in almost complete energy dissipation. Some wires remained intact, developed a 'kinked' deformation, and showed signs of heating through discolouration and damage of the enamel. The voltage and current waveforms were often under-damped oscillations. Thinner and shorter wires exploded into a shower of sparks, and only partially discharged the capacitors (fig. 2.11a). This was referred to as a 'sparky' discharge. It was suggested that the wire fragmented and conduction stopped before enough energy could be dissipated to complete the process.

At initial charge voltages of 30 kV and 45 kV, some wires were observed to form bright blue beads of plasma along the wire (fig. 2.11b). Smith referred to this as a 'beaded' discharge. In these experiments, there was only a partial discharge of the capacitor bank. Other experiments formed a full plasma path and completely discharged the capacitor bank (fig. 2.11c). In that case, the voltage and current waveforms often exhibited a restrike conduction period after an obvious dwell time. The thickest wires, 0.63 mm in diameter, still discharged most of the capacitor bank energy without producing much plasma. At an initial charge voltage of 60 kV, experiments produced only two outcomes; either a full discharge with a continuous plasma path or a partial discharge with plasma beads.

2.9 CONCLUSIONS

A review of the most relevant literature on EWs to date has been presented, delineating the boundaries of prior understanding. The AEF quantity was introduced, which provides one particularly useful measure of the distinction of this research from previous studies. The majority of the reviewed studies have been shown to focus on short lengths of wire with relatively high voltages, resulting in a high AEF. The AEF has usually been greater than 30 kV/m, with many studies using AEFs of 100 to 1000 kV/m. The AEF was described as being a key indicator as to which restrike mechanism will be induced. In this research on long distance EW, restrike was obtained using AEFs of about 4.5 to 11 kV/m, which was much lower than any study to date. The restrike mechanism that occurs at this lower AEF is different to the previously reported mechanisms, and will be presented in detail with many original observations and findings. Furthermore, the correlation between the AEF and the occurrence of restrike is refined with the formation of a mathematical model for long distance EW.

Another clear distinction of this research from previous studies is in the length of restrike that is obtained. In [Dannenberg and Silva 1969], restrike on EWs up to 2.95 m long was reported, up to 9 m in [Smith 2008], and even up to 20 m in [Mulholland 2004]. Most other research to date studied EWs that were much less than 1 m in length. In this research, restrike was produced on wires up to 60 m.

The literature review also covered fragmentation in EWs. Wires tend to fragment in the early stages of explosion, especially with lower current densities, which are also found in long distance

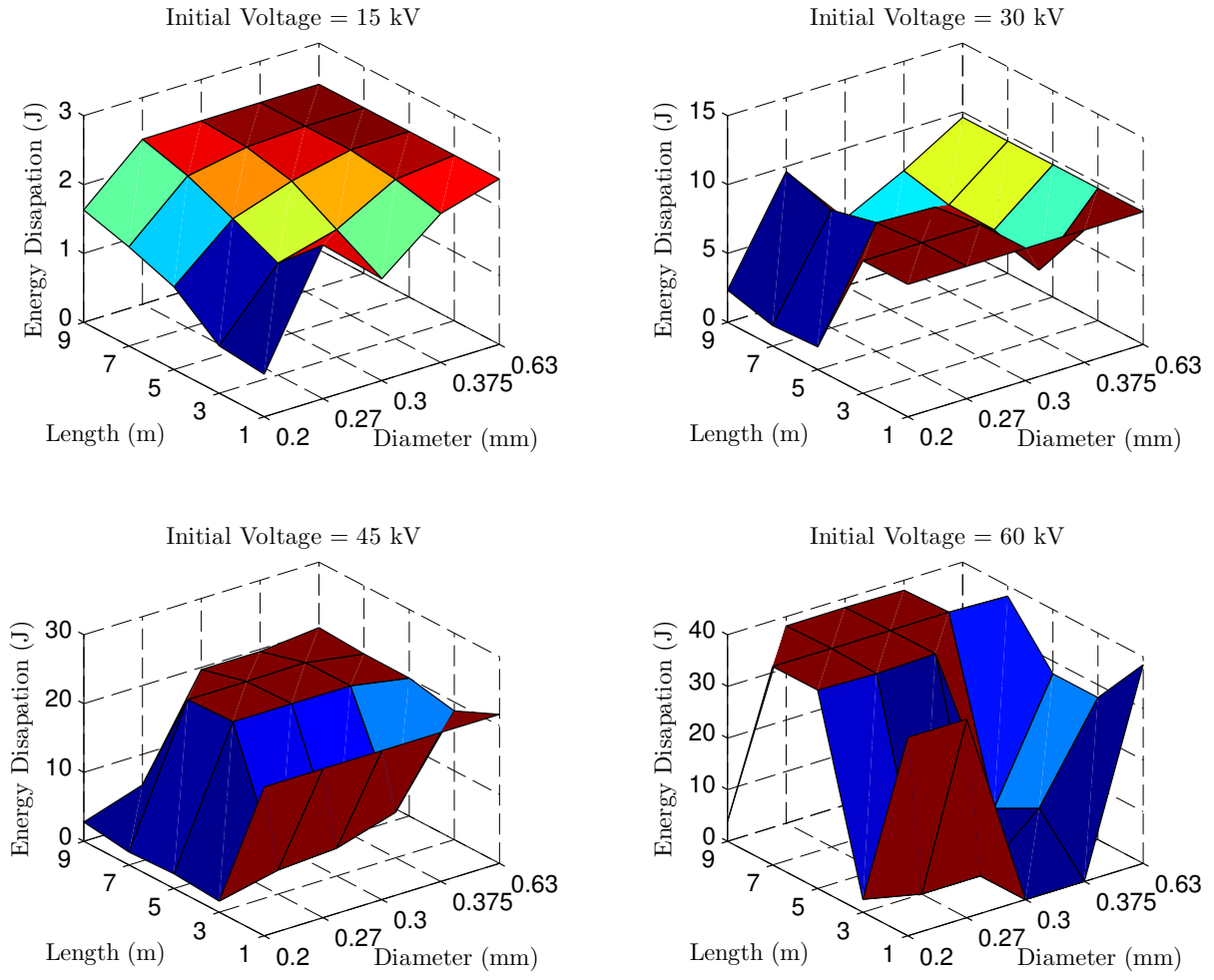

Figure 2.10 Analysis of the energy dissipation versus the wire length and diameter [Smith 2008].

EW experiments. Fragmentation has been reported to occur in either the solid or the liquid states. Fragmentation was identified as the cause of the formation of plasma beads, which was shown to be a mechanism that can initiate restrike. The formation of plasma beads has been a rarely reported phenomenon to date, but is a focal point of this research. This thesis presents extensive observations of the plasma beads, and how they can facilitate restrike.

Previously at the University of Canterbury, long distance EWs had been used to produce long plasma conductors. In the most recently work, which was a focused study of long distance EWs by [Smith 2008], no obvious formulation was found for the conditions that would reliably produce restrike. The research presented in this thesis extends Smith's work, presenting an improved understanding of the restrike mechanism and a model that can predict the occurrence of restrike.

(a) A ‘sparky’ discharge.

(b) A ‘beaded’ discharge.

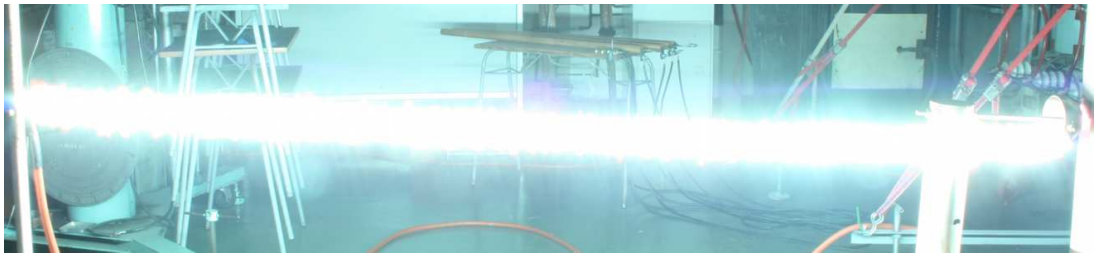

(c) A ‘full plasma’ discharge.

Figure 2.11 Smith’s observations of EW outcomes [Smith *et al.* 2007].

Chapter 3

THE EXPERIMENTAL ENVIRONMENT

3.1 INTRODUCTION

This research relied heavily on obtaining new experimental observations and data. Over the course of the research, an environment was developed in the high voltage laboratory in which experiments could be performed reliably, efficiently and safely. A substantial amount of work was completed in designing, constructing and testing equipment, instrumentation systems and operating procedures. Although some of the components could be acquired and integrated into the circuit without modification, many had to be constructed or modified and went through several development cycles before an adequate solution was found.

EW experiments require an electrical energy supply that can deliver large current impulses with fast rise-times. Capacitor banks, which are ideal for supplying such impulses, were used as the energy storage and supply devices. Two energy supply circuits were used in this research: a 60 kV capacitor bank circuit, and a Marx generator circuit. Either of these circuits could be charged using the same variable h.v. d.c. supply circuit. After it had been charged, the energy supply circuit was switched on to the EW using a triggered spark gap (TSG), which is a crucial component for reliable operation of the circuit.

This chapter has two purposes: to provide context for the subsequent experimental observations and results; and to describe the equipment in enough detail that other researchers can conduct their own long distance EW experiments. First, an overview of each energy supply circuit is given, describing the layout of the components and theory of operation. The physical construction of each component is then described in detail. Lastly, the safety considerations and the operating procedures are discussed.

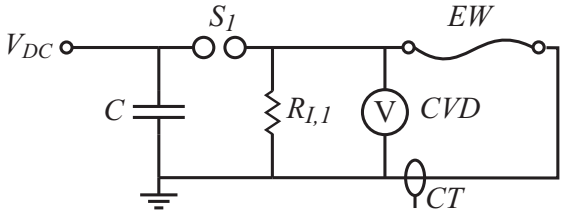

Figure 3.1 The schematic of the 60 kV capacitor bank circuit.

3.2 CIRCUITS

3.2.1 60 kV Capacitor Bank Circuit

A 60 kV capacitor bank was used as the energy supply for the earlier experiments presented in this thesis. The circuit was adapted from the equipment used in [Smith *et al.* 2007]. The capacitor bank, C, was charged using the charging circuit, connected at point V_{DC} (fig. 3.1). Once the capacitor bank had been charged to the required voltage, it was switched onto the specimen wire, EW, using the triggered spark gap, S_1. Resistor $R_{I,1}$ was included to maintain ionisation of the arc in S_1 during the experiment. A capacitive voltage divider, CVD, was used to measure the voltage across the EW and return cables. A current transformer, CT, was used to measure the current flowing through the EW.

3.2.2 Marx Generator

A Marx generator was used for experiments requiring voltages greater than 60 kV. The Marx topology is commonly used for generating high voltage impulses; the advantage over a single capacitor bank design is the output voltage can be many times greater than the charging voltage. The Marx generator built for this research has a different application than many high voltage impulse generators, which are designed to deliver high voltage impulses with limited energy for testing insulation systems. EW experiments need large current impulses, requiring more capacitance relative to the output voltage. Newer commercial impulse generators, however, would typically have enough capacitance to perform long distance EW experiments.

The maximum output voltage of the Marx generator was chosen to be 270 kV, achieved by using three 90 kV stages. The stage voltage was limited by the rating of the charging circuit, which was 110 kV d.c., and chosen to be a multiple of the individual capacitor rating, which was 15 kV. The Marx generator could be operated in one-, two- and three-stage configurations (fig. 3.2). For the three-stage configuration, the capacitor stages C_1 to C_3 charged in parallel through resistors R_1 to R_4 as the d.c. supply voltage V_{DC} was increased. When the desired stage voltage was reached, the TSG S_1 was triggered. Spark gaps S_2 and S_3 subsequently broke

down, effectively causing the stages to become reconnected in series and resulting in an output voltage equal to the sum of the stage voltages. The capacitors then discharged into the EW experiment. Resistor $R_{I,2}$ was included to maintain a small current flow through S_3 to keep it ionised and conductive for the duration of the experiment.

The coordination of the spark gaps in a Marx generator is crucial for reliable operation. The first spark gap is usually a TSG and the subsequent spark gaps break down due to transient over-voltages. The over-voltages form according to a voltage divider of parasitic capacitances between stages and across the spark gaps [Kuffel *et al.* 2000]. Most Marx generators are in a tower structure where the interstage capacitance is relatively high compared to the spark gap capacitance, and consequently the transient over-voltages in the spark gaps is relatively high. The Marx generator presented here, however, had lower interstage capacitances due to the physical separation of stages, reducing the spark gap over-voltage. So, to aid the breakdown of S_2, a 65 nF, 200 kV capacitor C_{SG} was connected between the bottom of C_3 and earth. Resistor R_{SG} was included to limit the current in C_{SG} and subsequently minimise earth potential rise. S_3 had one sphere effectively earthed through the EW and so experienced a sufficiently large transient over-voltage.

To reconfigure the Marx generator from a three-stage to a two-stage configuration, R_3, R_4 and S_2 were disconnected. The output of C_2 was connected to S_3. To reconfigure the Marx generator to a one-stage configuration, R_1 and R_2 were disconnected, and the output from C_1 was connected to S_1, which was then connected to $R_{I,1}$ and the EW. An overview of the Marx generator circuit is shown in Figure 3.3.

3.2.3 Charging Circuit

The charging circuit was a variable, half-wave rectified, high voltage d.c. supply (fig. 3.4). The variable transformer $VariAC$ was connected to the laboratory's 230 V a.c. supply, V_{AC}. $VariAC$ was then connected through a d.c. ammeter to measure the charging current I_C to a 230 V to 80 kV high voltage step-up transformer Tx. The transformer's high voltage output was connected through a 100 kΩ current limiting resistor R_L to a 360 kV, 1 A diode D. The full charging voltage was measured using a 100 kV resistive voltage divider RVD. A high voltage disconnector switch Sw_D, which was operated using a 230 V electromagnet, was used to connect the discharge resistor R_D to the circuit to remove the energy from the capacitor banks after an experiment.

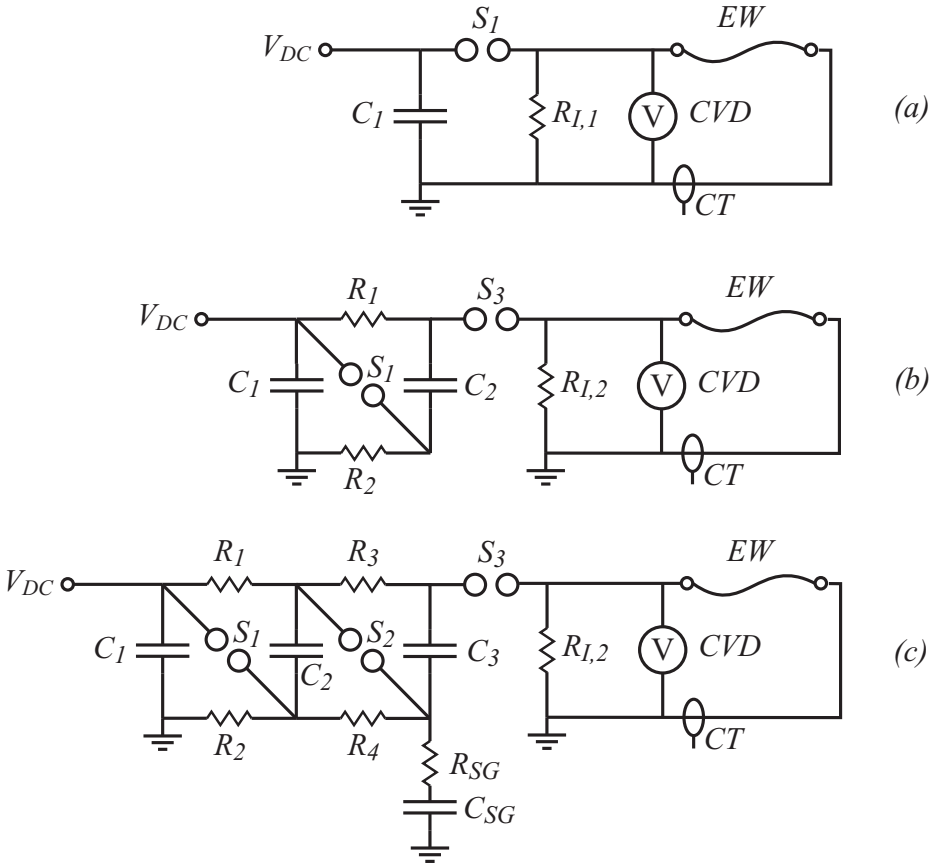

Figure 3.2 Circuit schematics of the Marx generator, in (*a*) one-stage, (*b*) two-stage and (*c*) three-stage configurations.

3.3 COMPONENTS

3.3.1 Capacitors

Unlike most previous EW studies, which required fast impulses and consequently low-inductance capacitors, long distance EW experiments are relatively slow, so DC-rated capacitors are acceptable. The capacitors that were available at the University of Canterbury were donated from the New Zealand High Voltage Direct Current Link project, where they had been used for about 40 years as part of a 12^{th} harmonic filter. Each capacitor had a rated voltage of 6.575 kV and a capacitance of 17.1 μF. They were foil electrode type, with oil-impregnated paper as dielectric and insulation, and housed in a sealed mild steel enclosure (fig. 3.5). The two terminals are the tip of the bushing and the metal enclosure.

Each capacitor had a 1.2 MΩ internal discharge resistor to ensure that the capacitor remained safely discharged while it was out of service. The discharge resistor in each capacitor dissipates 187 W at a charge voltage of 15 kV, so the 36 capacitors in the three-stage Marx generator,

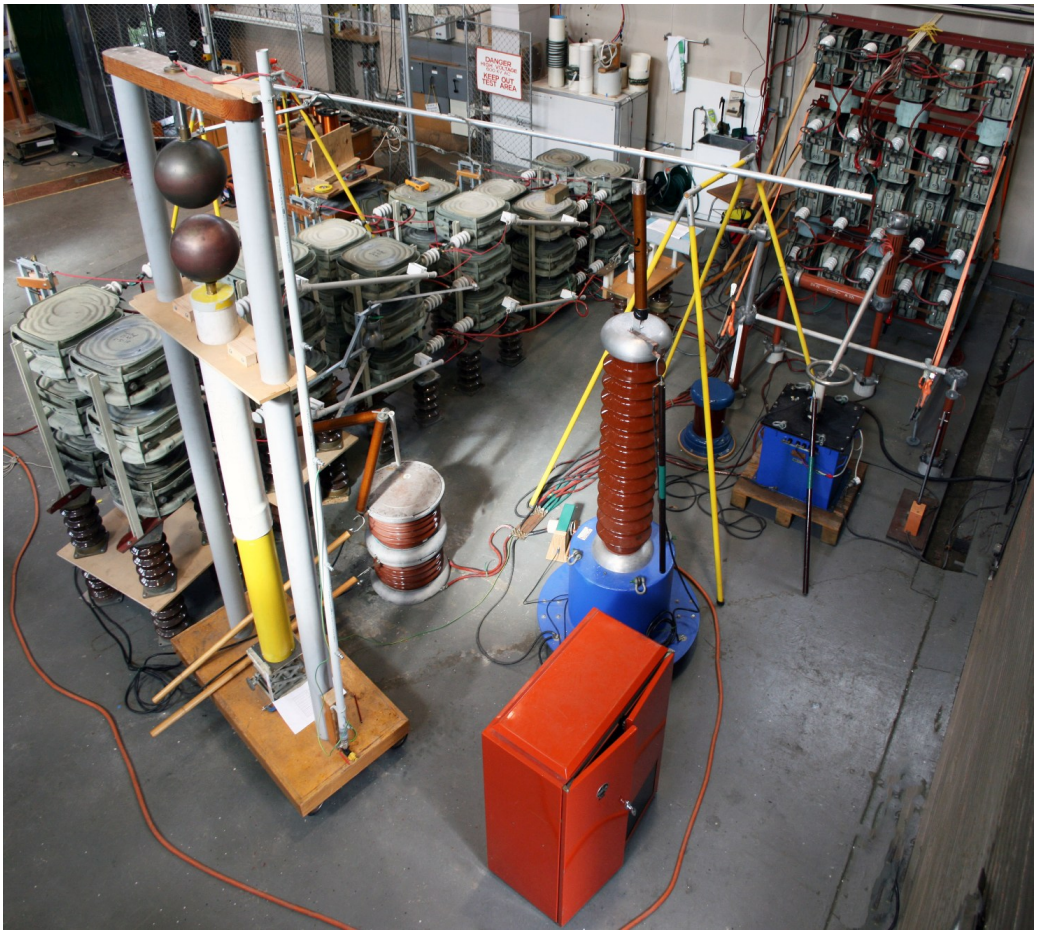

(a) A photograph.

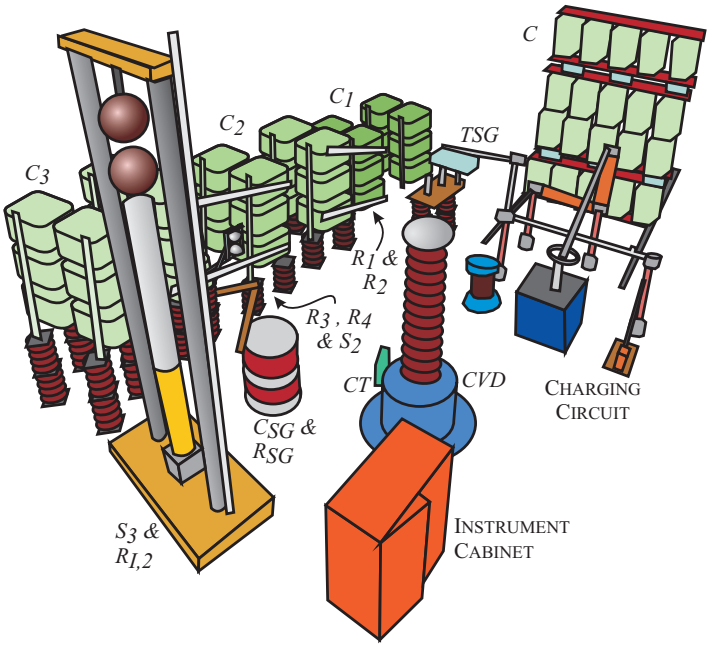

(b) A key to the photograph.

Figure 3.3 An overview of the complete 60 kV capacitor bank and Marx generator circuits.

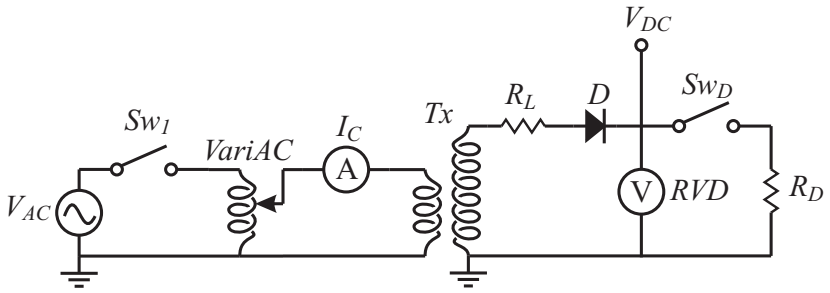

Figure 3.4 The electrical schematic for the charging circuit.

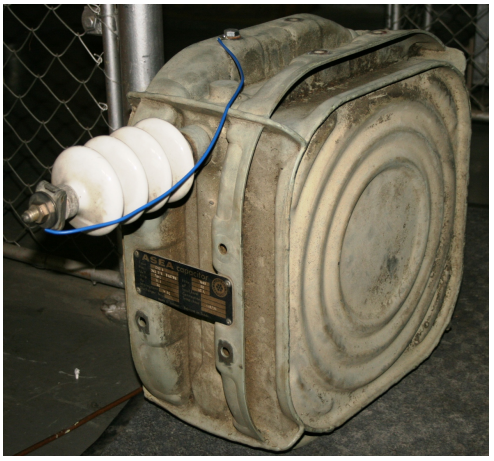

Figure 3.5 A capacitor, used in the capacitor banks.

for example, would consume 6.75 kW while at full charge. The available charging transformer would not have been able to supply this power and still charge the capacitors without exceeding the current rating of the high voltage winding. The capacitor voltage would also have decreased rapidly from when the charging circuit was isolated before the experiment was triggered, making it difficult to obtain accurate experimental voltages. Therefore, the discharge resistors were physically disconnected, and the safety discharge mechanism was replaced with an external earthing procedure.

To disconnect the discharge resistors in the capacitors, the oil level was reduced in each capacitor. Two holes were then drilled in the side of each capacitor's enclosure to allow 'key-hole' disconnection of the discharge resistor in two places. Cardboard and paper insulation had to be removed to reach the disconnection points. The resistor's wires were then cut and the two ends separated, but the resistor remained in place. The holes were then closed by welding steel plugs into place and the oil was replaced. Each modified capacitor was then electrically tested by charging it to 20 kV d.c. for 60 s. The capacitors generally leaked current so that the voltage decreased by 1 to 2 kV over the duration of the test. The capacitors that did not decrease by more than 2 kV or produce internal discharging sounds were deemed to have passed the test. They were then considered to be re-rated to 15 kV for the purpose of EW experiments.

Understanding the failure mode of the capacitors was important in the design of the capacitor banks. Previous investigation of a capacitor failure in [Smith 2008] indicated that during a fault, internal arcing under oil and the subsequent generation of gas created a build-up of pressure. This caused the side walls of the capacitor enclosure to swell. The side walls were ribbed to allow for expansion, and could expand by up to 20 mm without the enclosure rupturing. Under an extreme fault, the enclosure ripped open, spilling the capacitor's oil.

3.3.2 60 kV Capacitor Bank, C

The capacitor bank that was used primarily in the earlier parts of this research is described in detail in [Smith 2008]. It was rated to 60 kV, had a total capacitance of 21.375 μF and total stored energy of 38.475 kJ (fig. 3.6). The capacitor bank consisted of 20 capacitors, arranged as four series stages of five parallel capacitors. The capacitors were oriented vertically and bolted to mild steel angle-section supports. The clearance between capacitors was 100 mm to allow expansion of the side walls in the event of a fault, without causing mechanical failure of the entire capacitor bank. Insulation between each row of capacitors was provided by 100 mm long sections of 250 mm diameter poly-vinyl-chloride (PVC) culvert pipe. The entire capacitor bank was stabilised by Nylon tie-down strops connected to two outrigger-style horizontal supports constructed from 50 mm angle-section steel. The capacitor bank was earthed between experiments by applying temporary earth connections to each of the four rows of capacitors. The earth connections were applied using 1 m long wooden earth sticks with a metal hook and earthed cable on one end.

3.3.3 Marx Generator Capacitor Banks, C_1 to C_3

Six 90 kV capacitor banks were built and connected into three parallel pairs, constituting the three Marx generator stages. Each bank consisted of six capacitors in series. The criteria for the design of the banks included: structural strength to support the six capacitors, weighing 360 kg in total; a connection scheme to series-connect the bushings and enclosures; a minimial amount of insulating structural material; convenient locations for connection of each bank and the temporary earthing connections; and an ability to move each bank separately via a crane and a pallet trolley. The second and third stages had to be insulated from the earthed laboratory floor, withstanding voltages of 90 and 180 kV respectively. Porcelain insulators, rated to 100 kV, were used for this purpose.

Prototype Design

First, a prototype bank was constructed and tested up to 90 kV d.c. (fig. 3.7). The capacitor enclosures were bolted together in three pairs, each using four M10 bolts, to take advantage

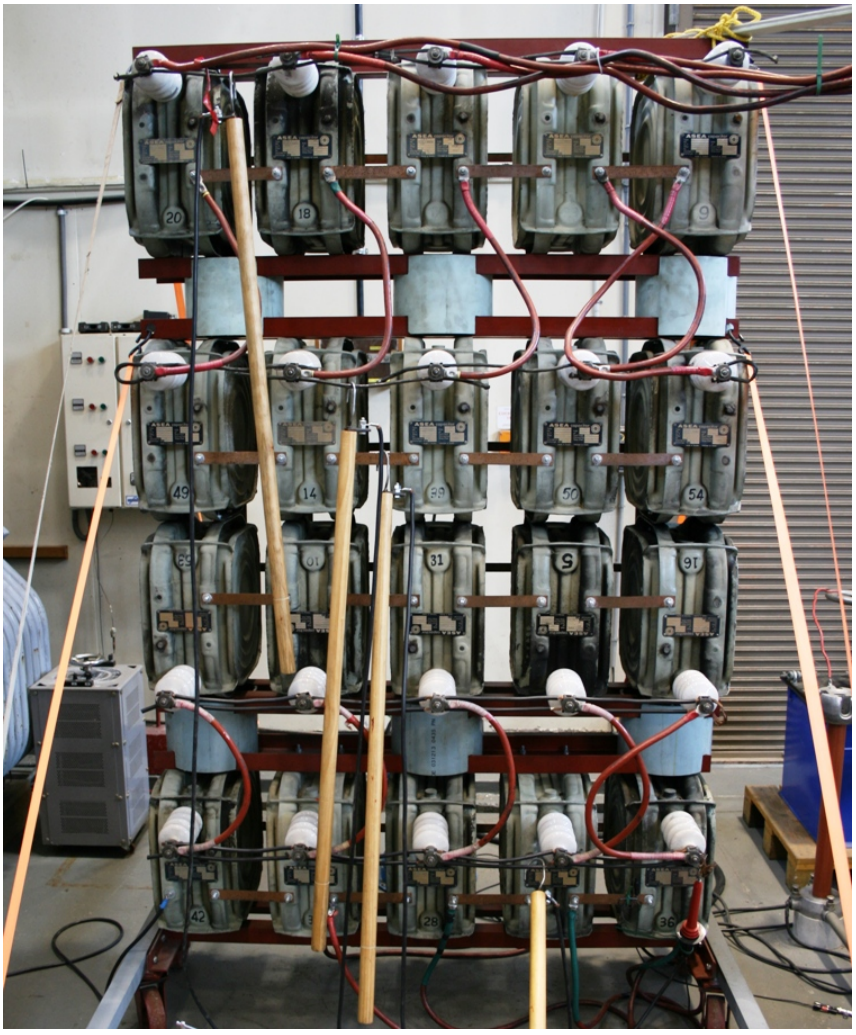

Figure 3.6 The 60 kV capacitor bank. Four temporary earth sticks are pictured in this photograph.

of the mechanically strong connection between capacitors and to reduce the required amount of structural insulating material. Insulating supports were constructed from four sections of 250 mm diameter PVC pipe. The prototype proved that the capacitor connection layout was suitable, but it was not mechanically stable enough to be used in a Marx configuration. Also, the PVC pipe sections would not have allowed for expansion of the capacitor enclosure in the event of a failure, and instead would have catastrophically toppled the whole bank.

Final Design

The final capacitor bank design used four lengths of channel-section pulltruded fibreglass as insulating supports (fig. 3.8a). The capacitors were connected using 95 mm^2 conductors according to Figure 3.8b, so that the insulation voltage requirement for the fibreglass supports could be evenly distributed. The connection arrangement also provided the most convenient layout of

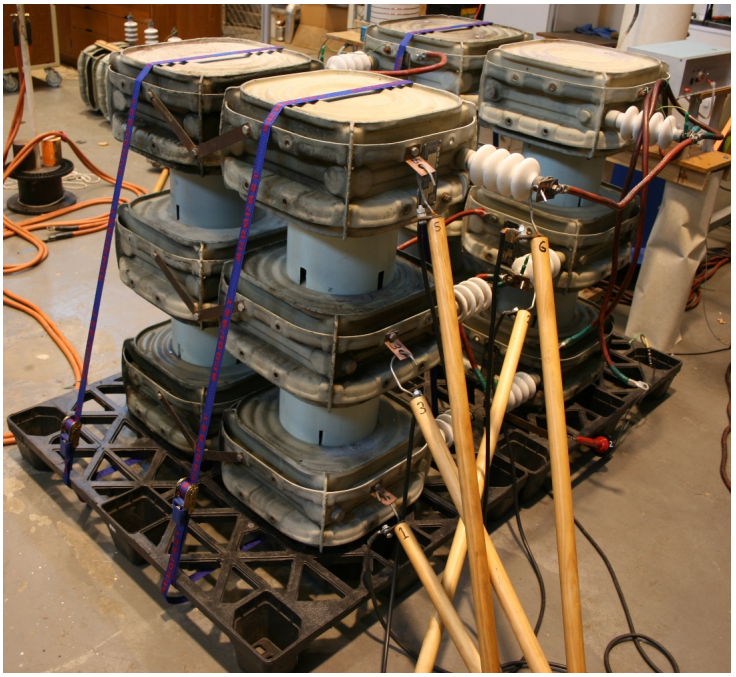

Figure 3.7 The prototype 90 kV capacitor bank, using PVC pipe insulators. Six earth sticks are applied to the bank to individually short out the capacitors.

the electrodes for temporary earthing to be applied. The connection arrangement required that the fibreglass insulators withstood 15 kV between the bottom of the bank and the first pair of capacitors, and 30 kV between each of the other two pairs. Gap lengths of 55 and 110 mm respectively were chosen and tested to withstand a d.c. voltage of $2U + 1$, where U is the designed withstand voltage, for 60 s.

Each pair of capacitor banks, constituting each stage of the Marx generator, was then connected by facing the bushings inwards and creating parallel connections using 95 mm^2 conductors (fig. 3.9). Two angle-section steel skids were bolted to the base of each bank for rigidity and to protect the ends of the fibreglass. The bank could be lifted by crane using strops around the top pair of capacitors. The capacitor banks, along with the rest of the circuit, survived without damage Christchurch's magnitude 7.1 and 6.3 earthquakes, and thousands of subsequent aftershocks.

Capacitor Bank Earthing

There were six capacitors in each stage that needed to be individually earthed after each experiment, creating a total of 20 nodes that required earthing in the three-stage Marx generator. It was not enough to earth each stage as a whole; due to uneven leakage currents in the capacitors, lethal voltages can remain within the capacitor banks after they are discharged. The earthing system needed to be fast and simple to apply to minimize experiment turn-around time and

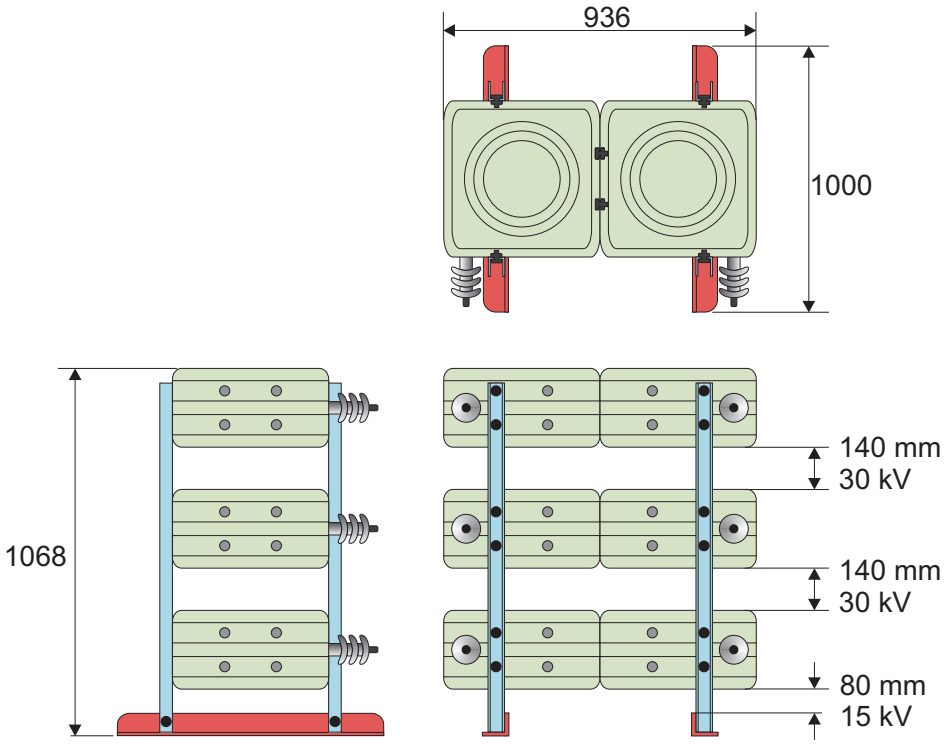

(a) The layout and dimensions of the capacitor banks.

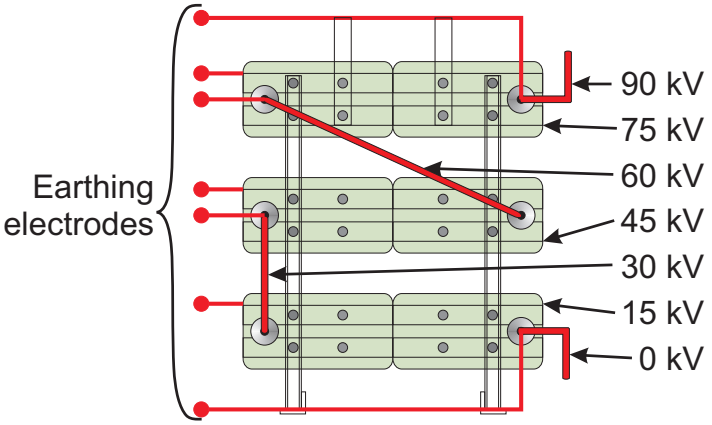

(b) The connection scheme for the capacitor banks, indicating the voltage of each conductor relative to the lowest voltage conductor of the bank. The layout of the electrodes for the application of temporary earths is also indicated.

Figure 3.8 Drawings of the Marx generator capacitor banks. Not to scale.

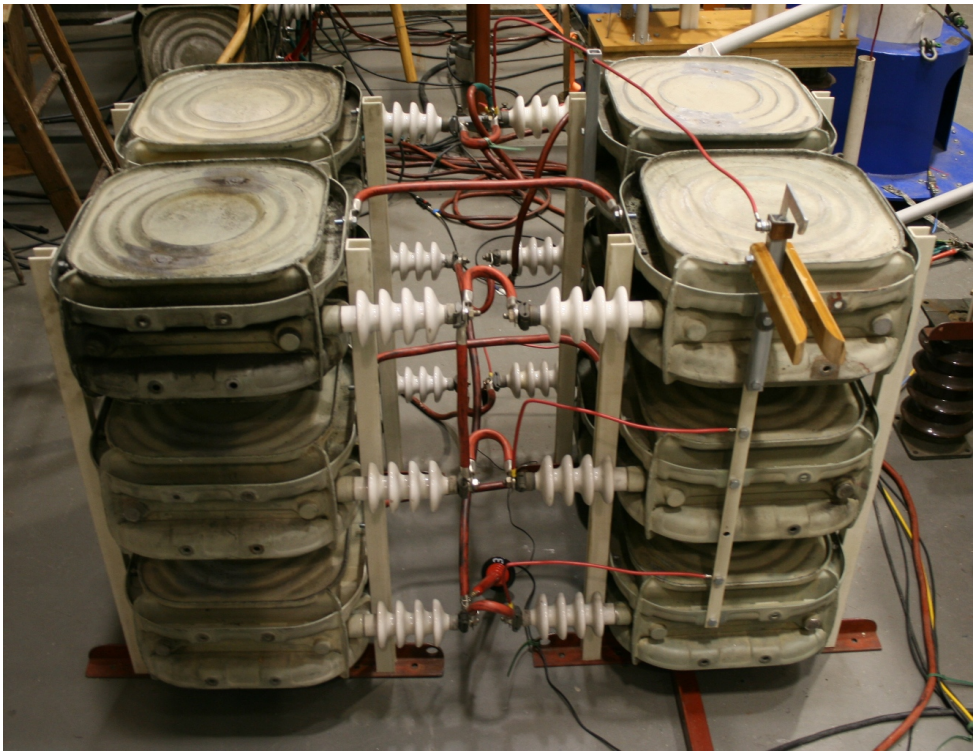

Figure 3.9 Two parallel-connected 90 kV capacitor banks, forming stage one of the Marx generator.

reduce the chance of an error by the operator.

Three earthing levers were built that rotated from a horizontal (disconnected) position to a vertical (connected) position, pivoting at floor level (fig. 3.10). Each lever had spring-loaded piston electrodes that pressed against contact electrodes on the capacitors. The levers were operated using wooden earth sticks rated to 100 kV and were secured into the connected position by an automatic latch. The earthing lever for the first stage required six electrodes because the bottom of the stage is connected solidly to the experiment neutral, whereas second and third stages required seven electrodes each.

3.3.4 Triggered Spark Gap, S_1

Design Criteria

A new triggered spark gap (TSG) was designed and built to match the requirements of long distance EW experiments. The previously used TSG, described in [Smith 2008], was a mechanically triggered design, consisting of a metal slider that was released from an electromagnet and fell under gravity into the spark gap. The major disadvantage of the design was that exact timing of the switching operation was not possible, making timing of long-exposure photographs unreliable and precise timing for short-exposure photographs and other instrumentation impossible.

(a) Earthing lever down.

(b) Earthing lever up (capacitors earthed).

Figure 3.10 The earthing lever for stage one of the Marx generator.

Another disadvantage was that the switch had to be manually reset, which took time and was occasionally forgotten.

Several types of TSG were considered for the design of a new TSG. Mechanical TSG designs, such as the one used by Smith, intrinsically have a very long delay between receiving the triggering signal and the break down of the spark gap, which is called the 'jitter time'. Laser-triggered spark gaps use a laser to ionise the gas in the gap, which is usually a specialised gas rather than atmospheric air. This type of TSG has jitter times that can be as low as 10 ns [Pendleton and Guenther 1965], but inclusion of a laser makes the design expensive and complicated. Three-electrode spark gaps use a triggering spark between a third electrode and one of the main electrodes to cause breakdown of the main gap. This is perhaps the most common type of TSG; it is used in most commercial impulse generators.

A three-electrode design was chosen for the new TSG. The Marx generator rating required that the main sphere gap was adjustable for a voltage range of 10 to 90 kV. As a safety consideration, the TSG was to be placed between the capacitor bank and the test wire in the circuit, so that the wire was not live while charging the capacitor bank. Therefore, the triggering circuit needed to be powered and signalled using a system that had 90 kV of electrical isolation. For reliability of the TSG, it was desirable to maximise the 'operating region', which is the range between the minimum voltage for reliable triggering and the maximum voltage before the main gap self-triggers. The operating region was dependant on the triggering mechanism of the TSG, which relied mainly on the disturbance of the electric field caused by the triggering spark. It was crucial that the triggering spark was near the positive electrode, and that it was of positive polarity with respect to the positive electrode [Kuffel and Bera 1968]; other variations of polarity have a

decreased operating region.

Prototype Designs

A prototype TSG was built for testing of the triggering mechanism (fig. 3.11a). It had two 12.5 cm diameter hemispheres for the main electrodes and a third triggering electrode that was a length of thick steel wire with its tip located in the axis of the main gap and 8 mm from the positive electrode. The triggering spark impulse was provided by a 12 V automotive ignition coil, supplied by a 12 V lead-acid battery and switched using a 400 V, 4 A metal-oxide silicon field effect transistor (MOSFET). The transistor's gate was switched via a pneumatic hose and actuator, providing high voltage electrical isolation to the circuit. The prototype was tested by energising the main gap with a 100 kV d.c. supply. For several lengths of the main gap, the self-trigger voltage was found by raising the voltage until breakdown occurred. The voltage was then reduced slightly until the minimum reliable triggering voltage was found. The prototype's operating range was only 3 kV; too low for reliable operation. Photographs of the prototype during tests showed that the main arc often hit the third electrode well below the tip. It was thought that the steel wire electrode was too irregular, causing unreliable flash-over of the main arc.

The prototype was rebuilt and the third electrode was exchanged for a 10 mm diameter aluminium rod with a small point facing the positive electrode (fig. 3.11b). The pneumatic trigger was replaced with a fibre-optic triggering circuit. The prototype was retested, but again the operating region was 3 kV. It was concluded that locating the third electrode between the two main electrodes distorted the electric field too much before triggering, and the triggering impulse did not add significant further distortion to the electric field. It was also thought that the 12.5 cm spheres were too large for the main gap voltage. Standard spark-gap tables [Standards Australia International Limited 2005] indicated that a more appropriate sphere diameter for voltages of up to 90 kV would be about 50 mm.

The Final Design

The main electrodes were replaced with two hemispheres that were turned from 40 mm diameter brass rods (fig. 3.12a). An M12 thread was tapped in to the back of each hemisphere to attach them to M12 threaded support rods. Four M6 holes were tapped in to the back of the hemispheres for connection cables. The third electrode was placed concentric to, and flush with the surface of the positive electrode such that the triggering spark was created perpendicular to the main gap axis. This was done by inserting a length of high voltage silicon insulated cable through an 8 mm diameter hole in the positive hemisphere, and cutting the cable flush with the surface of the sphere. The spheres and supporting rods were mounted on 150 mm long vertical Nylon

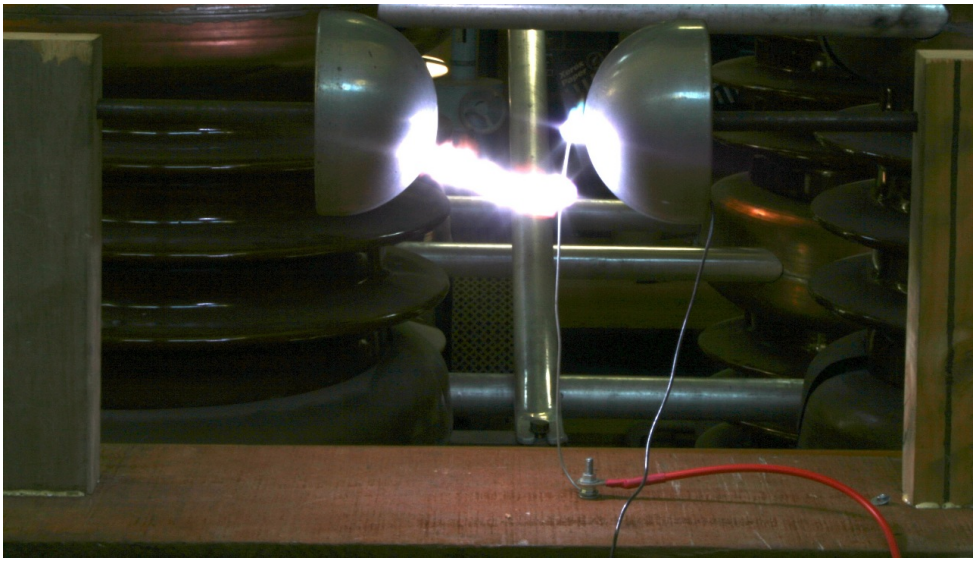

(a) The first TSG prototype during a test.

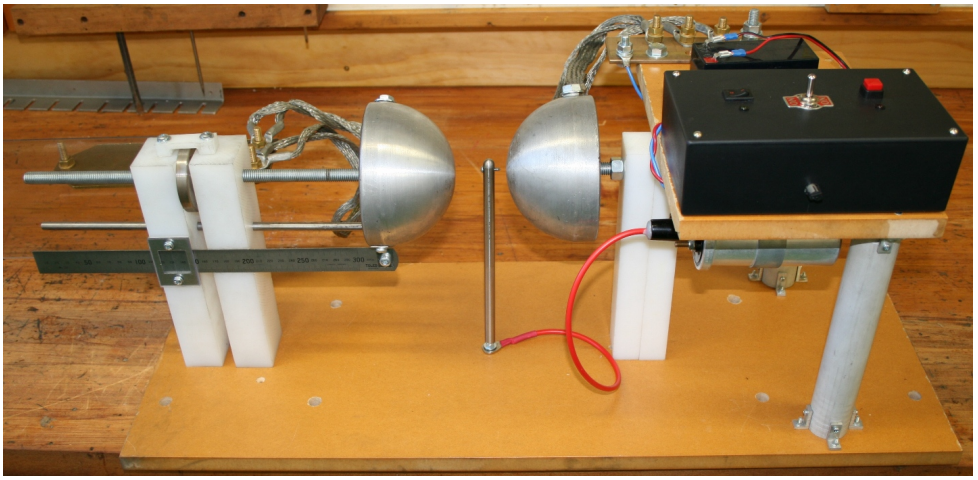

(b) The improved TSG prototype

Figure 3.11 Prototype triggered spark gaps.

insulators. The supporting rod for the negative electrode was adjusted using a large nut, and gap length indication was provided by a ruler attached to the negative electrode assembly (fig. 3.12b). Three flexible tinned-copper cables connected each hemisphere to brass plates, where connections could be made to other circuit components. The whole unit was supported by a wooden base that could be bolted to free-standing 100 kV porcelain insulators.

The triggering signal was provided by a fibre-optic connection (fig. 3.13a). The signal from the fibre-optic receiver was amplified by a bipolar junction transistor BJT, which was connected to the gate of a 400 V, 4 A MOSFET. The MOSFET switched the 12 V ignition coil supply. A 100 nF, 600 V snubbing capacitor and 400 V transient voltage suppressor (TVS) diode were connected across the MOSFET to prevent damage from the transient voltage spikes generated by the ignition coil . The circuit board, ignition coil and battery were housed in a metal enclosure

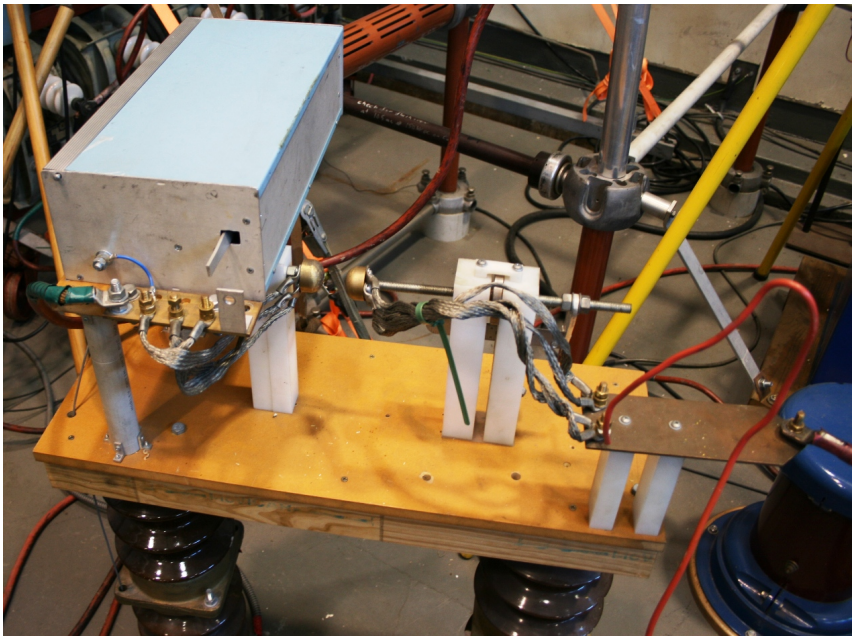

(a) The final construction of the TSG.

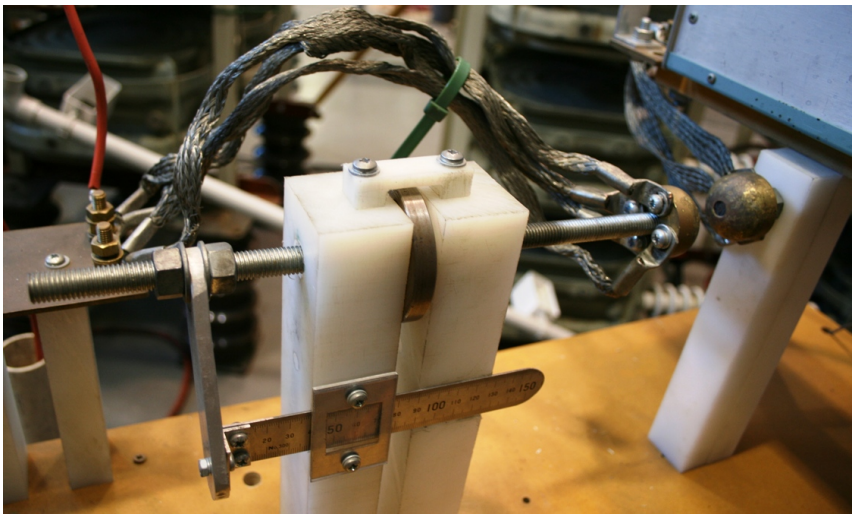

(b) Detail of the main gap, adjustment nut and gap length indicator.

Figure 3.12 Photographs of the final construction of the TSG.

and bonded to the positive electrode (fig. 3.13b).

The final design was found to have an adequate operating range of 13 kV at the lowest gap length, and up to 35 kV at longer gap lengths (fig. 3.14). The gap length was generally set to be closer to the reliable triggering voltage limit than the self-triggering voltage, because a self-trigger event was considered to be more damaging than a no-trigger event. Testing of the TSG in the EW circuit proved that triggering was reliable and that there was little surface damage to the spheres, even after high-current experiments.

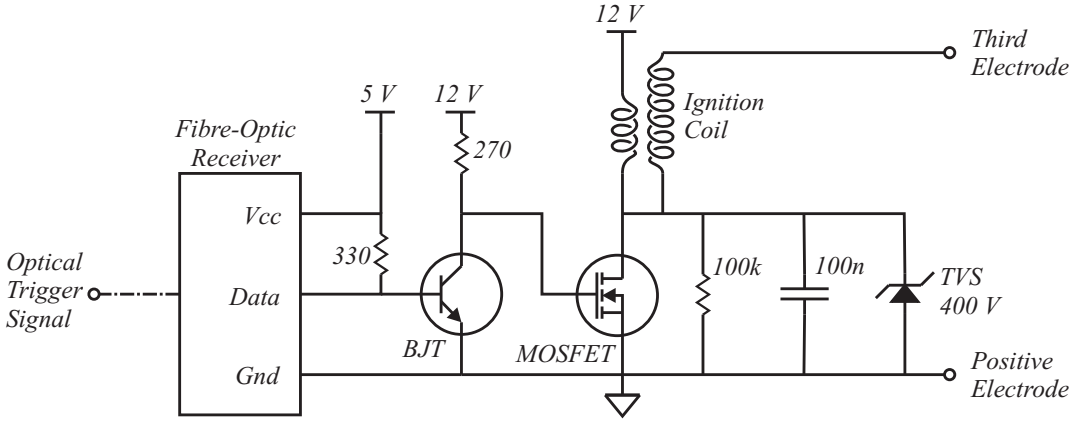

(a) The fibre-optic triggering circuit schematic.

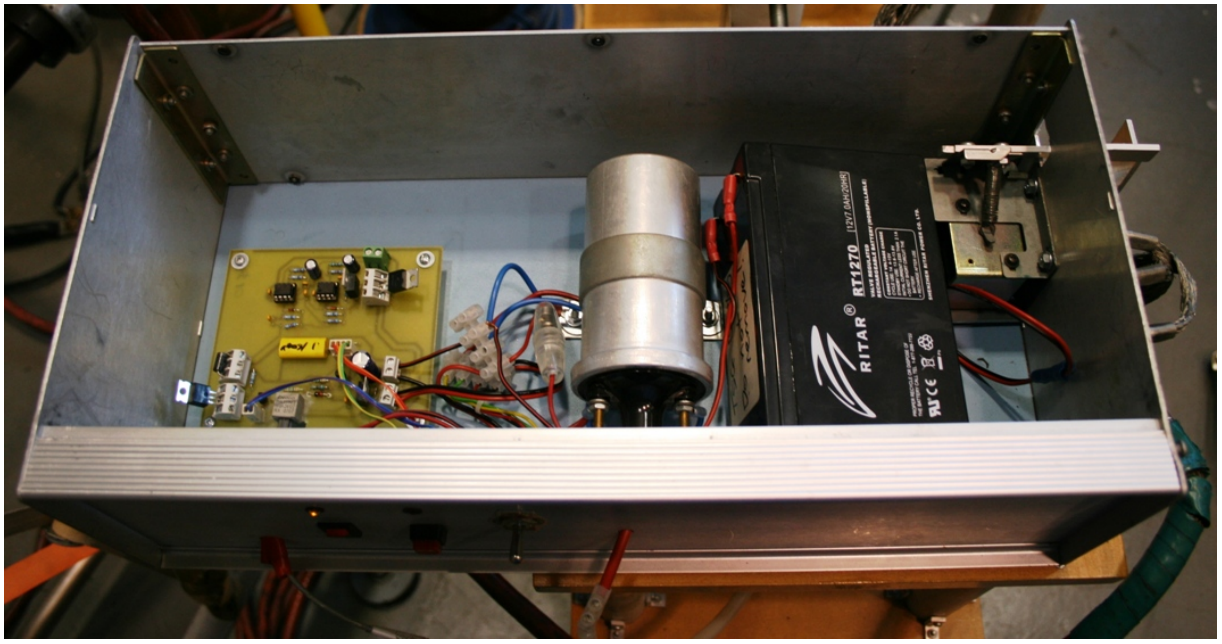

(b) The triggering electronics. From left to right: the circuit board, the ignition coil, and the battery.

Figure 3.13 The final design of the triggering circuit.

3.3.5 Spark Gap S_2, with C_{SG} and R_{SG}

Spark gap S_2 consisted of two 12.5 cm diameter hemispheres mounted on M10 threaded rods and supported by a fibreglass frame (fig. 3.15). The frame was bolted to the side of the lowest capacitor in capacitor bank C_3. The height of the top hemisphere could be adjusted to change the gap length. The gap length was adjusted to achieve a 50% impulse breakdown voltage, U_{50}, in accordance with [Standards Australia International Limited 2005]. The full range of the gap was from 20 to 110 kV. For reliable operation, S_2 was set to a U_{50} of 1.5 times the required stage charging voltage, a value that is approximately halfway between the stage charging voltage and the transient over-voltage, which itself was approximately twice the full-charge voltage.

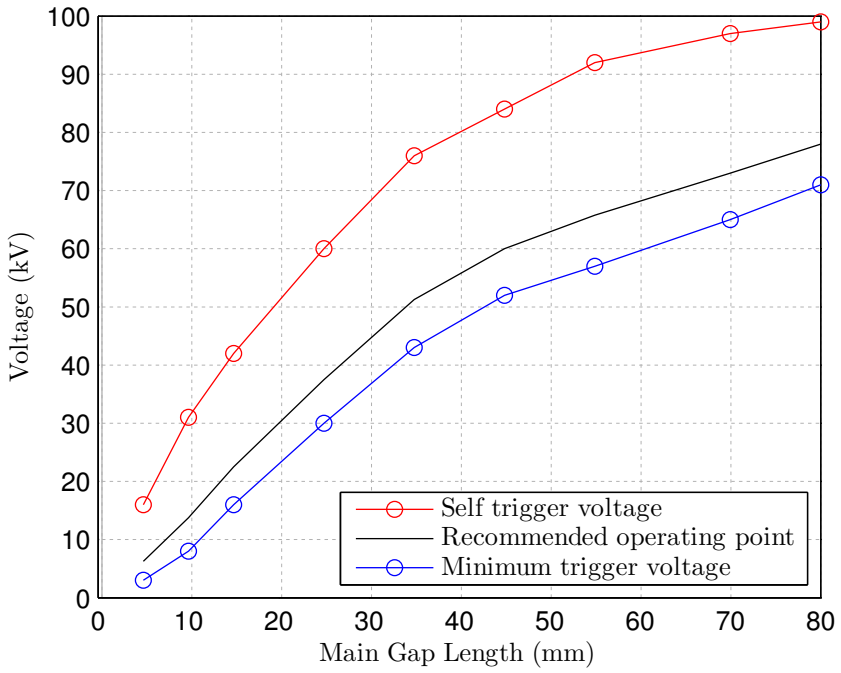

Figure 3.14 The operating region for the final TSG design.

Figure 3.15 Spark gap S_2. The top hemisphere was connected to C_2 and the bottom hemisphere was connected to C_3. An adjustment scale with a green pointer can be seen to the right of the top hemisphere.

Figure 3.16 Spark gap S_3. The bottom sphere height adjustment mechanism can be seen under the yellow pipe section. The ionising resistor $R_{I,2}$ can be seen on the right of the structure.

The capacitor C_{SG}, which was 65 nF and rated to 200 kV, was used to aid the breakdown of S_2 by enhancing the transient over-voltage across the gap. Between experiments, the capacitors were earthed for safety by temporary earth sticks. The resistor R_{SG} was included to limit the peak charging current of C_{SG} and prevent significant earth potential rise. R_{SG} was a 1.35 kΩ wire-wound resistor, limiting the peak charging current to 130 A at the maximum impulse voltage of 180 kV.

3.3.6 Spark Gap S_3

S_3 had two 25 cm spheres supported by a frame of PVC pipes (fig. 3.16). Both spheres were insulated from earth to a voltage of 270 kV. The gap length was adjustable to have a U_{50} voltage from 20 to 300 kV, and was set by adjusting the height of the bottom sphere. For reliable operation, S_3 was set to have a U_{50} of approximately two-thirds of the Marx generator output voltage.

Resistor	a	b	c	d	e	f	Maximum
R_1	0.83	3.9	3.6	35	10.2	11	35
R_2	0.83	6.2	4	32	10	20	32
R_3	0.21	2.7	2.3	5.9	22	25	25
R_4	0.21	2.4	2.2	5.9	37	6.5	37
$R_{I,2}$	0	59	57	0	0	16	59

[a] Charging to full voltage.
[b] Self-trigger while charging. Supply isolated after 3 s.
[c] Normal trigger with no EW load.
[d] S_1 self-triggers, S_2 and S_3 do not trigger.
[e] S_2 self-triggers, S_1 and S_3 do not trigger.
[f] S_3 self-triggers, S_1 and S_2 do not trigger.

Table 3.1 Simulated resistor energy absorption during contingencies (values in kJ).

3.3.7 Charging Resistors, R_1 to R_4

The resistance of the charging resistors R_1 to R_4 was designed to be low enough such that all capacitor stages reached an equal voltage within a few seconds, yet high enough to prevent significant discharge during the experiment. A transient simulation showed that a resistance of 30 kΩ produced a time constant of 1 s and a voltage drop after the first millisecond of less than 1%. Significant energy was absorbed by the resistors when the capacitors were not fully discharged during an experiment, so water was used as the resistive element due to its high thermal capacity. Water-filled resistors are easy and inexpensive to build using off-the-shelf PVC drainage pipe and fittings. Although the resistivity of tap water is variable, an approximate resistivity was measured by applying 40 kV d.c. to a 21 mm diameter, 650 mm long water column and measuring the current. The current was approximately 1 A, resulting in a resistance of 40 kΩ, and therefore a resistivity of 21 Ωm.

The volume of water in each resistor was calculated to ensure an acceptably low temperature rise. First, it was necessary to find the total energy that would be dissipated into each resistor. Several scenarios were simulated using a transient circuit simulator (Table 3.1). From these results, R_1 to R_4 were designed to be 1 m long and 32 mm in diameter, containing 1.2 L of water and resulting in a resistance of approximately 26 kΩ. The temperature rise was calculated to be 7°C using a maximum energy dissipation of 37 kJ and a specific heat capacity of 4.18 J/g/K.

3.3.8 Ionising Resistors, $R_{I,1}$ and $R_{I,2}$

Using the 60 kV capacitor bank, some experiments were observed to produce erratic voltage waveforms when the current through the EW was very low, for example during the dwell time. It was presumed that when the current was low, de-ionisation of the TSG occurred. The solution

Figure 3.17 The shunt-connected water resistor.

was to connect a resistor, $R_{I,1}$, from the output of the TSG to earth, such that current would flow through the spark gap continuously. A water-filled resistor design was used, consisting of a 21 mm diameter, 650 mm long PVC pipe, filled with tap water (fig. 3.17). A similar resistor, $R_{I,2}$, was built for use with the Marx generator to maintain ionisation in S_3. $R_{I,2}$ was 2.1 m long and 32 mm in diameter, containing 1.9 L of water and resulting in a resistance of approximately 50 kΩ. The temperature rise was calculated to be 7°C using a maximum energy dissipation of 59 kJ (Table 3.1). The pipe was supported by the structure of S_3 (fig. 3.16).

3.3.9 Charging Circuit Components

The high voltage components of the charging circuit are shown in Figure 3.18.

Charging Transformer, Tx

The charging transformer, Tx, was a 230 V to 80 kV, 8 kVA, step-up transformer. The charging transformer was earthed between experiments by applying a wooden earth stick, identical to the earth sticks used on the 60 kV capacitor bank, to the high voltage terminal.

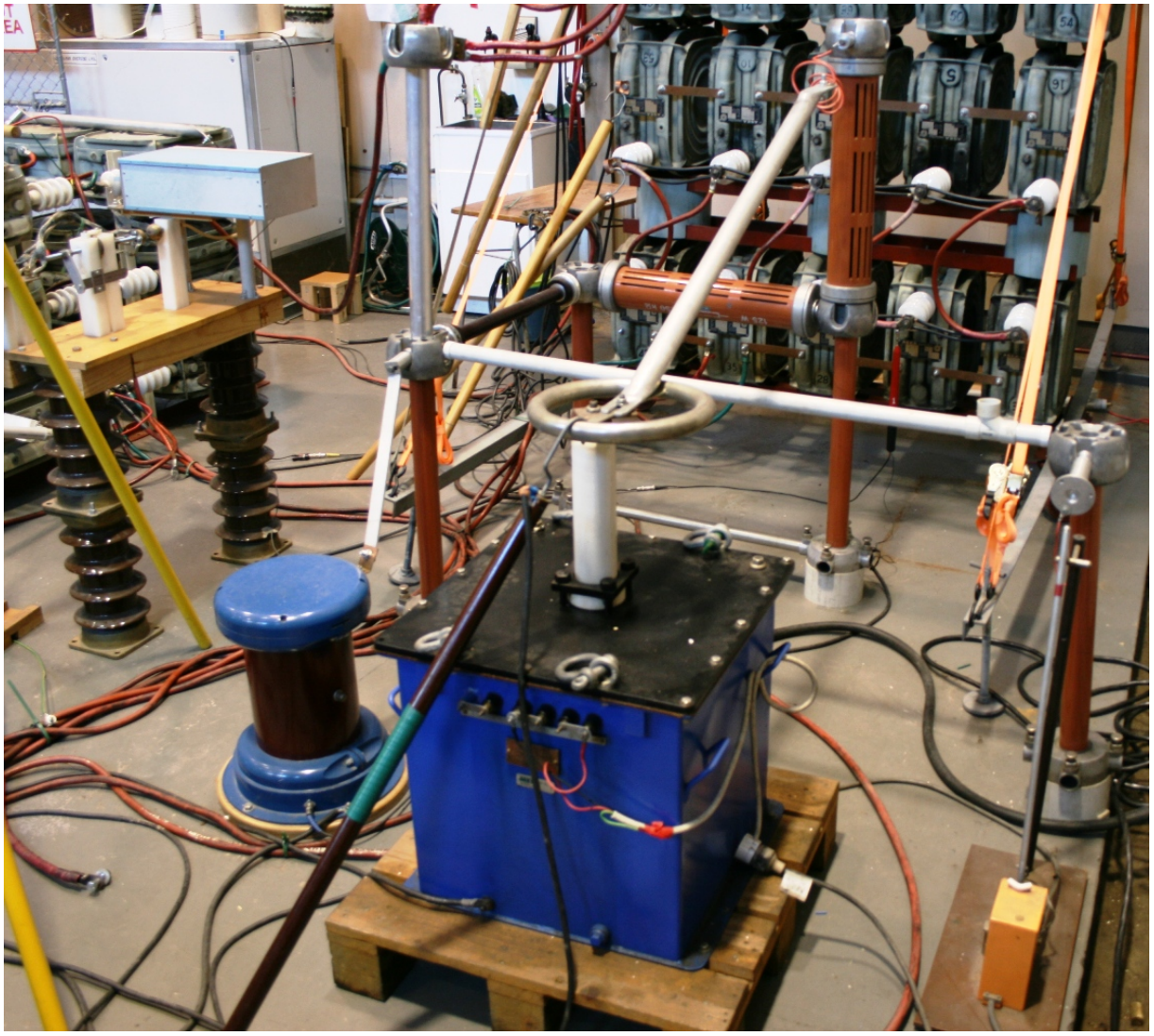

(a) Photograph.

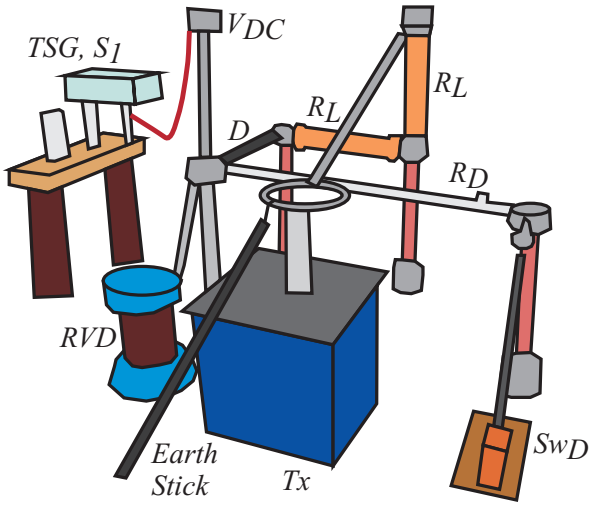

(b) Key to the photograph.

Figure 3.18 A photograph of the high voltage components of the charging circuit.

Rectifying Diode, D

The rectifying diode has been custom built out of 60 BYV90G high voltage diodes. Each diode is rated for a crest working reverse voltage of 6 kV and a continuous current of 1 A. The diode experiences a maximum reverse voltage of 200 kV when the capacitor bank is fully charged to 90 kV and the a.c. supply voltage is at a negative peak of 110 kV.

Current Limiting Resistor, R_L

The resistor R_L was comprised of two wire-wound, 50 kΩ, 125 W resistors in series. This limited the worst-case fault current through the diode to 1.1 A, which would have occurred during a short-circuit to earth on the output of the charging circuit at 110 kV.

Discharge Switch, SW_D

The discharge switch was an electromagnet-operated disconnector, rated to 100 kV when it was in the open position. The electromagnet required a 230 V a.c. supply to remain in the open position, and fell back into the closed position under gravity when the supply was removed.

Discharge Resistor, R_D

The resistor R_D was used to discharge the capacitor energy before applying temporary earth connections. R_D was a water-filled resistor, 36 mm in diameter and 1.5 m long. This gave a total water volume of 1.5 L, which could absorb the fully-charged Marx generator energy of 69 kJ with a temperature rise of 11 K.

3.4 CONTROL

3.4.1 Charging Meters

A 100 kV resistive voltage divider (RVD) was used to measure the total voltage on the 60 kV capacitor bank or the first stage of the Marx generator. Intermediate capacitor bank voltages were measured to ensure that the series-connected capacitors were charging evenly. A deviation of more than 10% of the expected value would be cause for concern that a capacitor had developed a fault. Fluke 80k-40 resistive voltage divider probes, rated to 40 kV peak, were used to measure the lowest capacitor row of the 60 kV capacitor bank, and across one-third of each Marx generator stage. Because the probes measuring the 60 kV capacitor bank and stage one of the Marx

Figure 3.19 The voltmeters and the ammeter, arranged on a table for viewing using the video camera and television screen.

generator were referenced to earth, they were connected to voltmeters using coaxial cables. The probes on stages two and three of the Marx generator had no earth reference, and so were connected to Fluke voltmeters that had radio-frequency, remotely updated displays. The non-remote voltmeters were viewed through a video camera, with a television screen in the Faraday cage, to provide electrical isolation from earth potential rise while still allowing the voltmeters to be read easily (fig. 3.19). A 20 A d.c. ammeter, I_C, was used to measure the charging current on the neutral connection to the step-up transformer, Tx, and was also viewed through the video system.

3.4.2 VariAC and Isolating Switches

The VariAC was a 230 V, 10 A variable transformer. It was positioned outside of the Faraday cage to avoid transferring earth potential rise into the cage. The control wheel that selects the voltage was operated using a pulley system with a rubber belt so that the operator did not need to touch the VariAC. The VariAC had a 10 A fuse, which protected the low voltage circuit and operated during a fault or self-trigger on the high voltage circuit. The low voltage isolating switch SW_1 was a domestic ceiling-mounted light switch, which was operated with a nylon pull-cord, again to avoid transferring earth potential rise the cage. The isolating switch for the SW_D electromagnet supply was also a pull-cord switch.

3.4.3 Triggering Control Unit

A digital electronic control unit was built to trigger the TSG and photographic camera (fig. 3.20b). It had an 8-bit microprocessor with flash memory, two LCD displays, five input buttons, a fibre-optic signal output and two electrical signal outputs (fig. 3.20a). It could be powered by an

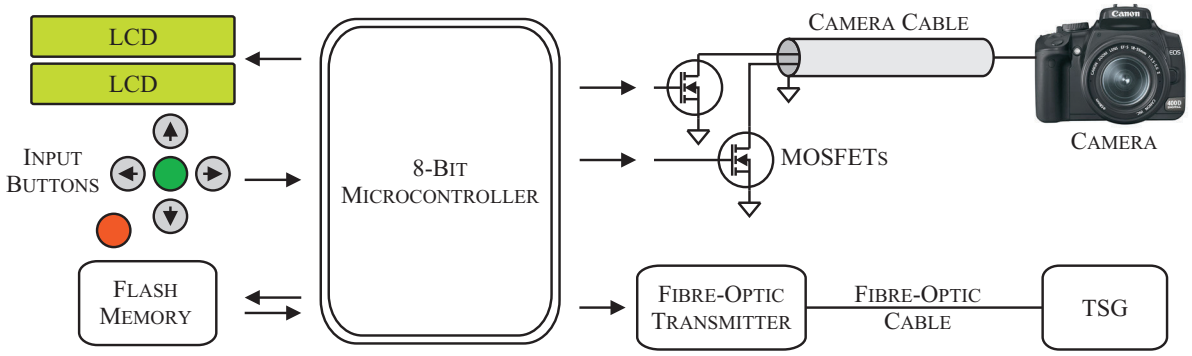

(a) A functional diagram.

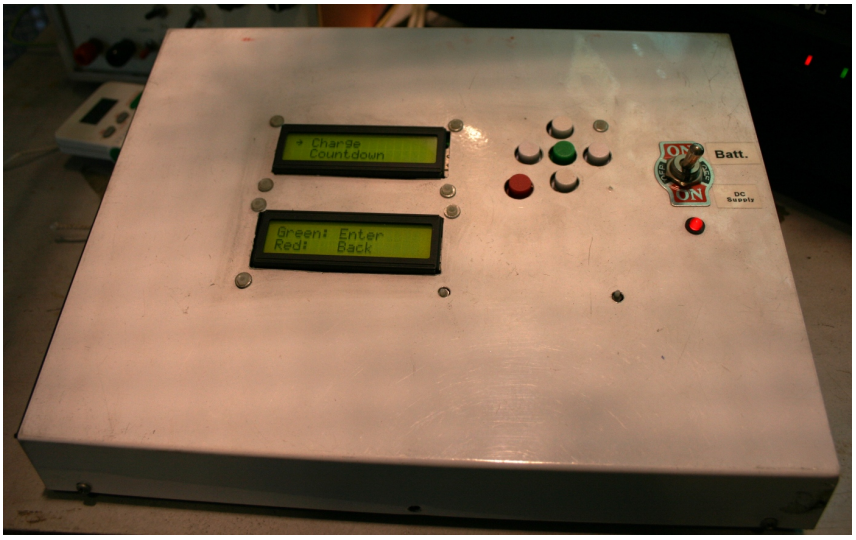

(b) A photograph.

Figure 3.20 The control unit used for triggering the TSG and the camera.

external 9 V d.c. supply or an internal 9 V battery. The buttons were used to traverse menus and to input signal delay values. The unit was programmable to set delay times between the triggering signals with a resolution of about 10 μs. The fibre-optic output was connected to the TSG. When the TSG signal was set high, the MOSFET in the TSG switched on, causing current to flow through the ignition coil. Then, when the TSG signal was set low, the MOSFET switched off, causing the triggering spark to appear. The electrical outputs connected to the camera were a 'camera ready' signal that allowed the camera to complete auto-focus and light metering, and another signal for the camera to operate the shutter. The camera outputs used MOSFETs to mimic a remote-controller switch for the camera.

When the menu option to trigger the experiment was selected, the unit began a three-second countdown (fig. 3.21). One second before the experiment commenced, the camera-ready and TSG signals were set high. At time zero, the unit began timing and set the camera-shutter signal high and the TSG signal low after the specified delays. At one second after the experiment, all output signals were set low. The countdown could only be cancelled before the TSG signal was

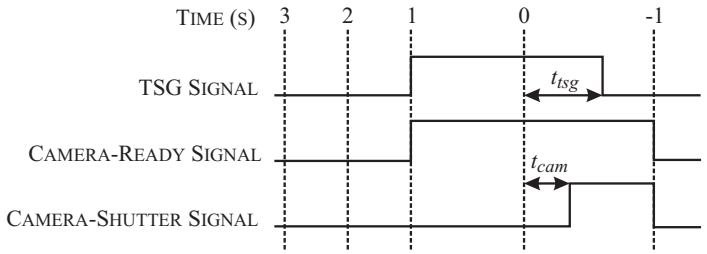

Figure 3.21 The controller for triggering the TSG and the camera.

set high, because after that, there was no way to switch off the MOSFET in the TSG without creating a triggering spark.

3.4.4 Faraday Cage

The experiments were operated and observed from a Faraday cage, which is a type of room used to create an equipotential zone around its occupants (figs. 3.22 and 3.22). The cage was approximately 2 m on all dimensions, made from a tight mesh of thick steel wire and solidly bonded to the laboratory earth grid. The cage was covered with a layer of 5 mm thick polycarbonate to protect the occupants from explosion fragments. The cage housed the controls for the charging circuit, the triggering control unit, and the television screen that was used to view the voltmeters. A welding screen was hung over one wall to allow researchers to observe the experiments without subjecting themselves to uncomfortably bright flashes of light.

3.5 INSTRUMENTATION

3.5.1 Transient Voltage Measurement, CVD

Voltage measurement was provided by a Ferranti 600 kV capacitive voltage divider (CVD). The top capacitor of the CVD was 200 pF and the bottom capacitor was 2 μF, giving a divider ratio of 10,000:1. A 2 kΩ wire-wound resistor was connected in series to the CVD to damp transient oscillations and prevent potential rise of the CVD's neutral connection. The resistor, in combination with the capacitance of the CVD, gave a time constant of 400 ns, which was fast enough for EW experiments. The resistor was then connected to the h.v. end of the EW using a 1 m long low-inductance copper ribbon cable and to the neutral connection plate using a 20 cm long ribbon cable. Since the CVD was a high voltage capacitor, a temporary earth was connected between experiments.

Figure 3.22 The Faraday cage, covered with 5 mm thick polycarbonate. A green welding screen covers one wall. The VariAC can be seen on the top of the cage, and the video camera for viewing the charging instrumentation is seen on the side.

3.5.2 Transient Current Measurement, CT

The transient current through the EW was measured using a Pearson 301X, which was a 50 kA rated, 200 ns usable rise-time, ferrite-cored current transformer (CT). The CT was placed on the neutral connection of the EW return cable and the signal cable was connected to the oscilloscope through a 20 dB in-line coaxial attenuator.

3.5.3 Oscilloscope

Voltage, current and emitted light intensity waveforms were recorded using a Tektronics TDS 2022B, 200 MHz oscilloscope. The oscilloscope was powered by a 230 V, sine-wave inverter and a 12 V lead-acid battery to eliminate an earth loop between the oscilloscope's power supply

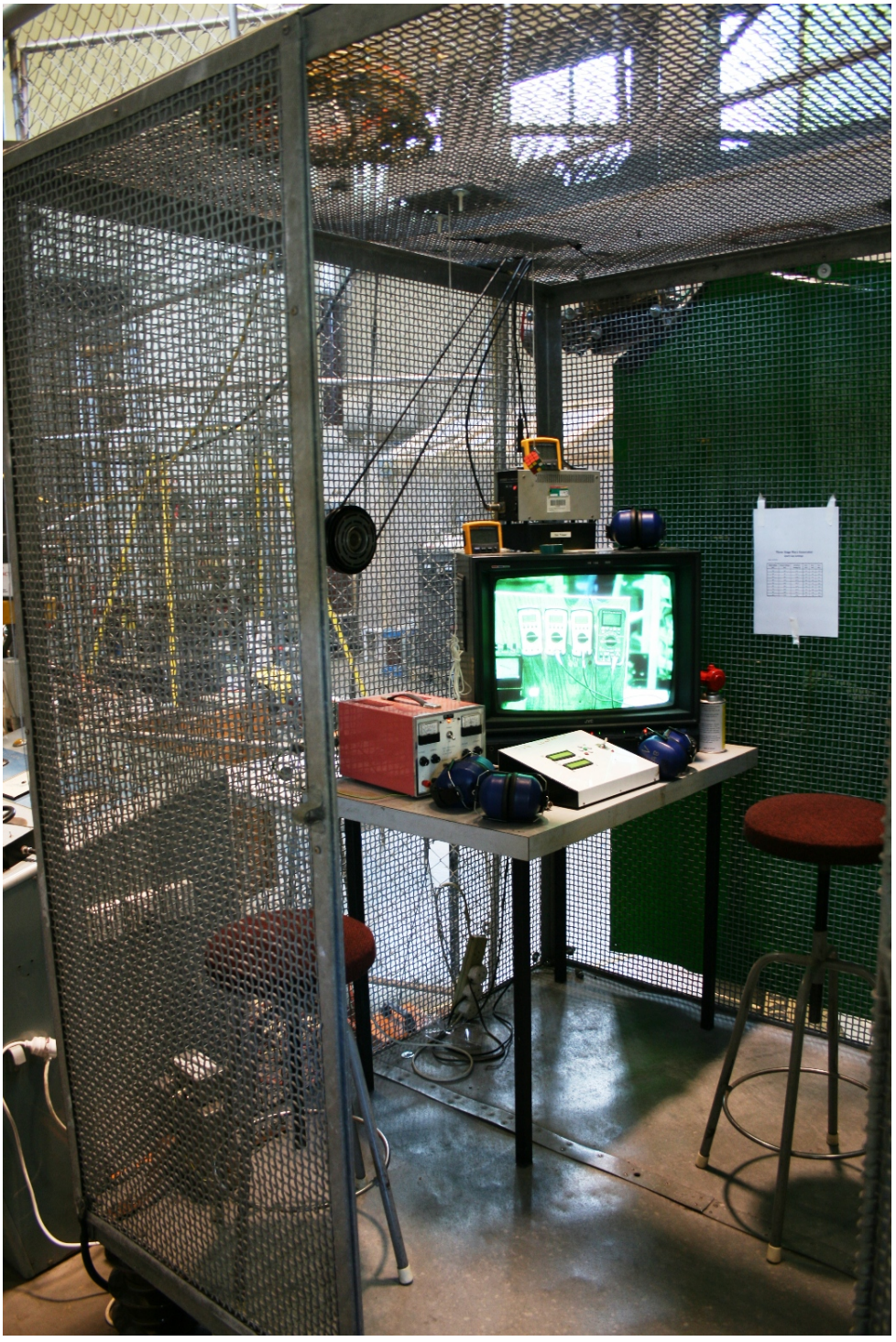

Figure 3.23 The inside of the Faraday cage. The television screen displays the video camera image of the charging instruments. The white box on the table is the TSG controller. Two yellow Fluke multimeter remote displays are on top of the television screen. The rubber belt-driven VariAC control wheel can be seen on the front wall of the cage.

and the CVD's neutral connection. An isolating transformer is insufficient for this purpose; the inter-winding capacitance is a low impedance path for the high frequency currents, produced by fast EW impulses. The oscilloscope and power supply were housed in a metal enclosure to shield them from the rapidly changing electric fields in the high voltage circuit.

3.5.4 Photography

The photographs presented in this thesis were taken using a Canon 400d digital single lens reflex camera, mounted on a tripod. Most photographs of experiments were taken using a long-exposure technique, whereby the camera's shutter was opened about one second before the experiment and closed about one second after the experiment, such that all emitted light was captured. Precise timing was not necessary, making this method reliable. Photographs of the restrike channel required extensive light attenuation, which was achieved using f-stop values of F22 to F36 and up to three neutral density 'ND8' darkening filters. Photographs of plasma beads required only one ND8 filter and an f-stop of F22.

Streak photographs were taken using a short-exposure technique, whereby the shutter time was set to 1/2500 s and the camera shutter was precisely timed to open simultaneously with the start of the experiment. Then, the wiping motion of the slit between the camera's two mechanical shutter curtains gradually moves along the wire as the experiment progresses. The precise timing depended on the delay of the camera's shutter, which was found through trial-and-error to be approximately 10.1 ms.

3.5.5 High Speed Camera

A MegaSpeed CPL MS 50K camera was used for high speed filming. The camera was capable of grey-scale 1264 x 48 pixel resolution at 10,240 frames per second. The camera was controlled by computer software, and so the camera's power supply and the computer's power supply were supplied by two separate battery and inverter systems to prevent creating an earth loop. The camera recorded continuously through a looping buffer, and was manually stopped immediately after the experiment finished.

3.5.6 Emitted Light Intensity Sensor

Time-varying measurement of the intensity of light emitted from the EW was provided using a high speed silicon photodiode. The photodiode was terminated with a 25 Ω load and connected to the oscilloscope using a 4 cm length of coaxial cable. The photodiode was placed facing the EW and at a distance of approximately 2 m. The data-sheet specifications stated that

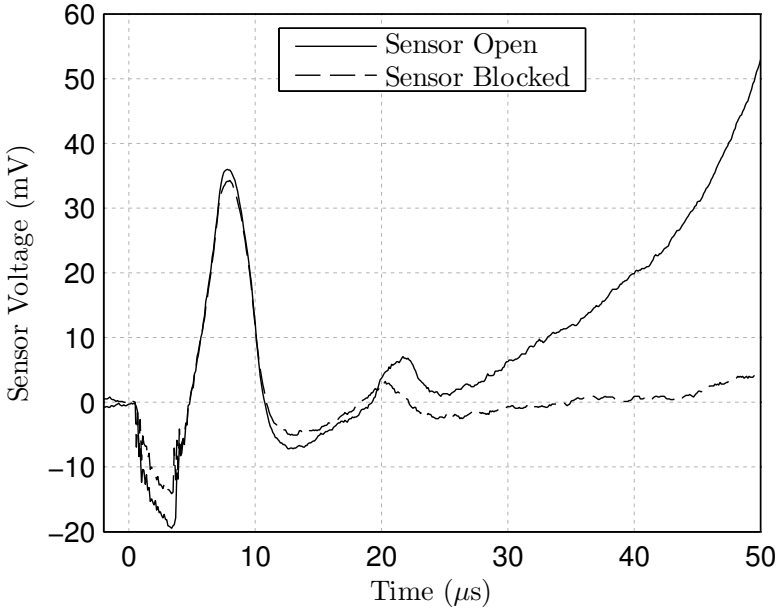

Figure 3.24 Two identical EW experiments, one with the photodiode open to the EW light and one with it blocked.

the photodiode had a 41 mm^2 sensitive area, a wavelength of maximum sensitivity of 800 nm, a peak responsiveness of 0.5 A/W and a response time of less than 40 ns. The open-circuit voltage versus irradiation characteristic chart in the data-sheet did not include the range of light intensity that the photodiode was subject to during EW experiments, so a high level of saturation was expected, which created a very non-linear output. The light intensity data should therefore be considered indicative of the relative intensity.

The light intensity waveforms included interference due to magnetic induction, mostly during the first 30 μs of the experiment, where the rate of change of current in the EW was the fastest. Two identical EW experiments were performed: one with the photodiode open to the EW light and one with the photodiode blocked from the EW light. The waveforms showed a very similar signal during the first 30 μs, showing that this component of the signal was induced noise rather than emitted light. This induced noise must be taken into account when interpreting the light intensity waveforms that are presented later in this thesis.

3.6 SAFETY

Safety was a major consideration throughout the experimental work conducted during this research. The safety of the operators and observers was the primary concern, followed by protection of the equipment and high voltage laboratory building. There were no guidelines for the operation of a high voltage laboratory in New Zealand. Instead, the electricity supply industry's best practices were applied where possible.

Implementing safety procedures and safe design of equipment begins with identifying the hazards. Hazards can then be isolated, minimised or eliminated. Isolation of a hazard implies that the dangerous mechanism still exists, but personnel are protected from it by using either physical barriers or procedures that prevent inadvertent contact with the hazard. Minimisation of a hazard implies that there is still a risk to personnel, but all practical steps have been taken to reduce the exposure and/or consequences of the hazard to an acceptable level. Eliminating a hazard is to remove the mechanism for danger completely, which although is the most effective mitigation of a hazard, is usually not possible in the high voltage laboratory environment. The following subsections detail each of the hazards that were identified during this research and the steps taken to mitigate them.

3.6.1 High Voltage

High voltages can cause current to be driven through a person, potentially causing burns and triggering fibrillation of the heart, either of which can be fatal. High voltages can also drive current through the air, causing the electricity to jump a considerable distance to a body that was not even in contact with the high voltage electrode.

Minimum Approach Distance

The a.c. high voltage hazard was isolated by applying an industry best practice minimum approach distance (MAD), which defines the minimum distance from a high voltage conductor that a competent person can be work (Table 3.2). The distances apply to 'competent persons', who must be able to demonstrate the necessary skills knowledge required to safely carry out work in the vicinity of live conductors. The MAD was also applied to cables that returned to the operators, such as the camera shutter triggering cable.

Supply Isolation

The high voltage hazard was isolated by physical disconnection of the low voltage supply to the charging transformer before operators approached the high voltage equipment. This did not isolate the high voltage stored in the capacitors; it only isolated the charging circuit and prevented inadvertent re-livening of the circuit.

Application of Temporary Earth Connections

The last line of defence against the high voltage hazard was to apply temporary earth connections before equipment was considered safe to touch. The location of temporary earth connections

Voltage	MAD (m)
±350 kV d.c.	2.8
±270 kV d.c.	2.3
±135 kV d.c.	2.2
220 kV a.c.	2.2
110 kV a.c.	1.5
66 kV a.c.	1.0
50 kV a.c.	0.75
33 kV a.c.	0.60
22 kV a.c.	0.45
11 kV a.c.	0.30
6.6 kV a.c.	0.25
1.0 kV a.c.	0.15

Table 3.2 The minimum approach distances for competent employees approaching exposed live equipment, as defined in [New Zealand Electrical Code of Practice for Electrical Safe Distances 2001].

and the order in which they were applied was carefully considered to ensure that all parts of the circuit were earthed and that the temporary earths could be applied while maintaining the MAD. The temporary earth connections were applied using wooden earth sticks that had been tested to withstand 100 kV a.c. The resistance between every temporary earth and the laboratory's earth grid was tested weekly to be less than 0.5 Ω using a 20 A continuity tester. This was to ensure that, for example, the cable had not been broken or disconnected.

3.6.2 Stored Energy

High voltage circuits that contain capacitors pose an additional major hazard: capacitors can store electrical energy at lethal voltages virtually indefinitely, and they can accumulate charge without physical connections through stray capacitances to live h.v. sources. Consequently, even after the electrical supply has been isolated, the circuit is still dangerous. Furthermore, stored electrical energy can be discharged explosively, and so must be dissipated in a safe manner. To mitigate the hazard of stored electrical energy, a water-filled resistor was applied to the capacitor banks to dissipate the stored energy. Then, temporary earth connections were applied such that both terminals of each capacitor were earthed.

3.6.3 Earth Potential Rise

When subjected to impulse currents, even a low impedance earth can develop a lethal voltage, or earth potential rise (EPR). For example, a 10 kA peak current impulse flowing through a 100 mΩ earth connection will produce a voltage of 1 kV. Impulse currents during faults can be several times larger, and the characteristic high frequencies present in an impulse can cause the

reactance of a short cable to be several Ohms or more. EPR can affect measurements, damage equipment and cause dangerous touch and step potentials to appear around the laboratory.

EPR was minimised by careful design of the earthing system. A clear distinction was made between neutral and earth connections. Neutral connections carried the normal operating current of the circuit, so it was acceptable that they experienced some EPR and they were designed accordingly. Earth connections were provided for safety of personnel and equipment and did not carry current in normal operation. They were rated to carry a fault current without significant earth potential rise (EPR) or damage to the conductors or joints. The neutral cables, which lay on the concrete floor of the laboratory, were routed according to Figure 3.25. They did not touch or cross earth, instrument, or low voltage supply cables, so that the EPR on the neutral cables could not be transferred.

An example of EPR that occurred during this research occurred when capacitor C_{SG} was installed without the current limiting resistor R_{SG}. During the transient condition created when S_2 broke down, C_{SG} charged from 0 to 180 kV almost instantaneously, causing a very large flow of current. An incident eventually occurred during an experiment where there was a flash-over from the neutral of C_{SG} to the laboratory earth grid, blasting a 150 mm diameter hole into the concrete. An investigation revealed that the peak EPR on the neutral of C_{SG} was about 100 kV. It transpired that the EPR had been occurring for many previous experiments, and had damaged coaxial instrumentation cables throughout the circuit and even been responsible for some damage to the oscilloscope's inverter. The problem was fixed by installing R_{SG} and choosing a larger conductor size for the neutral of C_{SG}.

The operators were protected from EPR by residing in the Faraday cage during the experiments. The cage had conductive walls, floor and ceiling to create an equipotential zone, eliminating hazardous touch and step potentials. Cables from the experiment area were not brought into the cage, and the charging circuit isolating switch Sw_1, the R_D electromagnet supply switch, and the $VariAC$ were operated remotely using insulated controls.

3.6.4 Earth Loops

Care was taken in the design of the earthing system to avoid earth loops. Earth loops are formed when earth connections, which may be made through a chassis, instrument cable, or by metal parts unintentionally contacting, form a complete circuit. Then, rapidly changing magnetic flux, generated by the experiment current, passes through the loop area and creates a large circulating current that may damage equipment. Earth loops were avoided by applying a single-point earthing policy, so that there was only one path to earth from any point in the circuit. For example, the oscilloscope was run from an isolated battery and inverter power supply because the voltage measurement channel needed a reference to the CVD neutral, which

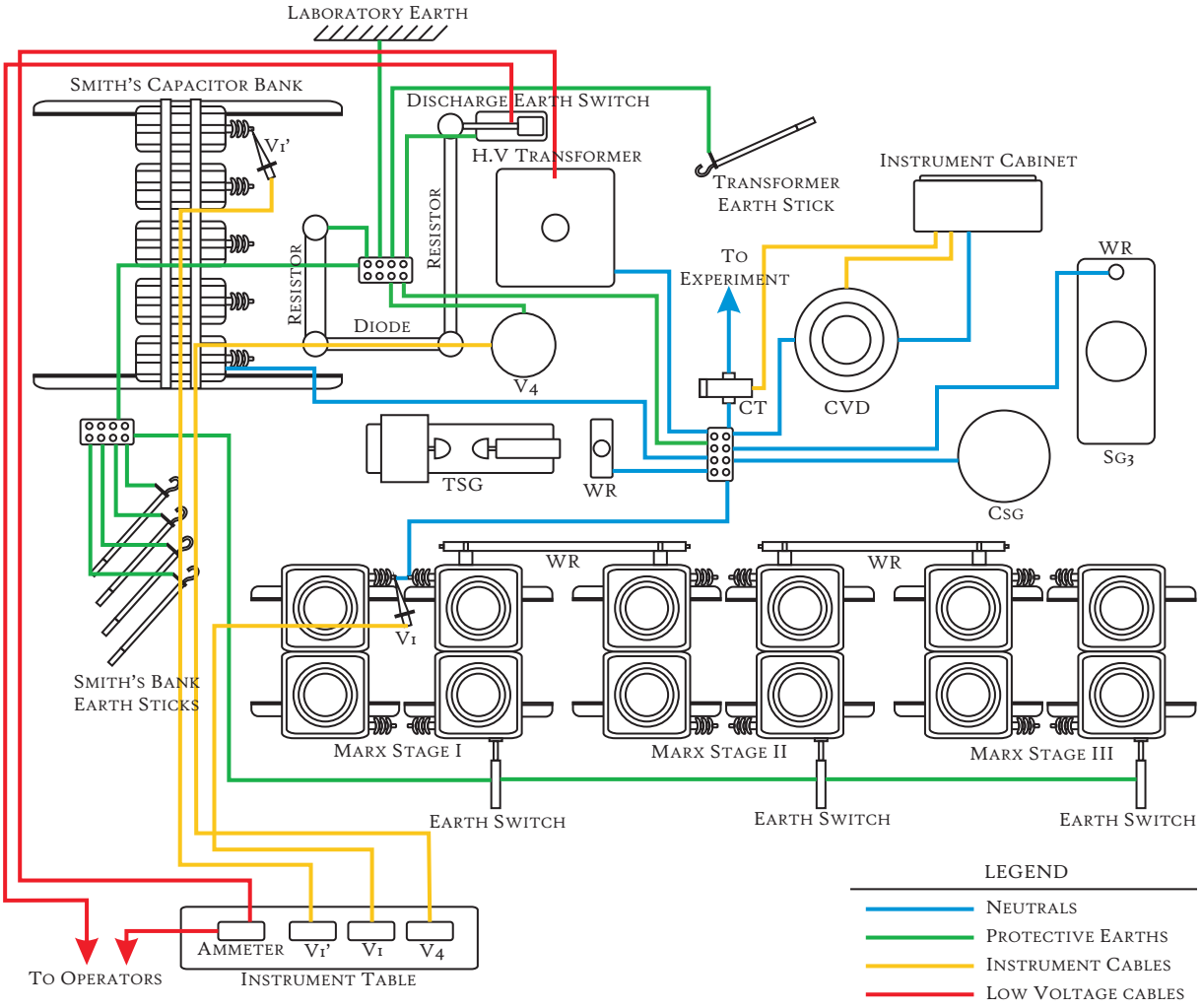

Figure 3.25 The layout of the cables for the equipment used in this research. The neutral cables, which experience potential rise during experiments, did not come into contact with the protective earth conductors, instrument cables or low voltage cables. Two exceptions were the instrument cable for the CVD, which was bonded to the neutral circuit to give the CVD a reference voltage, and the instrument cable for the CT, also bonded to the neutral circuit to prevent damage to the oscilloscope.

was itself earthed. An earth reference on the oscilloscope's power supply would have otherwise formed an earth loop.

3.6.5 Explosion

The fully-charged Marx generator could store up to 69 kJ of energy. While the total energy was relatively small (about a fifth of the energy that it takes to boil a litre of water from room temperature), it could be released almost instantaneously, with a peak power dissipation of 1 GW or more. Such a discharge could explosively damage equipment and create a shower of high velocity fragments of metal, porcelain or concrete. EWs and unintended explosions can also be extremely loud, and may damage hearing.

The explosion hazard was minimised by requiring that all personnel were inside the Faraday cage, which had a polycarbonate covering, from when the capacitors were charged to when they were discharged. All personnel were also required to wear personal protective equipment (PPE), including earmuffs, safety glasses and clothing that covered their arms and legs. When experiments were performed outside the laboratory, all observers were required to maintain a distance from the experiment that was deemed safely away from the reach of explosion fragments.

3.6.6 Fire

The capacitors and the charging transformer are filled with insulating oil. Oil fires can burn extremely hot and are very difficult to extinguish. A situation where an oil fire could occur begins when there is an arcing fault inside a capacitor. Gas is produced in the oil, which pressurises the capacitor's enclosure and can cause it to burst open, spilling the oil. Further arcing can then ignite the gas and oil. This hazard was minimised by positioning the operators as far from the capacitors as possible and near a fire escape. Carbon dioxide and dry-powder fire extinguishers were available so that the operators could fight the fire while they were comfortable to do so and could still maintain the MAD. The laboratory has a fire alarm system that has a direct connection to the local emergency fire service.

3.6.7 Hazard Identification Forms

A Hazard Identification (HID) form was filled out prior to commencing experiments each day. Completing the HID form helped to remind operators of the existing hazards and stimulated thoughts on any additional hazards. The HID form also provided useful reminders, such as the regular checking of temporary earth connections, ensuring that the discharge water resistor was filled, and securing the second laboratory entrance, which could have provided access for an unsuspecting person directly into the live equipment area. An example HID form is presented in Table 3.3.

3.7 OPERATING PROCEDURES

A set of operating procedures were carefully designed and discussed with all operators before any work began. The operating procedures became more important when repetitious experiments were performed, where there was a risk of complacency and increased probability of human error. In such circumstances, it was useful to instigate extra procedures, such as counting the number of temporary earth connections as they were applied and removed, employing a safety observer, and taking regular breaks.

Hazard	I/M/E	Controls
High voltage - up to 270 kV impulse	I	Remain in the Faraday cage while triggering is possible, generating the full impulse voltage.
High voltage - up to 90 kV d.c.	I	Use a MAD of 1.5 m. Isolate the charging transformer and apply temporary earth sticks before entering the MAD.
Stored energy	I	Apply R_D to discharge the energy before applying the temporary earth connections. Ensure that the resistor is full of water.
Earth potential rise	M	All personnel must be in the Faraday cage when the isolations and earths are removed.
Explosion	M	All personnel must wear PPE.
Fire	M	Sound the alarm. Fight using the fire extinguishers if comfortable (maintain MAD). If not, evacuate.
Continuity of temporary earth connections	M	Inspect and test all protective earth connections weekly. The resistance of each earth to the local earth grid must be less than 0.5 Ω when tested with a 20 A earth tester.
Other Laboratory Users	E	Secure all laboratory entrances.

Table 3.3 A example of the content in a HID form, used for an EW experiment session. Hazards were either (I)solated, (M)inimised or (E)liminated using the controls.

The following is an example of the operating procedure used when performing an EW experiment.

(1) Complete the Hazard Identification form.

(2) Configure the circuit for the 60 kV capacitor bank or Marx generator.

(3) Prepare the experiment by measuring out the appropriate length of wire and connecting it to the terminals.

(4) Set the gap lengths of the spark gaps.

(5) Turn on the TSG, voltmeters, oscilloscope, camera and power supply to the Faraday cage equipment.

(6) Remove all of the temporary earth sticks and levers.

(7) Remove the isolation of the charging circuit and enter the Faraday cage.

(8) Open the discharge switch, Sw_D, and close the VariAC switch, Sw_1.

(9) Slowly turn the VariAC control, maintaining a charging current I_C of about 10 A and ensuring that the capacitor banks are charging evenly by comparing the voltmeters.

(10) When the desired voltage has been reached, open Sw_1 and turn the VariAC control to zero.

(11) Trigger the controller and observe the experiment.

(12) Close Sw_D and ensure that the voltage remaining on the capacitor banks reduces to less than 200 V.

(13) Isolate the charging circuit and apply temporary earth sticks and levers.

(14) Record results and return to step (3) for the next experiment.

It was considered that unexpected situations presented a period of increased hazard to the operators. Even a minor problem could often be a symptom of a more serious fault. In the case of an emergency, false triggering or an unexpected event, the following procedure was used.

(1) Open Sw_1 and turn the VariAC control to zero.

(2) Close Sw_D.

(3) Isolate the charging circuit.

(4) Approach the equipment carefully, and apply temporary earth sticks and levers.

(5) Check, test and recommission equipment if necessary.

3.8 CONCLUSIONS

A complete experimental environment was developed for performing EW experiments. The environment proved to be reliable and safe during the extensive use it had, gathering the observations and data for this research. During its development, new equipment was constructed, including a TSG, the triggering control unit, two spark gaps, seven water resistors, six capacitor banks and three earthing levers. Descriptions of the operation of the 60 kV capacitor bank and Marx generator circuits as well as the construction details of the individual components were presented in this chapter. The safety of the environment was carefully considered, and was managed by a system of hazard identification and mitigation. The major hazards were high voltage, stored energy and earth potential rise. Descriptions of the normal and emergency operating procedures were presented in this chapter.

Chapter 4

OBSERVATIONS OF EXPLODING WIRES

4.1 INTRODUCTION

The mechanism that causes long arcs to form using EWs was not well understood, so detailed observations were necessary to determine as much as possible about the processes. The insights gained into the EW mechanism could then be used in the creation of the restrike prediction model.

EW experiments are extremely fast and violent; they last less than 500 μs and reach a peak power dissipation of over 1 GW. Gathering data about the inception and evolution of the restrike channel therefore presented one of the major challenges of this research. The most useful mediums for the observation of EWs were: voltage and current waveforms; short and long exposure still photography; high speed camera photography; transient light emission waveforms; and direct observation of the wires' remains. Observations of these mediums and inferences about the EW processes are presented throughout this chapter.

There are many different outcomes that can result from an EW experiment, ranging from the wire being nearly unaffected through to a very powerful plasma-producing explosion. The average electric field (AEF), which will be discussed in depth in Chapter 5, provides a reliable method of categorising an experiment's outcome. The AEF is defined as $E_0 = V_0/\ell$, where V_0 is the initial capacitor bank voltage, and ℓ is the wire's length. The wire's diameter d has less of an effect on the experiment outcome when it is in the range of 0.2 to 0.3 mm. All experiments presented here used enamelled copper wire.

This chapter contains sections for the four main AEF regions of experimental outcome:

Region I Insufficient AEF: $E_0 = 0$ to 4.5 kV/m;

Region II Restrike region: $E_0 = 4.5$ to 11 kV/m;

Region III Excessive AEF: $E_0 = 11$ to 30 kV/m;

Region IV Upper restrike region: $E_0 = 30$ kV/m and above.

The majority of observations were collected from EWs in Region I, where the fragmentation and plasma formation mechanisms can be observed in their infancy before the evidence is destroyed by subsequent more powerful restrike process. Extensive data of the restrike channel forming was collected from EWs in Region II. Observations of experiments in Regions III and IV are brief, because this research was focused on producing long arcs, rather than restrike on short EWs using higher voltages. Some additional observations of interest are included in the final section of this chapter.

The usefulness of voltage waveforms as a key indicator of the experimental outcome was common to experiments in all regions (fig. 4.1a). Most EW voltage waveforms exhibit at least one inductive voltage spike within about 20 μs after the experiment is triggered. It will be shown in Chapter 5 that this is due to a rapid increase in resistance of the copper wire in the solid state. Some experiments will also exhibit a second smaller voltage spike within about 50 μs after triggering that is due to another rapid increase in resistance. In this chapter, it will be demonstrated that the second spike corresponds to the formation of plasma beads in Regions I and II, and the formation of a gas column in Region III. The occurrence of restrike in Region II could be easily identified on the voltage waveforms as a smooth decay to zero after the dwell time. All of these features could also be found in the current waveforms (fig. 4.1b). The rapid resistance changes were seen as sharp falls in the current, and the restrike was seen as a smooth hump of current.

4.2 REGION I: INSUFFICIENT AEF

An EW with an AEF less than approximately 4.5 kV/m will not restrike, and is said to have insufficient AEF. The study of EWs in this region has allowed for useful observations of some mechanisms that are otherwise difficult to detected when there is a restrike. Three distinct outcomes occur within the insufficient AEF region, further subdividing it into the following categories: the wire remains intact; the wire shatters with no plasma beads; and the wire shatters and plasma beads are formed. Four EW experiments were performed to demonstrate these typical outcomes. The wires, referred to as wires A through D, were 6 m long, 0.2 mm in diameter and had AEFs of 1.0, 1.5, 1.75 and 2.0 kV/m. The voltage and current waveforms were recorded (fig. 4.2) and the wire remains were examined.

4.2.1 The Wire Remains Intact

Wire A remained intact in one continuous piece, but broke free at the h.v. terminal. The wire was kinked in a wave-like pattern, and had lengthened by approximately 50 mm, or 1%. The

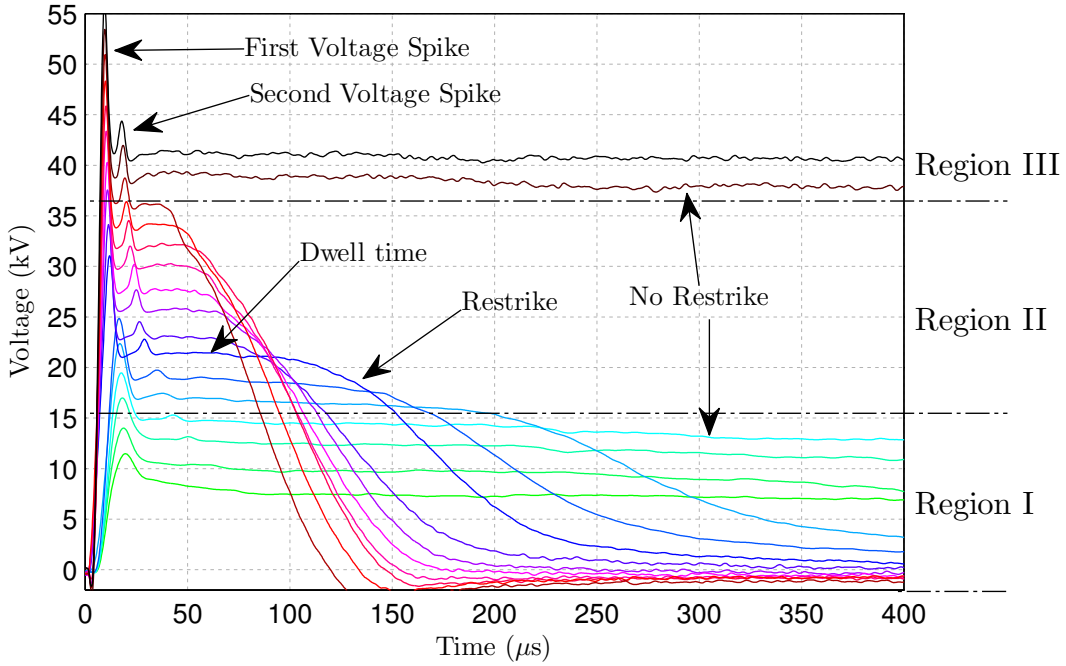

(a) Voltage waveforms.

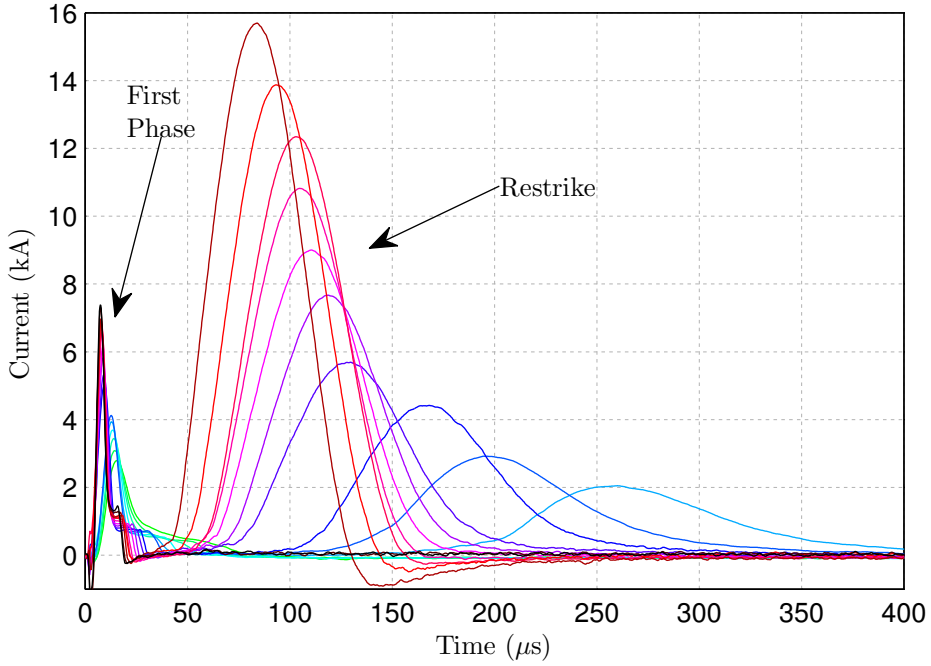

(b) Current waveforms.

Figure 4.1 Voltage and current waveforms from a set of EW experiments that transcends AEF regions I, II and III, with common features labelled. $\ell = 3$ m, $d = 0.2$ mm, $V_0 = 10$ to 40 kV, $E_0 = 3.3$ to 13.3 kV/m.

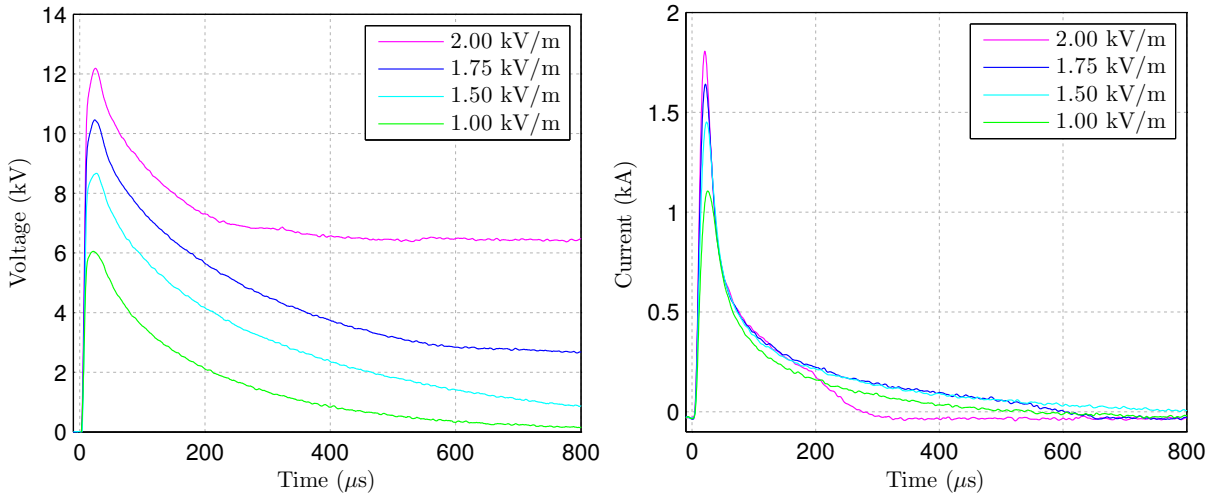

(a) Voltage waveforms.

(b) Current waveforms.

Figure 4.2 Voltage and current waveforms of EWs with insufficient AEF. $\ell = 6$ m, $d = 0.2$ mm, $V_0 = 6$ to 12 kV, $E_0 = 1$ to 2 kV/m.

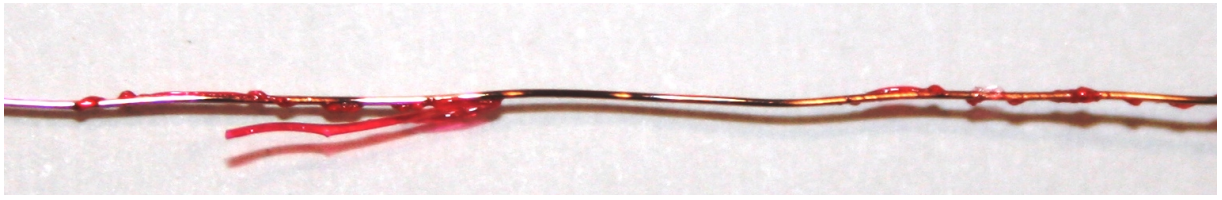

(a) Wire A: $V_0 = 6$ kV, $E_0 = 1.0$ kV/m.

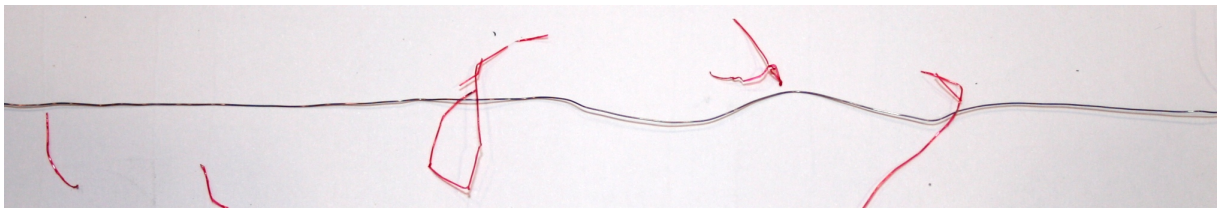

(b) Wire B: $V_0 = 9$ kV, $E_0 = 1.5$ kV/m.

Figure 4.3 Solid remains of wires with insufficient AEF. $\ell = 6$ m, $d = 0.2$ mm.

kinking appeared to be consistent with thermal expansion, because at some of the kink locations, the copper had torn out of the enamel coating, which itself does not expand significantly. The enamel insulation was heat damaged; in some places it had completely detached from the copper and was partially melted where it had remained in contact with the copper (fig. 4.3a). Wire B produced a similar outcome except that almost none of the enamel insulation remained on the copper and stronger kinking had occurred (fig. 4.3b).

(a) Sausage instabilities. (b) Pinched ends.

Figure 4.4 Fragments of wire show signs of sausage instabilities caused by MHD forces, eventually causing fragmentation when the copper is liquid. $\ell = 6$ m, $d = 0.2$ mm, $V_0 = 10.5$ kV, $E_0 = 1.75$ kV/m.

4.2.2 The Wire Shatters

Wire C, which had only a slightly higher AEF than wire B, shattered into small fragments. No sections of copper longer than 20 mm were found, but tubes of enamel insulation up to 60 mm remained. The discrepancy in the copper and enamel lengths indicates that the enamel and wire fractures via different mechanisms. The shape of the remnant fragments of wire was reminiscent of magneto-hydro-dynamic (MHD) 'sausage instabilities' [Dattner *et al.* 1959] (fig. 4.4a). These form due to electromagnetic Lorentz forces squeezing the metallic liquid radially inwards, with stronger forces on thinner diameter sections of the wire, thereby causing the instability. On Wire C, the thick sections appeared to be slightly thicker than 0.2 mm in diameter and the thin sections appeared slightly thinner than 0.2 mm. The ends of the fragments had been squeezed into sharp points, which suggests that the breaks had formed when the copper was liquid, rather than fracturing while the wire was still solid (fig. 4.4b).

Wire D ejected a shower of liquid copper droplets from the wire (fig. 4.5a). No solid sections of wire could be found, however solidified spherical droplets of copper were found after the experiment, the size of which ranged from less than 0.5 mm in diameter a dust-like particle size. Sections of enamel insulation no longer than 10 mm remained.

The liquid copper droplets ejected from similar wires have been observed to both bounce quite elastically and explode into small fragments upon impact (fig. 4.5b). Most droplets also exhibit a varying degree of eccentricity in their trajectories that describe helix-shaped trails in long-exposure photography (fig. 4.5c). This effect could be related to Taylor's photo of a spinning copper fragment (fig. 2.1b).

4.2.3 The Appearance of Plasma Beads

As the AEF approaches the upper boundary of Region I, bright blue-green spots were observed to form along the axis of the wire (fig. 4.6). These were called 'plasma beads', and can be detected with the naked eye.

(a) Liquid copper droplets ejected from a wire.

(b) Liquid copper droplets bouncing and exploding on an aluminium plate.

(c) Helical trajectory of a copper droplet.

Figure 4.5 Observations of liquid copper droplets.

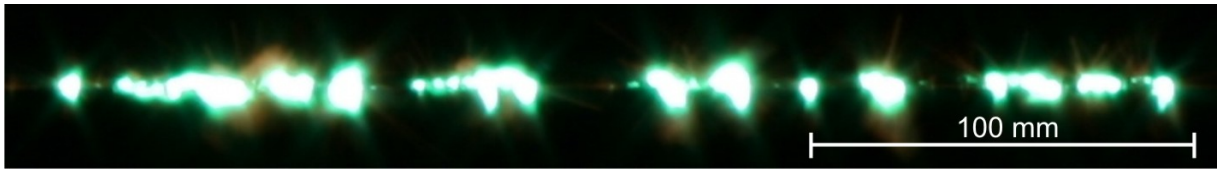

(a) A close-up photograph of plasma beads. $\ell = 3$ m, $d = 0.2$ mm, $V_0 = 15$ kV, $E_0 = 5$ kV/m.

(b) A photograph of plasma beads on a very long wire, seen as a punctuated line of green plasma across the entire length of the image. $\ell = 60$ m, $d = 0.2$ mm, $V_0 = 270$ kV, $E_0 = 4.5$ kV/m.

Figure 4.6 Examples of long-exposure photographs of plasma beads.

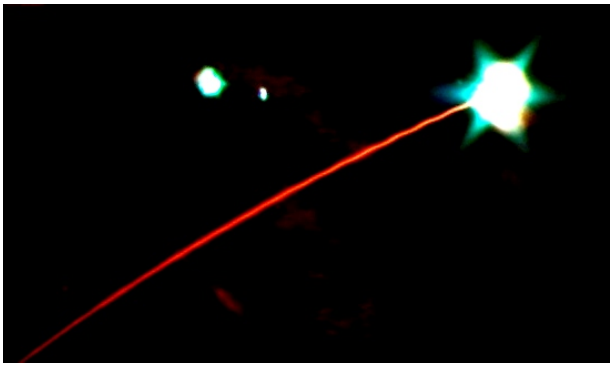

Figure 4.7 A plasma bead ejecting a liquid copper droplet.

Photography

Long-exposure photography was used to capture images of the plasma beads. The long exposures intrinsically portray the plasma in its most expanded form before it deionises and stops emitting light. The plasma beads appeared to be randomly distributed along the length of the wire, but were centred on the wire's axis. Liquid copper droplets were often seen being ejected from the plasma bead locations (fig. 4.7).

An experiment was performed to determine the correlation between the quantity of plasma beads that formed to the wire's AEF. The method had similarities to an experiment in [Taylor 2002b], where photography was used to calculate the total length of plasma shrouding a wire, and thus observe the evolution of the plasma channel. Long-exposure photographs were taken of a set of six EWs, each 3 m long, 0.2 mm in diameter and with AEFs from 4.1 to 5.8 kV/m (fig. 4.8). An additional EW with an AEF of 6.1 kV/m produced a restrike. Using digital image processing, the location of plasma was identified using a brightness threshold on each column of pixels, and then the total plasma column length was calculated as a percentage of the total wire length. The quantity of plasma forming on the wire was positively correlated to the AEF, including the

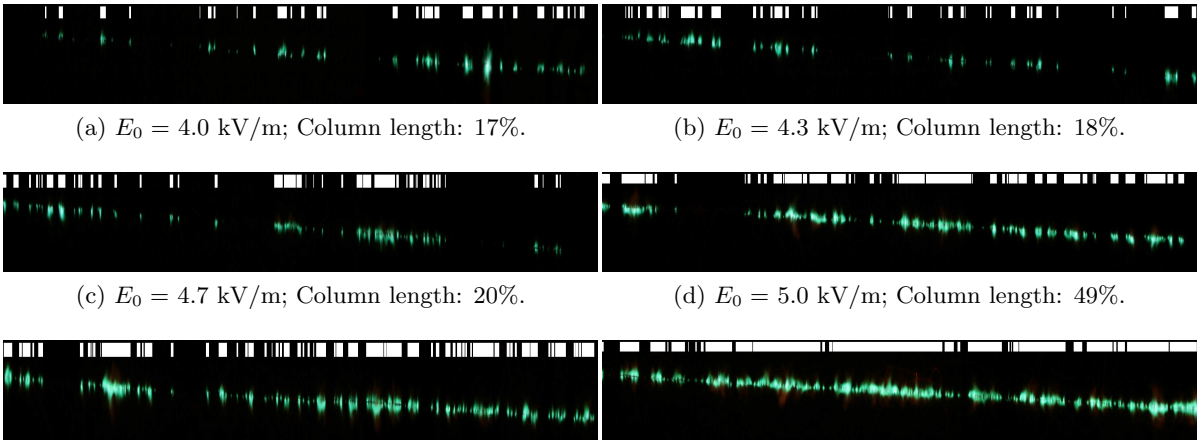

(a) $E_0 = 4.0$ kV/m; Column length: 17%. (b) $E_0 = 4.3$ kV/m; Column length: 18%.

(c) $E_0 = 4.7$ kV/m; Column length: 20%. (d) $E_0 = 5.0$ kV/m; Column length: 49%.

(e) $E_0 = 5.4$ kV/m; Column length: 45%. (f) $E_0 = 5.8$ kV/m; Column length: 80%.

Figure 4.8 The calculation images used to find the effective plasma column length. The white patterns at the tops of the images indicate where plasma was detected. The images have been compressed horizontally. $\ell = 3$ m, $d = 0.2$ mm.

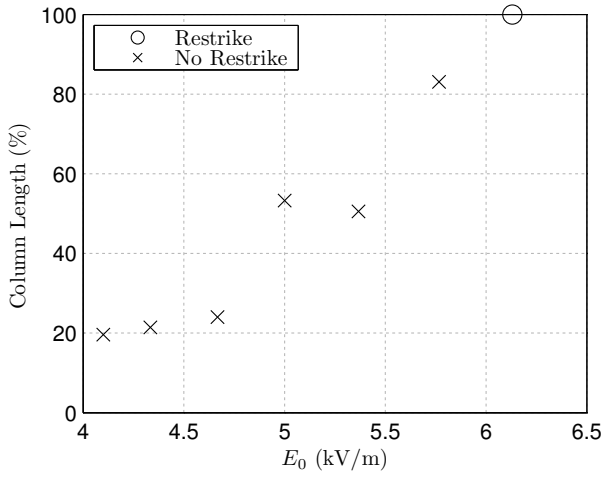

Figure 4.9 The plasma column length as a percentage of wire length. The circle denotes an experiment that produced restrike, where the plasma column length was considered equal to the wire length. $\ell = 3$ m, $d = 0.2$ mm.

experiment that produced restrike, which was considered to have a plasma column length of 100% (fig. 4.9).

Another observation was obtained from a photograph where the plasma beads had illuminated the sections of wire that had not yet been shrouded by plasma, effectively capturing the wire's position at the instant of plasma bead formation (fig. 4.10). The wire appeared to be kinked, again reminiscent of thermal expansion, but there is very little motion blur, which suggested the wire was not moving quickly at that time.

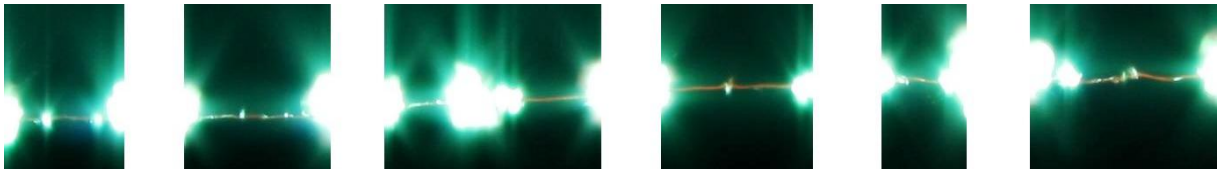

Figure 4.10 The sections of an EW illuminated by plasma beads are seen to be kinked; the wire was initially straight.

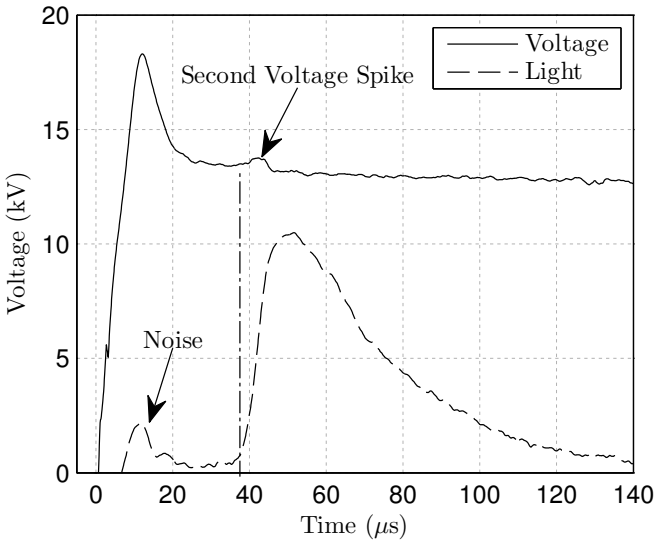

Figure 4.11 Voltage and emitted light intensity waveforms recorded for an EW that did not produce restrike. The dash-dot annotation delineates the start of the second voltage spike and the first emitted light. The emitted light intensity has an arbitrary scale. $\ell = 3$ m, $d = 0.2$ mm, $V_0 = 15$ kV, $E_0 = 5$ kV/m.

Emitted Light Intensity Waveforms

A photodiode light sensor was used to record the emitted light intensity waveforms of EWs in Region I. When it was compared to the voltage waveforms, the first detected light (discounting the switching noise, which was discussed in Section 3.5.6) was simultaneous to the second inductive voltage spike (fig. 4.11). The light increased at the fastest rate during the voltage spike as the plasma beads formed. The light increased more slowly as the plasma beads expanded, and then tapered off as the plasma deionised. This was the first evidence found that plasma beads form during the second voltage spike.

Voltage and Current Waveforms

Voltage waveforms can be seen in the above plasma column length experiment show as the AEF is increased (fig. 4.12). The second voltage spike is barely distinguishable on the lowest AEF, where the least amount of plasma was formed, and is most pronounced when the most amount of plasma is formed. The second voltage spike also occurs sooner with increased AEF because

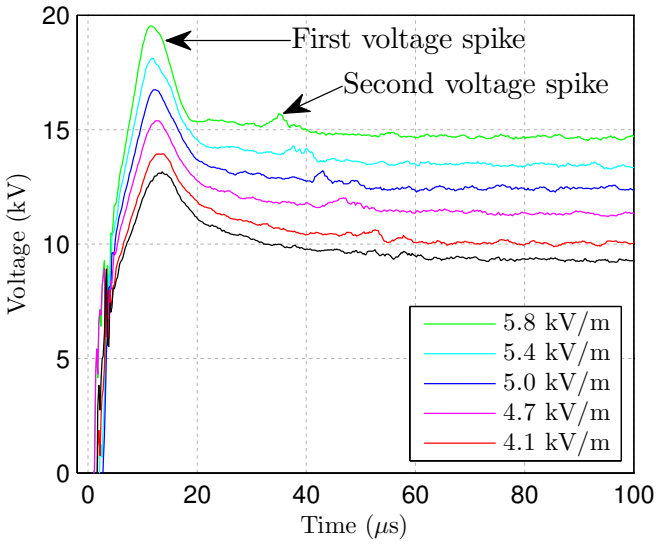

Figure 4.12 Voltage waveforms of the plasma column length experiments, which are in Region I. ℓ =3 m, d =0.2 mm, V_0 =12.3 to 17.4 kV, E_0 =4.1 to 5.8 kV/m.

the larger current melts the wire more, causing the plasma beads to form sooner.

When the second voltage spike was examined using a faster sampling rate on the oscilloscope, it was found not to be a smooth hump (fig. 4.13). Instead, the inductive voltage flickered as the current reduced into the dwell time; it was the average of the flickering that gave a positive voltage spike. The possible implication of this finding was that the formation of each fracture caused a spike in resistance, a rapid change in current, and subsequent inductive voltage spike. The voltage spike then aided the breakdown of the fragmentation site, forming a small arc, or plasma bead. When the current had fallen to a low level, inductive voltage spikes were no longer created at the fragmentation sites and so no more plasma beads were formed.

High Speed Camera

An EW with insufficient AEF was filmed using a high speed camera. The captured frames from the experiment show the plasma beads seed from small points, grow in size and intensity and then begin to fade before they coalesce (fig. 4.14).

4.3 REGION II: RESTRIKE REGION

Photography

The plasma beads are easily observed via long-exposure photography in EWs which do not produce restrike. However, for EWs that produce restrike, the camera is over-exposed with the

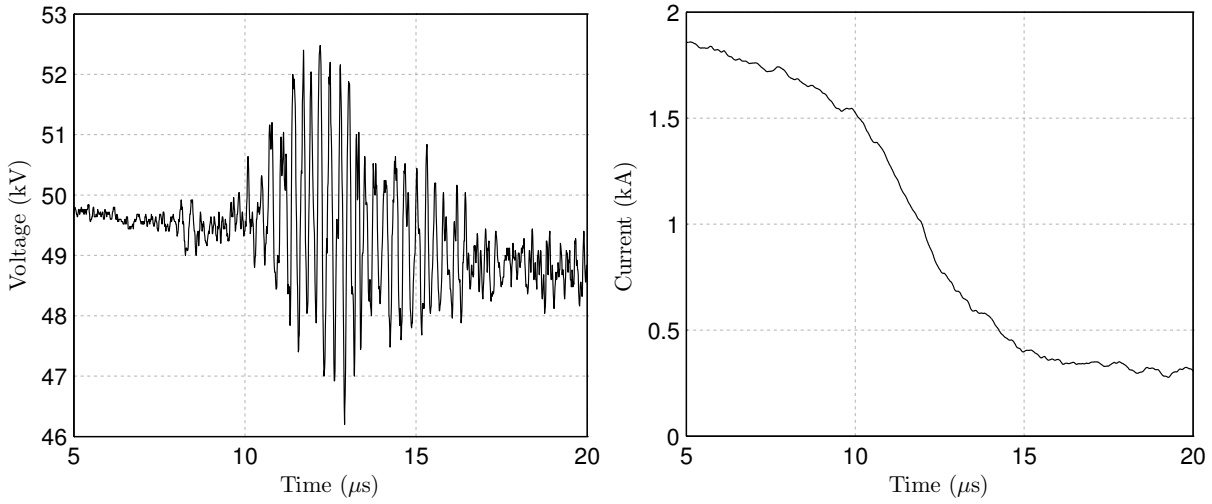

(a) Voltage waveform.

(b) Current waveform.

Figure 4.13 Detailed waveforms of the second voltage spike. The damping resistor was not connected to the CVD for this experiment, but the resolution of the voltage measurement is still limited by the sampling rate of the oscilloscope. $\ell = 6$ m, $d = 0.2$ mm, $V_0 = 50$ kV, $E_0 = 8.3$ kV/m.

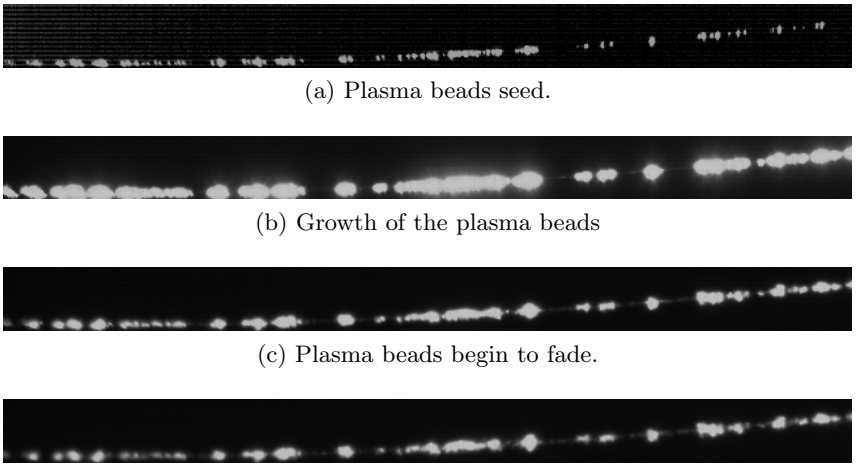

(a) Plasma beads seed.

(b) Growth of the plasma beads

(c) Plasma beads begin to fade.

(d) Fading continues.

Figure 4.14 Consecutive frames captured from high speed camera footage of an EW with insufficient AEF. Each frame represents approximately 100 μs. $\ell = 5$ m, $d = 0.3$ mm, $V_0 = 30$ kV, $E_0 = 6$ kV/m.

extremely bright light emitted during the restrike, obscuring the plasma beads that may have been previously recorded. To capture the presence of the beads forming on EWs that produce restrike, a short-exposure photography technique was employed, in which the mechanical shutter of the camera was triggered precisely to obscure the wire just before the restrike occurs. Using this technique, it was found that plasma beads are present just prior to restrike (fig. 4.15).

The short-exposure technique was used again, but this time the camera was turned 90°, such that the camera shutters moved along the axis of the wire. This allowed a 'streak photograph' of an EW that produced restrike to be captured (fig. 4.16). On the left of the photograph, the

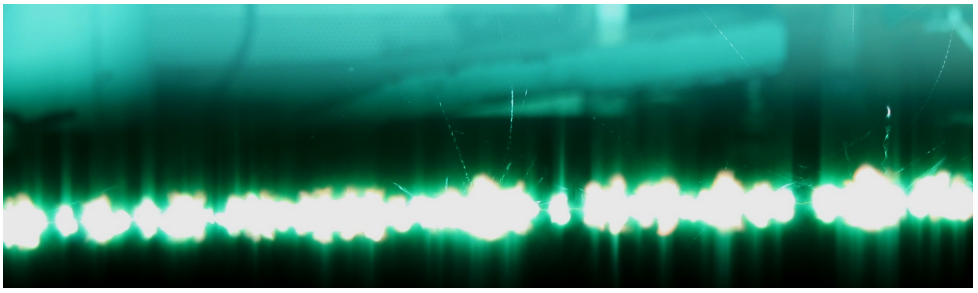

Figure 4.15 A short-exposure photograph of plasma beads with an EW that produced restrike. Due to the sliding shutter mechanism in the camera, time increases from bottom to top in the photograph. The bright band across the top of the photograph is the light from restrike reflected off the laboratory wall. $\ell = 9$ m, $d = 0.2$ mm, $V_0 = 40$ kV, $E_0 = 4.4$ kV/m.

Figure 4.16 A streak photograph, using the short-exposure technique, of a wire that produced restrike. The camera was rotated 90° such that the camera shutters move along the axis of the wire. Time increases from left to right in this photograph. Approximately 2 ms of time is represented. $\ell = 3$ m, $d = 0.2$ mm, $V_0 = 25$ kV, $E_0 = 8.3$ kV/m.

plasma beads can be seen expanding radially until the bright restrike channel is formed, which lit up the laboratory in the background. Then, the plasma deionises and fades into a dull orange, and expands slightly in the radial direction but much more in the axial direction. The liquid copper fragments can been seen near the axis of the wire; they are much slower than the other processes in this photograph.

Emitted Light Intensity

The emitted light intensity waveform was recorded for an EW that produced restrike. The waveform showed that the plasma beads again form at the second voltage spike and then continue to grow during the dwell time (fig. 4.17a). The emitted light intensity, and therefore the plasma's degree of ionisation, increases dramatically at the inception of restrike and reaches a maximum when the current peaks (fig. 4.17b). The plasma then continues to emit light until the current has dropped to a relatively low level.

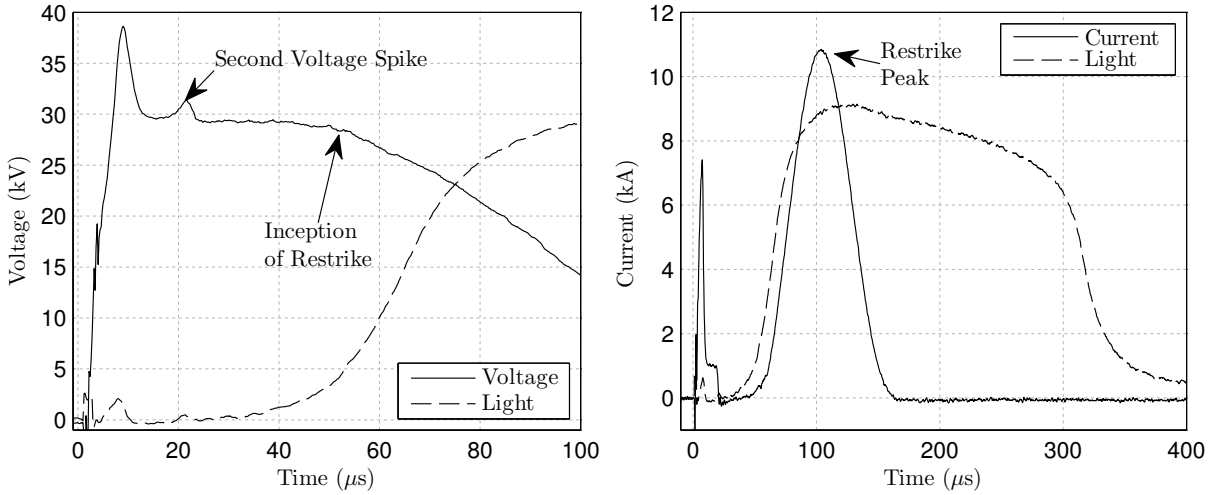

(a) Voltage waveform with first phase detail.

(b) Current waveform with full detail.

Figure 4.17 Voltage and current waveforms compared to the emitted light intensity for an EW that produced restrike. The emitted light intensity has an arbitrary scale in each plot. $\ell = 3$ m, $d = 0.2$ mm, $V_0 = 30$ kV, $E_0 = 10$ kV/m.

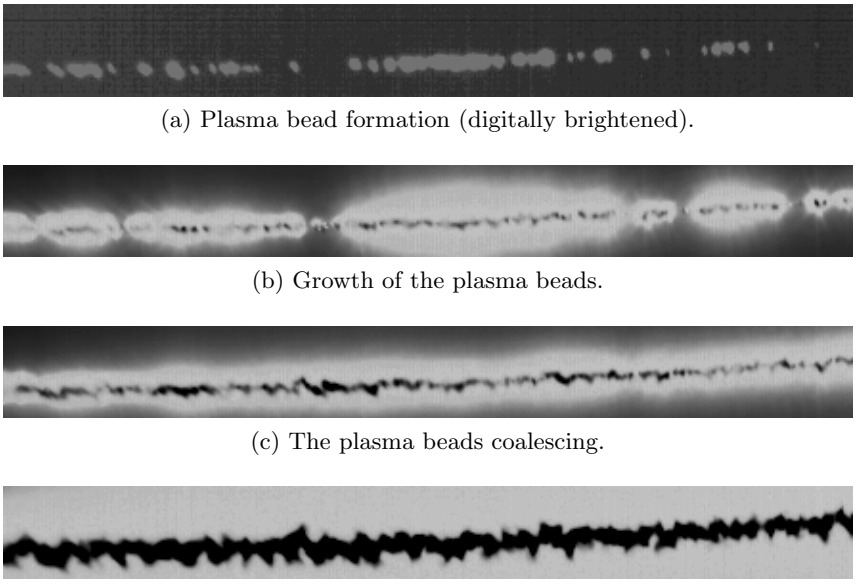

(a) Plasma bead formation (digitally brightened).

(b) Growth of the plasma beads.

(c) The plasma beads coalescing.

(d) Restrike through the continuous plasma channel.

Figure 4.18 Consecutive frames captured from high speed camera footage of an EW that produced restrike. Each frame represents approximately 100 μs. $\ell = 5$ m, $d = 0.3$ mm, $V_0 = 30$ kV, $E_0 = 6$ kV/m.

High Speed Camera Photography

A high speed camera was used to film an EW that produced restrike (fig. 4.18). The captured frames show that the plasma beads appear prior to the onset of restrike, then expand and eventually coalesce. Once a continuous column of plasma beads has been created, the brighter restrike channel forms.

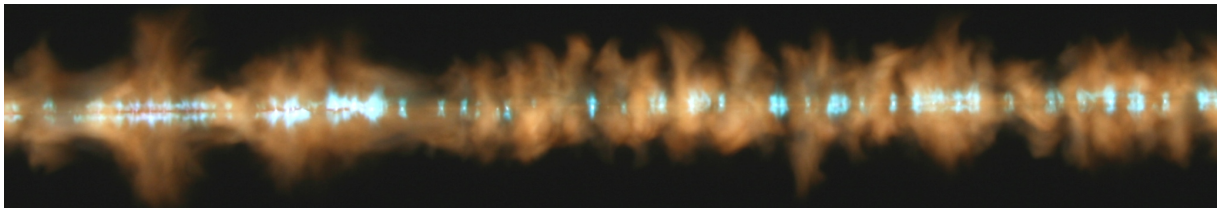

(a) $\ell = 2$ m, $d = 0.2$ mm, $V_0 = 30$ kV, $E_0 = 15$ kV/m

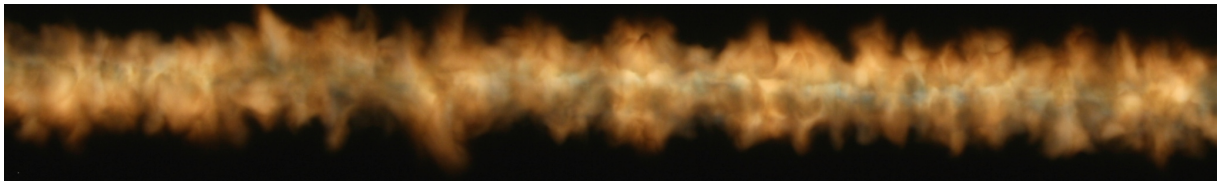

(b) $\ell = 2$ m, $d = 0.2$ mm, $V_0 = 45$ kV, $E_0 = 22.5$ kV/m

Figure 4.19 Long-exposure photographs of EW experiments in Region III.

4.4 REGION III: EXCESSIVE AEF

When the AEF exceeds around 10 kV/m, restrike becomes unlikely to occur. No experiments with an AEF between 15 and 30 kV/m have been observed to produce restrike. This result is not intuitive; there are very few breakdown mechanisms that fail to occur when the electric field is increased. Experiments in this region could be identified by the voltage waveforms, which exhibited a large second voltage spike and no restrike feature (fig. 4.1a), and because they were notably quieter and less bright than the experiments in Region II.

Photography

Photographs of experiments in Region III showed a column of orange gas with small quantities of symmetrical plasma (fig. 4.19a). The orange gas is thought to be the copper vapour that has formed before fragmentation can occur. The symmetrical plasma is possibly a few plasma beads that have formed and then been blasted apart radially by the vaporising copper. For experiments with an even higher AEF, the quantity of copper gas was greater and the symmetrical plasma beads were entirely absent (fig. 4.19b).

A possible theory on the failure of the restrike mechanism to operate with an excessive AEF is that the wire was heated too quickly. The consequence of a higher voltage per unit length of wire was a large current, a higher power dissipation and a faster temperature rise. After the wire had melted and the sausage instabilities began to form, the fast temperature rise may have boiled the copper before the sausage instabilities fragmented the wire. Thus, no plasma beads were formed and restrike was not produced.

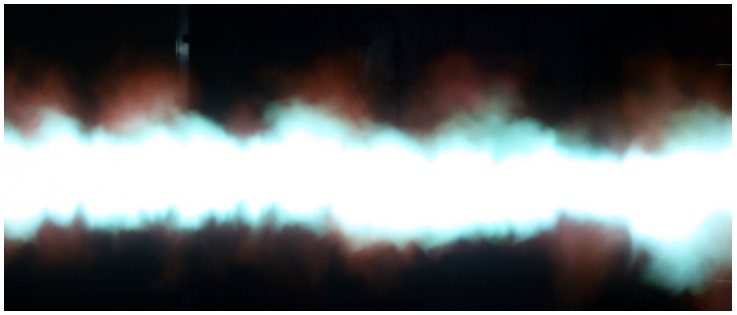

Figure 4.20 A long-exposure photograph of an experiment in Region IV. $\ell = 1$ m, $d = 0.2$ mm, $V_0 = 35$ kV, $E_0 = 35$ kV/m.

4.5 REGION IV: UPPER RESTRIKE REGION

With an AEF of more than 30 kV/m, experiments produced restrike again. From the operators' perspective, these were very violent due to the larger amount of energy being dissipated in a much shorter length. Long-exposure photography shows a bright restrike channel (fig. 4.20). It is thought that this mode of restrike is the direct breakdown of the copper gas.

4.6 OTHER OBSERVATIONS

4.6.1 The Effect of Additional Inductance

A set of experiments was performed where extra series inductance was added to the circuit for several sets of EW experiments. The additional inductance was varied from 0 to 670 μH, and sets of experiments using 6 m long, 0.2 mm diameter wire with AEFs of 4, 5 and 6 kV/m were performed. As expected, no restrike was produced using 4 kV/m. With no additional inductance, an AEF of 5 kV/m produced restrike, but with any additional inductance, no restrike was produced. The 6 kV/m set only produced restrike with less than 430 μH of additional inductance.

Adding inductance slowed down the initial rate of current increase, which would have resulted in a slower transition from solid to liquid (fig. 4.21b). This caused the size of the first voltage spike to decrease (fig. 4.21a). The additional inductance meant that when the wire fragmented, which must have still been a rapid process, the second voltage spike was much larger. In all sets, the photos showed that fewer plasma beads were created and more liquid copper was ejected as the additional inductance was increased. The velocity of the ejected liquid copper droplets also increased markedly with increased additional inductance (figs. 4.21c and 4.21d).

From the experiments, it was concluded that an increase in circuit inductance is detrimental to the formation of plasma beads. This is possibly due to the slower rate of heating and lower

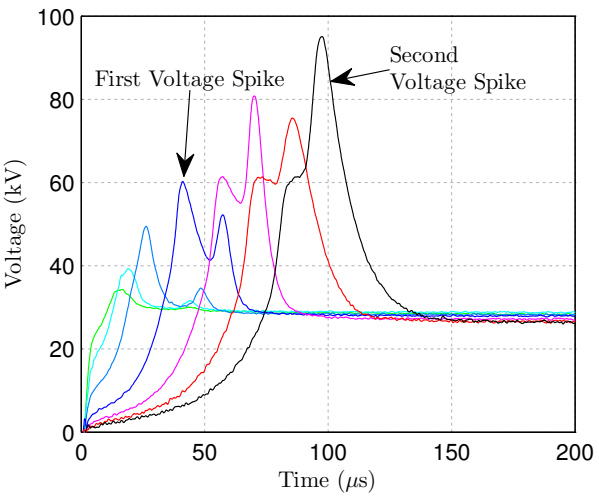

(a) Voltage waveforms.

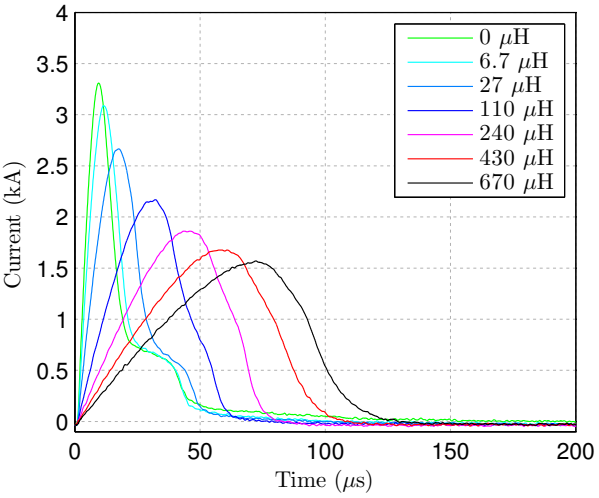

(b) Current waveforms.

(c) With 6.7 μH additional inductance.

(d) With 240 μH additional inductance.

Figure 4.21 A set of EWs with extra series inductance added to the circuit. Only the EW with no additional inductance produced restrike in this set. $\ell = 6$ m, $d = 0.2$ mm, $V_0 = 30$ kV, $E_0 = 5$ kV/m.

peak current in the first phase, causing only weak sausage instabilities and therefore limited fragmentation. It was also concluded that minimising the circuit inductance may help to achieve restrike on longer EWs.

4.6.2 Multiple-Diameter EW

A brief study was conducted in which lengths of different diameters wires were connected in series. One experiment used a 0.7 m length of 0.26 mm diameter wire that was connected in series between two lengths of 0.25 mm wire, creating a total wire length of 3 m. The capacitor voltage was 30 kV, resulting in an AEF of 10 kV/m. It was expected that, despite the slight difference in wire diameter, both wires would explode in a similar manner in Region III. The long exposure photograph showed that the 0.25 mm wire was in Region III (fig. 4.22a). Surprisingly, the 0.26 mm wire remained intact and fell to the floor in a single length, and so was in Region I. This finding led to the idea that a thin wire could be used as the return path for the EW current, instead of thick, heavy cables.

(a) Left: ℓ =0.7 m, d =0.26 mm EW remains intact; Right: ℓ =1.3 m, d =0.25 mm EW forms plasma beads. V_0 =30 kV.

(b) Left: ℓ =0.7 m, d =0.26 mm EW forms plasma beads; Right: ℓ =1.3 m, d =0.25 mm EW produces restrike. V_0 =18 kV.

Figure 4.22 Photographs of multiple-diameter EW experiments.

The experiment was then repeated with the voltage decreased to 18 kV, such that the AEF on the 0.25 mm wire was in Region II at 7.8 kV/m, since the 0.26 mm wire appeared to conduct without exploding. This resulted in a restrike on the 0.25 mm wire and caused the 0.26 mm wire to form plasma beads (fig. 4.22b). It could be seen on the voltage waveform that the capacitor voltage stops decreasing near the end of the restrike, indicating when the 0.26 mm wire explodes. Restrike on two different diameter wires was later achieved using 1 m of 0.25 mm wire and 2 m of 0.2 mm wire at 17 kV. The photo showed a complete plasma channel through both sections of wire, and the voltage waveform (fig. 4.23) shows first restrike in the 0.2 mm wire, then a very delayed restrike in the 0.25 mm wire after about 2 ms. It was thought that the restrike current from the 0.2 mm wire was effectively the first-phase current for the 0.25 mm wire. In these experiments, the outcome of each diameter wire could be categorised into one of the AEF regions. This allowed the AEF to be adjusted accordingly until restrike was achieved.

4.7 CONCLUSIONS

Long distance EW experiments were observed to result in several different outcomes. The outcomes were categorised into four regions, defined by the AEF. In Region I (0 to 4.5 kV/m), experiments did not produce restrike, allowing the mechanisms that caused restrike to be more easily observed. The wire was found to thermally expand during the solid copper heating phase. Fragmentation appeared to have been caused by sausage instabilities that formed while the wire was in the liquid state. The sausage instabilities were strong enough to squeeze points of the wire until it fragmented. It is thought that plasma beads were arcs that formed across the fragmentation sites, perhaps aided by inductive voltage spikes that were driven by sudden increases in resistance at the fragmentation sites. The summation voltage spikes at each fragmentation site

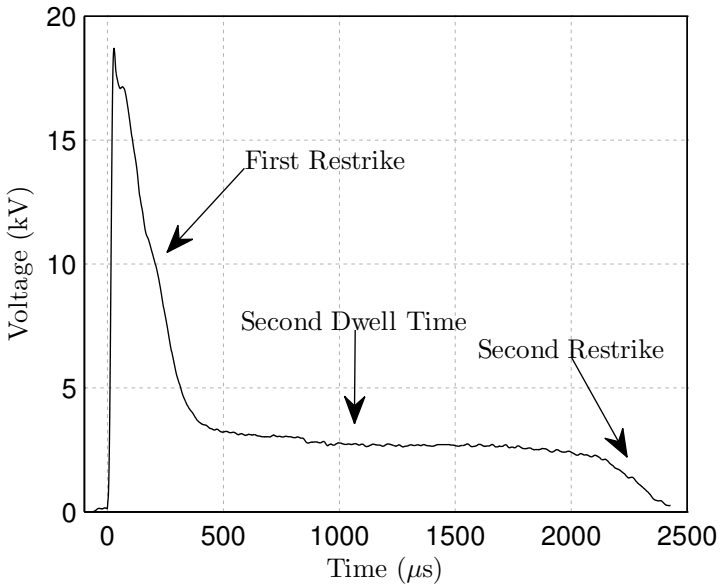

Figure 4.23 A voltage waveform of 0.2 mm diameter and 0.25 mm diameter EWs in series, where both produce restrike. V_0 =17 kV.

produced the second inductive voltage spike, which was shown to coincide with the formation of plasma beads. When the AEF was too low, few or no plasma beads formed on the wire. This may have been due to insufficient Lorentz forces for the formation of sausage instabilities.

In Region II (4.5 to 11 kV/m), the plasma beads were observed to expand and coalesce, forming a continuous chain of plasma that facilitated restrike. In Region III (11 to 30 kV/m), when the AEF was too high, no plasma beads were formed and instead the wire was vaporised. It was thought that the wire reached boiling point before the sausage instabilities had time to form. In Region IV (30 kV/m and above), restrike by a different mechanism was produced.

Observations of some alternative experimental configurations were then presented. When extra inductance was added to the circuit, the AEF required for restrike increased, highlighting the importance of minimising the circuit inductance to maximise the length of restrike. When two wires of different diameters were connected in series, it was found that the wires could have independent experimental outcomes. This finding led to the idea that a thin wire can be used as the return path for the EW current, rather than using thick and heavy cables. The use of a thin return wire is presented in Chapter 6.

The experimental observations presented in this chapter have advanced understanding of the processes that occur during long distance EWs. It has been determined that the long distance EW restrike mechanism is completely dependent on the formation of plasma beads. It has also been shown that the AEF is a reliable metric in defining the regions of experimental outcome, a phenomenon that is developed and explored in the next chapter.

Chapter 5

DEVELOPMENT OF A MODEL

5.1 INTRODUCTION

The primary aim of this research was to develop a useful mathematical model that could predict the occurrence of restrike in long distance EWs. The experimental variables were the length and diameter of the wire and the energy supply's characteristics and initial charge voltage. The output of the model was a prediction of whether or not restrike will occur. The model could then be used to aid experimental work in the study of applications of EW or by other research groups who wish to investigate long arcs using EWs. The development of a model also further developed the understanding of the processes which occur in long distance EW.

The development of the model is presented chronologically in this chapter. It begins with the analysis of the dataset presented in [Smith 2008], which was the most comprehensive long distance EW data in the literature at the commencement of this research. Useful trends that are found in Smith's data prompt new experiments in an attempt to find correlations between the model inputs. Next, a transient simulation study is presented, which uses an electro-thermal model of the EW. A model to predict the occurrence of restrike is then presented. The model was used to design the Marx generator for performing experiments from 10 to 60 m long. Lastly, a complete model is developed using a combination of the current understanding of the restrike mechanism and empirical data.

For the purpose of analysis, the whole EW process was split into two consecutive phases, which are separated by the dwell time: the first phase and the restrike phase. The first phase occurs in every EW; it encompasses all of the heating, melting, fragmentation and plasma bead creation processes. The first phase is completed when the wire enters the dwell time, after which the restrike phase of the process begins, where a continuous plasma channel may form. The focus of this chapter is on the first phase and its effect on the initiation of restrike.

5.2 ANALYSIS OF SMITH'S DATASET

The dataset published in [Smith 2008] provided a comprehensive experimental dataset with which to begin studying long distance EW. The purpose of the analysis was to determine which experiments had produced restrike, and to look for trends that may indicate why restrike had occurred. The dataset contained 100 experiments, using initial capacitor voltages of 15, 30, 45 and 60 kV; wire diameters of 0.2, 0.27, 0.375 and 0.63 mm; and wire lengths of 1, 3, 5, 7 and 9 m. Voltage and current waveforms had been recorded for each experiment. The final capacitor voltage after each experiment was also recorded. Although some of the voltage and current waveforms exhibited a dwell time and restrike, many of the voltage waveforms had recording durations which were too short to show whether or not a restrike was produced.

5.2.1 Energy Dissipation and Energy Density

It was hypothesised that the outcome of each EW experiment would be correlated to the amount of energy available in the capacitor bank per unit volume of copper in the wire; a large amount of energy that was dissipated into a thin and short wire would be expected to produce a very different result to a small amount dissipated into a long and thick wire. Thus, a new quantity called 'energy density', with units of J/mm^3, was defined:

$$D = \frac{\text{Energy}}{\text{Volume}} = \frac{W_0}{\pi \left(\frac{d}{2}\right)^2 \ell} \tag{5.1}$$

where W_0 is the initial capacitor bank energy, d is the wire's diameter and ℓ is the wire's length. Next, the proportion energy dissipated was calculated as

$$w = \frac{W_T}{W_0} \tag{5.2}$$

where W_T is the total energy dissipated into the wire.

The correlation between D and w was then examined (fig. 5.1). It was found that experiments with very low energy densities had near-complete energy dissipation. This was because the wire had remained conductive, probably in the solid state, until the capacitor bank had mostly or entirely discharged. The energy dissipation then began to decrease in experiments where the energy density exceeded approximately 10^1 J/mm^3, presumably because wire fragmentation and/or melting caused a wire to eventually become open-circuit before much energy was dissipated. When the energy density increased beyond 10^2 J/mm^3, the energy dissipation became dual-valued. This region is a clear depiction of Smith's observations of the partial-plasma and

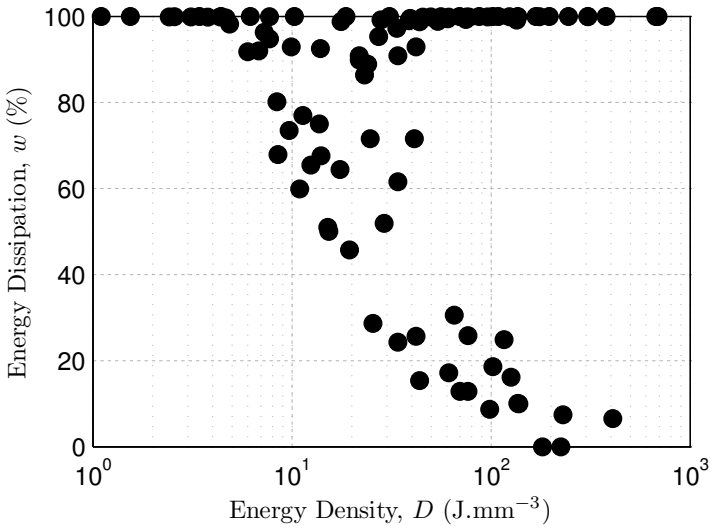

Figure 5.1 The energy dissipation of Smith's EW experiments as a function of their energy density.

full-plasma outcomes, and delineates the critical region of investigation needed to create long arcs using EW.

5.2.2 Average Electric Field

The quantity of average electric field (AEF), $E_0 = V_0/\ell$, was applied to Smith's dataset. To analyse the effect of the AEF on the experiment outcome, the energy dissipation of experiments which fell within the dual-valued energy density region that was identified in Figure 5.1, i.e. $D < 10^{1.6}$ J/mm^3, were plotted against E_0 (fig. 5.2). A grouping of experiments with near-complete energy dissipation appears; these are EWs that produced restrike, and were seen to occur exclusively, but not necessarily, in a region of AEF between 6 and 12 kV/m. This AEF region of restrike was the beginning of the restrike prediction model formulation.

5.3 SOME EXPERIMENTAL SETS

The region of energy density in Smith's data that produced two distinct EW outcomes, along with the AEF categorisation of restrike, provided the first evidence of predictability in long distance EW experiments. New experiments were designed to focus on this region, abandoning investigation into the rest of Smith's wide range of experiments. The aim of the new experiments was to test simple hypotheses that may contribute to the formulation of a restrike prediction model.

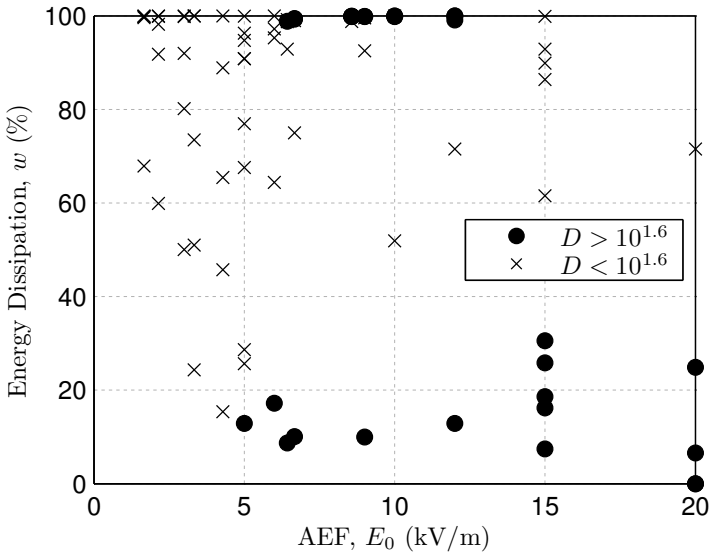

Figure 5.2 The energy dissipation of Smith's EW experiments as a function of the AEF. The grouping of experiments with $D < 10^{1.6}$ J/mm^3 and near-complete energy dissipation were identified as experiments that produced restrike.

5.3.1 First Phase Energy and Copper Volume

It was hypothesised that the plasma formation mechanism in the restrike phase was dependent on the voltage across the EW during the dwell time, V_1. The voltage reduction in the capacitor bank was dependent on the amount of energy that was dissipated during the first phase, W_1. Then, W_1 would be correlated to the mass or volume of the wire, assuming that the energy supply losses were negligible and that the EW heated and changed state homogeneously. A simple model could then predict W_1 from the wire dimensions, and hence calculate V_1 and predict the occurrence of restrike.

Two sets of EW experiments were performed; one set with each wire having a copper volume of 200 mm^3 and the other set with 300 mm^3 (fig. 5.3). Each set consisted of five different wire diameters, with lengths calculated to give the required volume. All experiments used V_0 =30 kV. For each experiment, the dwell-time voltage was taken to be the average of 50 μs following the second voltage spike, and then the energy dissipated during the first phase, W_1, was calculated as

$$W_1 = \frac{1}{2} C \left(V_0^2 - V_1^2 \right) \tag{5.3}$$

The first phase energy of EWs within each set were not identical as the hypothesis suggested. The difference between the two sets was insignificant and instead W_1 appeared to be more strongly correlated to the diameter. The reason for the dependence of W_1 on the diameter was

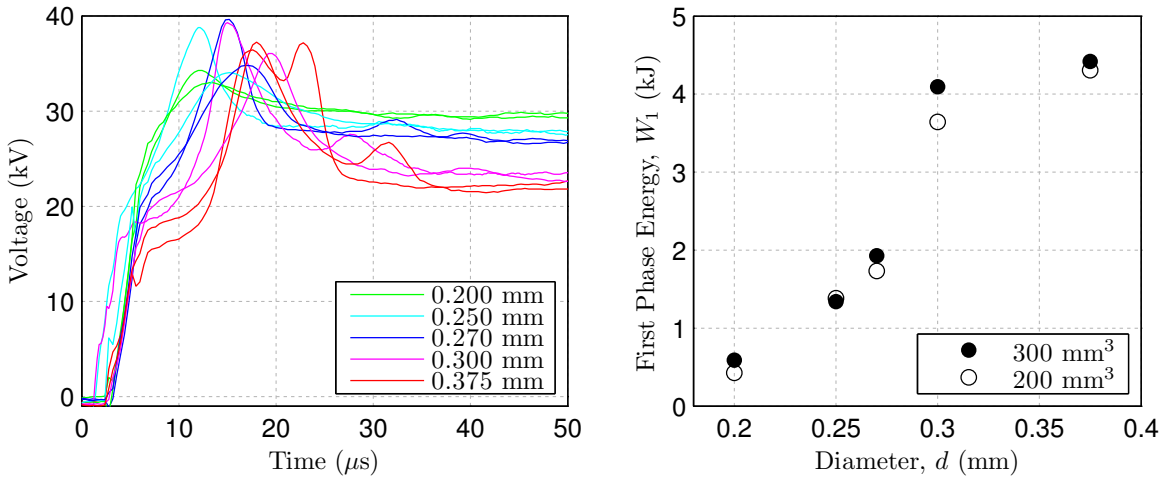

(a) Voltage waveforms.

(b) First phase energy.

Figure 5.3 Two sets of experiments, with EWs in each set having identical volume but various lengths and diameters. V_0 =30 kV.

unclear, but it is possibly due to non-uniform heating in the radial direction due the skin effect. This research henceforth compared only wires of the same diameter, rather than attempting to create a model that encompassed various diameters.

5.3.2 Identical Diameters

New experimental data was collected that focused on the region of AEFs that was found to produce restrike in Smith's data. Two sets of EW experiments were performed using a comprehensive range of initial voltages, but each set contained identical diameter and length wires (fig. 5.4). Set 1 used 5 m long, 0.27 mm diameter wires and set 2 used 9 m long, 0.355 mm diameter wires. The initial voltage was varied from 15 to 60 kV in 5 kV steps, resulting in AEFs from 3 to 12 kV/m for set 1 and from 1.7 to 6.7 kV/m for set 2.

Two inductive voltage spikes could be seen in the first phase detail of both sets. The first and largest spike occurred at 10 to 20 μs in all of the waveforms. The second, and much smaller, voltage spike occurred around 20 to 40 μs in set 1 and became undetectable on the lowest voltage waveforms. The second voltage spike was less distinct in set 2. Both voltage spikes became more pronounced as V_0 was increased. The occurrence of restrike could be easily identified on the voltage waveforms as a fast voltage decay following the dwell time. Four experiments in set 1 and three experiments in set 2 produced restrike. The AEF restrike region was very apparent in set 1, where experiments that had an AEF between 7 and 10 kV/m produced restrike. These waveforms also demonstrated that the dwell time decreased and the rate of discharge in the restrike becomes faster as the initial voltage was increased.

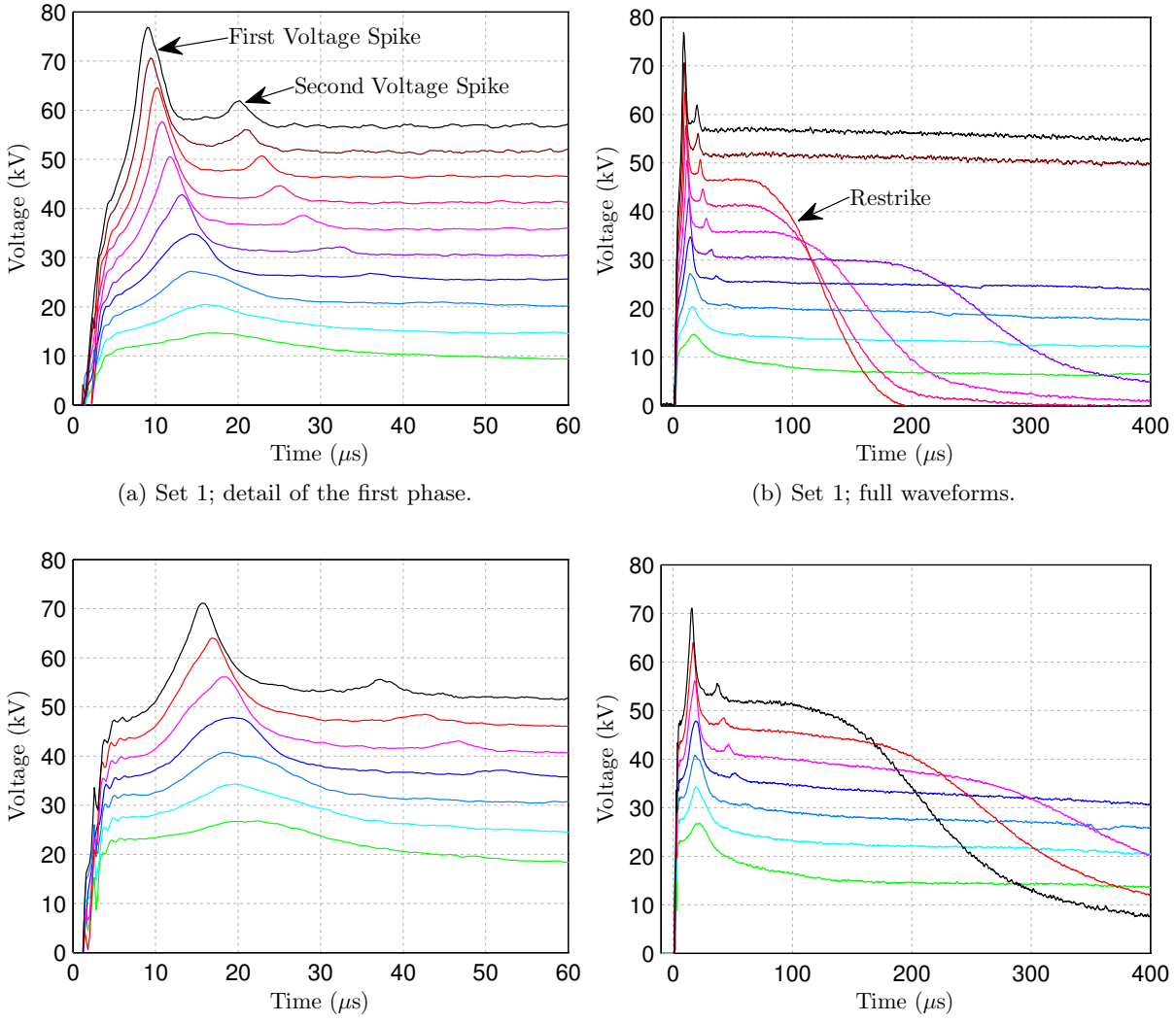

(a) Set 1; detail of the first phase.

(b) Set 1; full waveforms.

(c) Set 2; detail of the first phase.

(d) Set 2; full waveforms.

Figure 5.4 Voltage waveforms from two sets EW experiments. Set 1: $\ell = 5$ m, $d = 0.27$ mm. Set 2: $\ell = 9$ m, $d = 0.355$ mm. In both sets, $V_0 = 15$ kV (bottom waveform) to $V_0 = 60$ kV (top waveform), increasing in steps of 5 kV.

5.4 A TRANSIENT STUDY

It was still hypothesised that the occurrence of restrike might depend on the dwell time voltage, V_1, although a simple method for predicting W_1 had not yet been found. So, the first phase of the EW process was simulated on a computer using a transient model, with the aim of producing a calculation method for W_1. The 60 kV capacitor bank circuit was modelled as shown in Figure 5.5. The capacitor bank and supply cables were modelled by a 21.375 μF capacitor in series with an 85 mΩ resistor and a 6.5 μH inductor. The inductance and resistance were calculated from the under-damped response of the circuit, obtained in an experiment where the output of the circuit was shorted to earth. The TSG was modelled by a perfect switch. The inductance of the EW and the return cables was calculated using

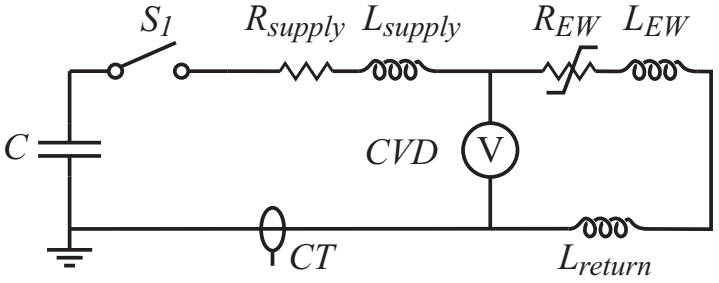

Figure 5.5 The electrical schematic of the transient simulation of the 60 kV capacitor bank circuit and EW.

$$L = \frac{2\ell}{10^7}\left[log\left(\frac{4\ell}{d}\right) - \frac{3}{4}\right] \tag{5.4}$$

a formula for the inductance of a circular cross-section conductor [Rosa 1908]. The wire's inductance was calculated to be 1.83 μH/m, and the 10 m long return cable's inductance was calculated to be 10.3 μH. The return cables were assumed to have negligible resistance.

The EW was modelled by a variable resistor, whose resistance was re-calculated each simulation step. The time-varying energy dissipated into the EW resistor, $W(t)$, was calculated as

$$W(t) = \int_0^t v(t)i(t)dt \tag{5.5}$$

where $v(t)$ and $i(t)$ were the resistive component of the EW voltage and the current through the EW. The energy dissipation was then used to calculate the wire's temperature,

$$T(t) = \frac{W(t)}{cm} + T(t_0) \tag{5.6}$$

where m is the wire's mass, c is the specific heat of copper (0.385 $\mathrm{Jg^{-1}K^{-1}}$) and $T(t_0)$ is room temperature (293 K). Initially, the EW was assumed to remain in the solid state, where the resistance is easily calculated by the linear equation

$$R(t) = R(t_0)\left[1 + \alpha\left(T(t) - T(t_0)\right)\right] \tag{5.7}$$

where $R(t_0)$ is the initial resistance of the wire and α is the temperature coefficient of copper (0.0039 $\mathrm{K^{-1}}$) [Wesley *et al.* 2008].

Sixty experiments with various wire lengths, wire diameters and initial capacitor bank voltages were simulated. In most cases, the simulation of the first inductive voltage spike and the transition into the dwell time provided a good fit for the experimental data. However, the simulated

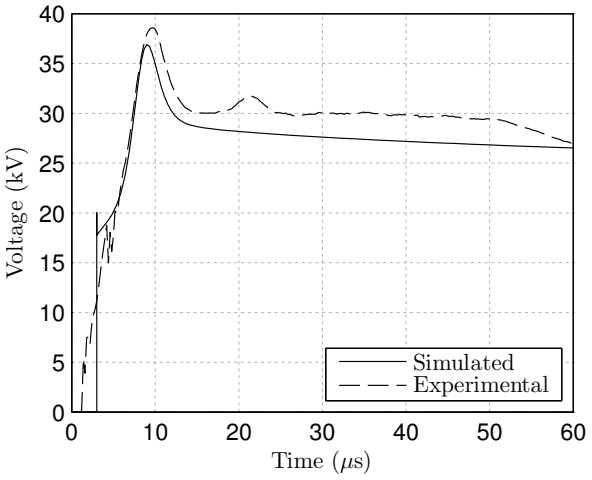

(a) Simulated and experimental voltage waveforms.

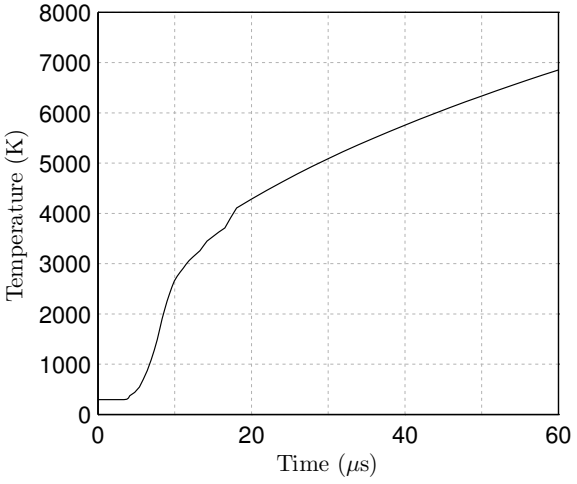

(b) Simulated temperature of the EW.

Figure 5.6 A transient simulation of an EW using a solid copper temperature-resistivity relationship. $\ell = 3$ m, $d = 0.2$ mm, $V_0 = 30$ kV, $E_0 = 10$ kV/m.

voltage was lower than the experimental voltage after the first voltage spike, and decreased too quickly during the dwell time (fig. 5.6a). The explanation for the discrepancy was found by examining the simulated temperature, which showed that the EW quickly exceeded the melting point of copper (1358 K) and consequently invalidated the solid temperature-resistance model (fig. 5.6b).

The temperature-resistance model was modified to include the resistivity of liquid copper, using data found in [Dyos and Farrell 1992]. The resistivity of copper increases significantly at the melting point, which caused the second voltage spike to then appear in the simulation. However, the step-increase was too fast, causing the spike to be much too tall. An attempt was then made to smooth out the resistivity transition at the time of melting by modelling the wire as a series of 500 segments, each with their own diameter and temperature. Thermal instabilities were seeded by applying a bell-shaped distribution of diameters with a mean value of the wire diameter

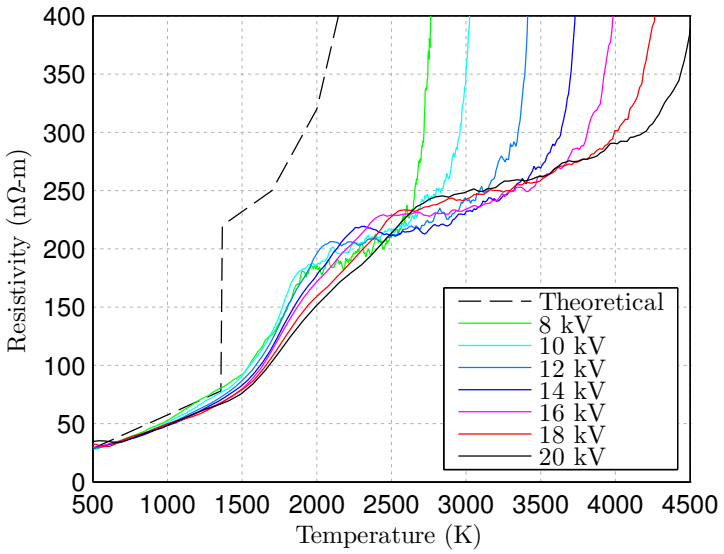

Figure 5.7 Calculated temperature-resistivity data from experimental results, compared to the theoretical data in [Dyos and Farrell 1992]. $\ell = 1.05$ m, $d = 0.2$ mm, $V_0 = 8$ to 30 kV, $E_0 = 7.6$ to 19 kV/m.

and a standard deviation of 1%. Although the simulation could be adjusted to predict that a handful of segments might prematurely vaporise, representing fragmentation and plasma bead formation, the assumptions became too impractical for the model to be believable.

The difficulty in finding a useful temperature-resistance model was illustrated by calculating the actual relationship from experimental results. EW experiments performed at the Institute for High Voltage Engineering in Graz, Austria, provided voltage and current waveforms for this purpose (fig. 5.7). A set of 1.05 m long, 0.2 mm diameter wires, were exploded using a Haefely high current impulse generator with a capacitance of 20 μF. Initial voltages from 8 to 20 kV were used. The energy dissipation, temperature, and wire resistance were calculated from the waveforms. In the calculated curves, the resistance was seen to increase much more slowly with temperature than the theoretical data suggested, although it had approximately the correct shape. The assumption that the wire heated homogeneously was clearly false, and an improvement would require a much more sophisticated model.

5.5 A SIMPLE RESTRIKE PREDICTION MODEL

A simple restrike prediction model was empirically developed. The model was derived from the AEF region of restrike that was found during analysis of Smith's results. The region of restrike was substantiated by analysing a collation of new experiments. The selected results were from EW experiments with diameters of 0.2 to 0.3 mm and lengths of 1 to 9 m. By examining the frequency of restrike produced at each level of AEF, it was found that the region of restrike was between AEF values of 5 and 15 kV/m (fig. 5.8). The frequency does not indicate

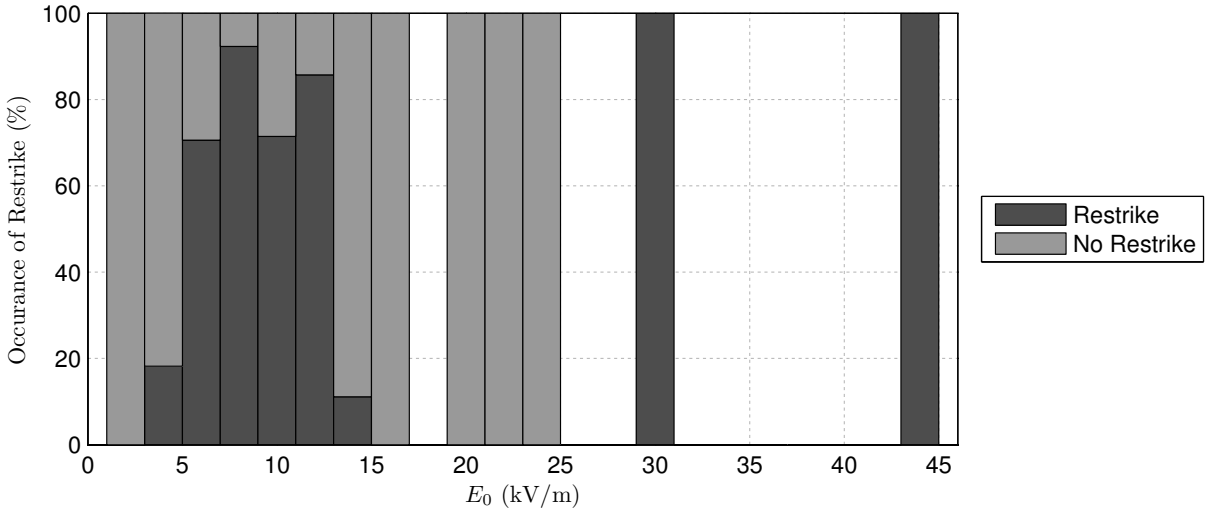

Figure 5.8 A histogram of the occurrence of restrike in EW experiments as a function of the initial AEF, E_0. A total of 86 experiments is represented in this figure.

the probability that an experiment will produce restrike at a given level AEF, but rather the number of experiments that produced restrike, with consideration given to wide variations in the experimental environment during development.

The model was further refined for 0.2 mm wire, which was observed to produce restrike on wires up to 9 m long using an AEF of 4.5 kV/m. After this finding, the use of other diameters of wire was discontinued, because it was considered that 0.2 mm diameter wires could produce restrike using the lowest AEF.

It is interesting to note that in the study of long distance EWs in [Dannenberg and Silva 1969], restrike was not produced using copper wires. However, the study only used AEFs of 11.5 to 29.2 kV/m. It is now known that this falls almost exactly between the upper limit of the plasma bead restrike mechanism and the upper restrike region, which occurs via a different mechanism above 30 kV/m. Had they attempted to use a slightly lower voltage, restrike would have probably been produced.

There were two serious limitations with the simple model for restrike. Firstly, it was observed that shorter wires actually required slightly higher AEFs to produce restrike than longer wires. It was thought that, because the lower voltage results in less energy in the capacitor bank, the voltage reduction during the first phase would be greater. Secondly, it was considered unlikely that the model would be reliable when using capacitor banks with a lower capacitance, again because the voltage reduction during the first phase would be greater. Both of these limitations hinged around the capacitance. So, a set of experiments was performed where the capacitance of the 60 kV capacitor bank was reduced by sequentially disconnecting columns of capacitors, giving capacitance values from 4.3 to 21.4 μF. All experiments used 7 m lengths of 0.2 mm diameter wire. For each capacitance value, the minimum voltage that would produce restrike

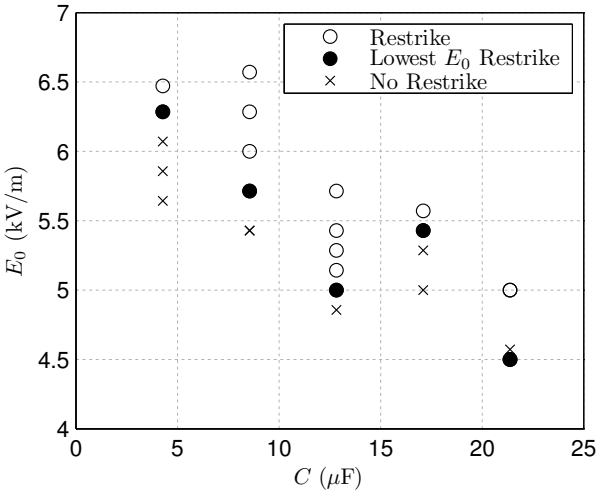

Figure 5.9 Experiments performed to find the minimum AEF needed to produce restrike for various capacitances.

was found. There was a clear correlation between an increase in capacitance and a decrease in the minimum AEF that was required to produce restrike (fig. 5.9).

5.6 A COMPLETE RESTRIKE PREDICTION MODEL

In this section, a model is derived that can predict the occurrence of restrike for any length of wire. The model is based on data that was collated from a variety of experiments using the Marx generator in two- and three-stage configurations.

5.6.1 Finding the First Phase Energy

The first phase energy, W_1, was calculated from the experimental transient current waveforms, $i(t)$, by firstly integrating the current to obtain the charge that leaves the energy supply,

$$Q_1 = \int_0^{t_1} i(t)\, dt \tag{5.8}$$

where t_1 is the end of the first phase, defined by the current falling below 400 A. The first phase energy can be derived from the equations for the charge in a capacitor, $Q = CV$ and the energy in a capacitor, $W = 0.5CV^2$,

$$W_1 = \frac{Q_1^2}{2C} \tag{5.9}$$

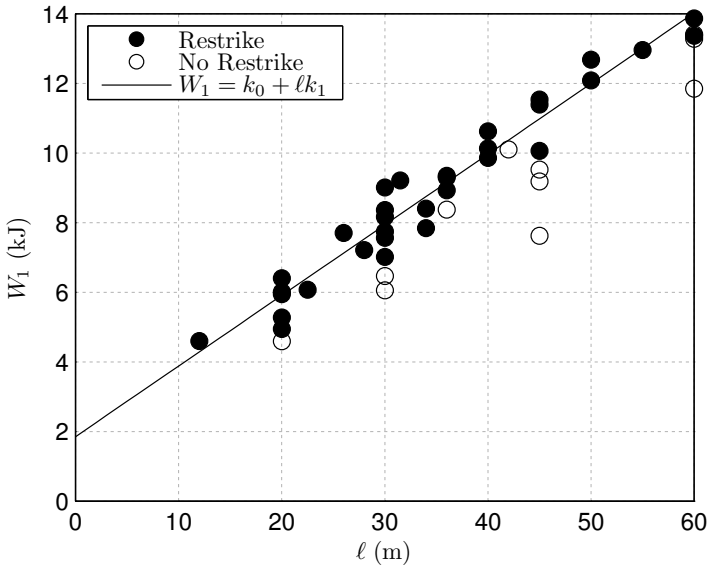

Figure 5.10 The energy dissipated in the first current pulse is correlated with the wire length. Results from two- and three-stage Marx generator configurations are shown. Only the experiments that produced restrike were used to derive the linear fit.

The energy calculated from the transient current waveforms produced a more consistent result than the energy calculated from directly the voltage waveforms. The voltage waveform was too noisy and had an inductive component that was difficult to remove.

W_1 was found to be correlated with ℓ with a linear fit given by

$$W_1 = k_0 + k_1 \ell \tag{5.10}$$

where constants k_0 and k_1 were found to be 1850 J and 203 J/m respectively (fig. 5.10). The regression coefficient of determination for the linear fit was $R^2 = 0.95$. The linear correlation implied that there was a constant amount of energy dissipated per unit length of wire to produce a state that was conducive to the formation of restrike. The constant k_1 is specific to 0.2 mm diameter enamelled copper wire, and would need to be recalculated if other wire types are used. The constant k_0 represents the losses in the energy supply when an average first-phase current waveform flows through the energy supply's resistive components, presumably the majority of which is in the spark gaps. As it will be shown later, this value of k_0 can be adjusted to provide a better fit for the restrike occurrence data.

5.6.2 Finding the Plasma Bead AEF

It was assumed that the formation of plasma beads was due to electrical breakdown of the gas medium in the fragmentation sites and was therefore dependent on the electric field at those

sites. The quantity of plasma beads that formed therefore depends on the AEF at the time of plasma bead formation, E_1. As shown in Chapter 4, the dwell time is caused by the expansion of the plasma beads and the restrike is delayed until they coalesce. Hence, when E_1 increases, and consequently more plasma beads are formed, the dwell time decreases (fig. 5.11). Conversely, when E_1 is insufficient, the plasma beads will deionize before they coalesce. From the two- and three-stage Marx generator results, the minimum E_1 needed to produce restrike, k_E, was 4.0 kV/m and the longest dwell time was 630 μs. The value of k_E is only valid for 0.2 mm diameter enamelled copper wire, and would need to be recalculated if other wire types are used.

The same correlation of dwell time and AEF was presented in [Vlastos 1973a]. In that work, the dwell time of the 'short type' was fitted by an equation derived from the time-varying energy input into the medium surrounding the wire as it attains conditions which will produce a conducting plasma sheath. The equation for the dwell time of the 'long type' was derived from Paschen's law as the electric field is applied to a radially expanding medium described by a shock wave. In both cases, the form of the equation is the same:

$$t_d = \frac{k_d}{E_0 - k'_E} \tag{5.11}$$

where t_d is the dwell time and k_d and k'_E are constants. Because the plasma bead mechanism in this thesis depends heavily on the complicated fragmentation processes, a derivation from first principles was not feasible. However, Equation 5.11 provided a good fit for the the experimental data, with a regression coefficient of determination of $R^2 = 0.79$. The value of k'_E, which determines the asymptote of the fit, was not the same as k_E, presumably because there was a practical limitation on the length of dwell time before the plasma beads deionise.

5.6.3 The Maximum Restrike Length Formulation

The voltage the time of plasma bead formation, V_1, can be related to the first phase energy using an expression for the energy dissipated from the capacitor bank,

$$W_1 = \frac{1}{2}C\left(V_0^2 - V_1^2\right) \tag{5.12}$$

Equating Equations 5.10 and 5.12, and using $V_1 = \ell k_E$, we obtain

$$k_0 + k_1\ell = \frac{1}{2}C\left(V_0^2 - (\ell k_E)^2\right) \tag{5.13}$$

Substituting $V_0 = \ell E_0$ and rearranging for E_0, we obtain

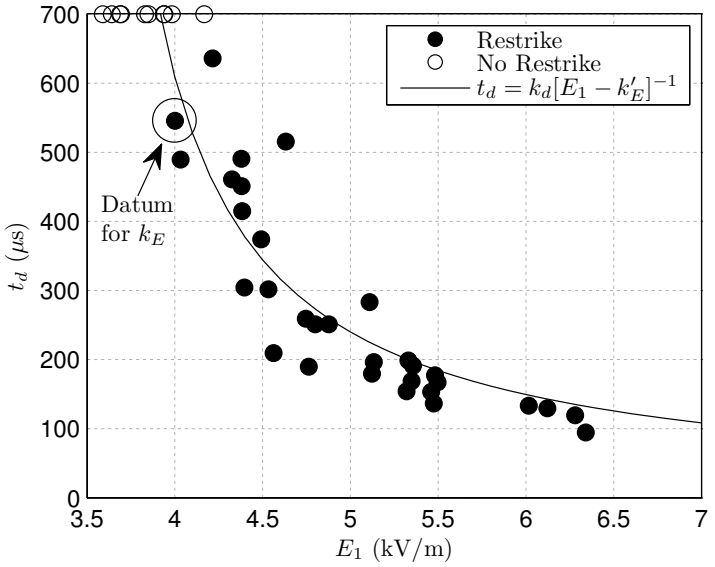

Figure 5.11 The dwell time of the plasma bead restrike mechanism is correlated to E_1. The data from experiments that did not produce restrike have been shown with an arbitrary dwell time in this figure, and were not used in the fit of the curve. The circle denotes the experiment with the lowest E_1 that produced restrike, which determined the constant k_E.

$$E_{0,min} = \sqrt{\left(\frac{2k_1}{C\ell} + \frac{2k_0}{C\ell^2} + k_E^2)\right)} \tag{5.14}$$

an expression for the minimum initial AEF that will produce restrike for a given wire length and energy supply parameters (fig. 5.12). This correctly predicts that using shorter lengths of wire requires a greater initial AEF to produce restrike, a phenomenon that had been noted during this research. It also shows that there is a minimum length of restrike that can be produced with a given energy supply capacitance; shorter lengths that theoretically require an E_0 greater than 11 kV/m will enter the excessive AEF restrike region and therefore will not produce restrike.

Equation 5.13 can also be rearranged to give

$$\ell_{max} = \sqrt{\left(\frac{k_1}{Ck_E^2}\right)^2 + \frac{V_0^2}{k_E^2} - \frac{2k_0}{Ck_E^2}} - \frac{k_1}{Ck_E^2} \tag{5.15}$$

the maximum length of restrike that can be obtained for a given voltage V_0, which is useful for calculating the limits of untested energy supplies.

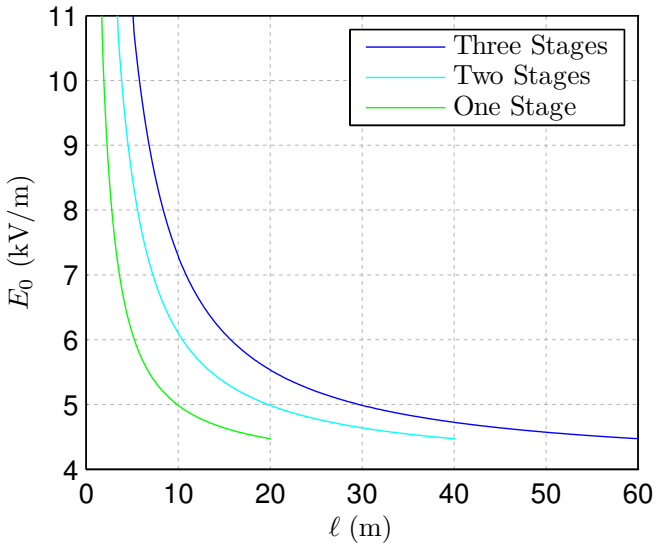

Figure 5.12 The minimum initial AEF that is required to produce restrike as a function of wire length. The three Marx generator configurations are shown.

5.6.4 Capability Diagrams

Capability diagrams are commonly used to allow for the reliable use of service equipment, such as electrical generators. Most of the limitations of the device can be presented in one simple diagram for easy reference. The three limitations for producing restrike were the lower AEF restrike boundary, the upper AEF restrike boundary and the voltage rating of the energy supply. The lower boundary is given by Equation 5.14. The upper AEF restrike boundary was assumed to be a linear boundary at the empirically chosen value of 11 kV/m, represented by

$$\ell = \frac{V_0}{11 \times 10^3} \tag{5.16}$$

The voltage rating of the energy supply, V_{rated}, was integrated into the capability diagram as a straight line at $V_0 = V_{rated}$.

Capability diagrams were constructed for the Marx generator using these three boundaries (fig. 5.12). The values of k_0 were adjusted to provide a better fit for the empirical data at each configuration of the Marx generator. Although the value of k_0 became less significant at longer lengths, where the $k_1\ell$ term dominates the result of Equation 5.10, the point of intersection between the upper and lower boundaries was significantly dependant on k_0. The new k_0 values were 500, 1000 and 1500 J for the one-, two- and three-stage configurations respectively. It was useful to note that k_0 was proportional to the number of stages, hinting that k_0 for new energy supplies could be estimated as $k_0 = 500n$ J, where n is the number of stages in a multi-stage impulse generator. The scatter data on the Marx generator capability diagrams

shows a very good fit, especially around the lower AEF restrike boundary. The upper AEF restrike boundary, which has not been extensively studied, does not give an accurate fit, but rather represents the maximum AEF that will reliably produce restrike.

The capability diagrams have similarities to the voltage-length plane of outcomes presented in [Bhat and Jordan 1971], reproduced in Figure 2.5. The upper and lower AEF restrike boundaries represent the observed limits of the restrike mechanism in both the voltage-length plane and the capability diagrams, although in the voltage-length plane, a different restrike mechanism was observed to occur at voltages immediately above the upper boundary, rather than no restrike.

5.7 CONCLUSIONS

The development of the restrike prediction model began with an analysis of Smith's experimental data. The data provided a diverse set of results by using a wide range of voltages, lengths and wire diameters. Analysis of the results initiated the concept of applying the AEF quantity to long distance EW, and indicated that the region of interest was around $E_0 = 6$kV/m to 12 kV/m. New experiments were then designed, focusing on that region. No obvious trends were found relating ℓ, d and V_0 to the energy dissipated in first phase or occurrence of restrike, so the diameter variable was excluded and experiments focused on 0.2 mm diameter wires. A transient study concluded that although the resistance of the wire can be modelled accurately when in the solid state, beyond the melting point it becomes inhomogeneous. A simple restrike prediction model was presented, which used the initial AEF to predict the occurrence of restrike, with limited accuracy.

Lastly, a complete restrike prediction model was formulated using some assumptions about the plasma bead restrike mechanism and some empirically derived constants. The model used the AEF at the end of the first phase, E_1, as a reliable indicator for the facilitation of restrike. The minimum E_1 that produced restrike, k_E, was determined empirically to be 4.0 kV/m. The energy removed from the energy supply during the first phase, W_1, was linearly related to the wire length with constants $k_0 = 500n$ J and $k_1 = 203$ J/m. An equation for the maximum length of restrike that could be produced was then derived. The three boundaries for producing restrike, which were the upper AEF restrike boundary of 11 kV/m, the lower AEF restrike boundary and the voltage rating of the capacitor bank, could then be used to draw capability diagrams for the production of restrike. The capability diagrams were shown to provide a good fit for the collation of a wide range of experimental data.

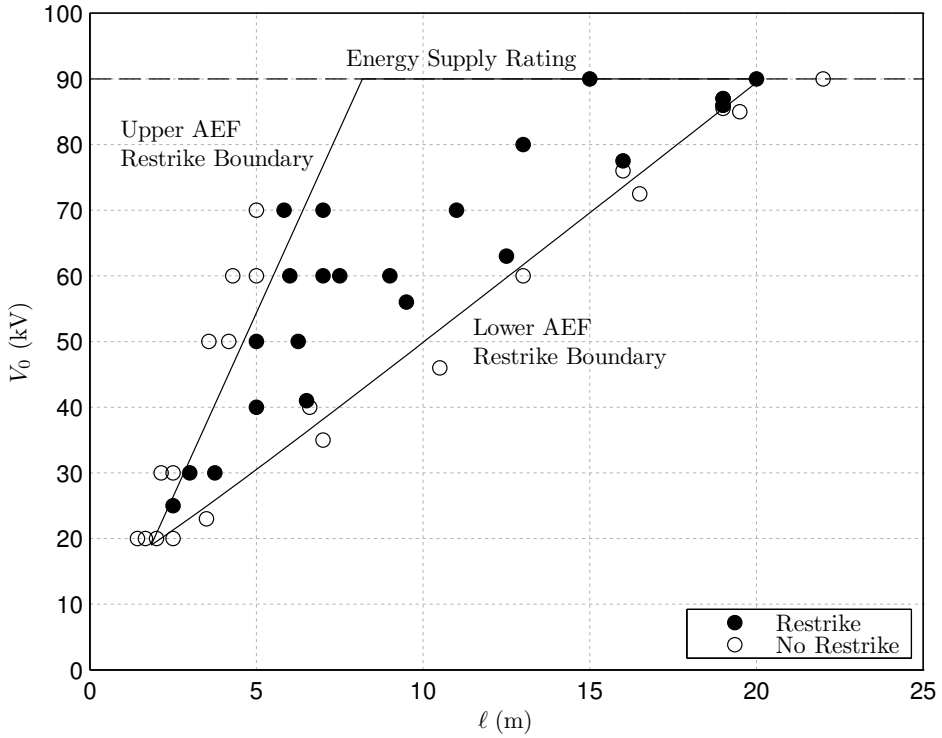

(a) One-stage configuration.

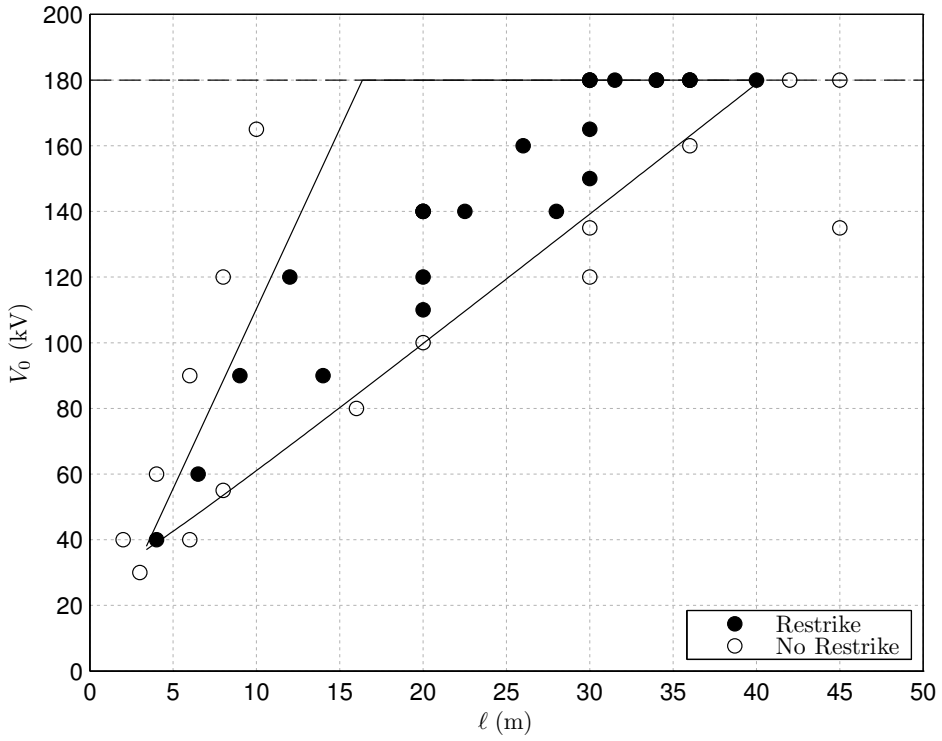

(b) Two-stage configuration.

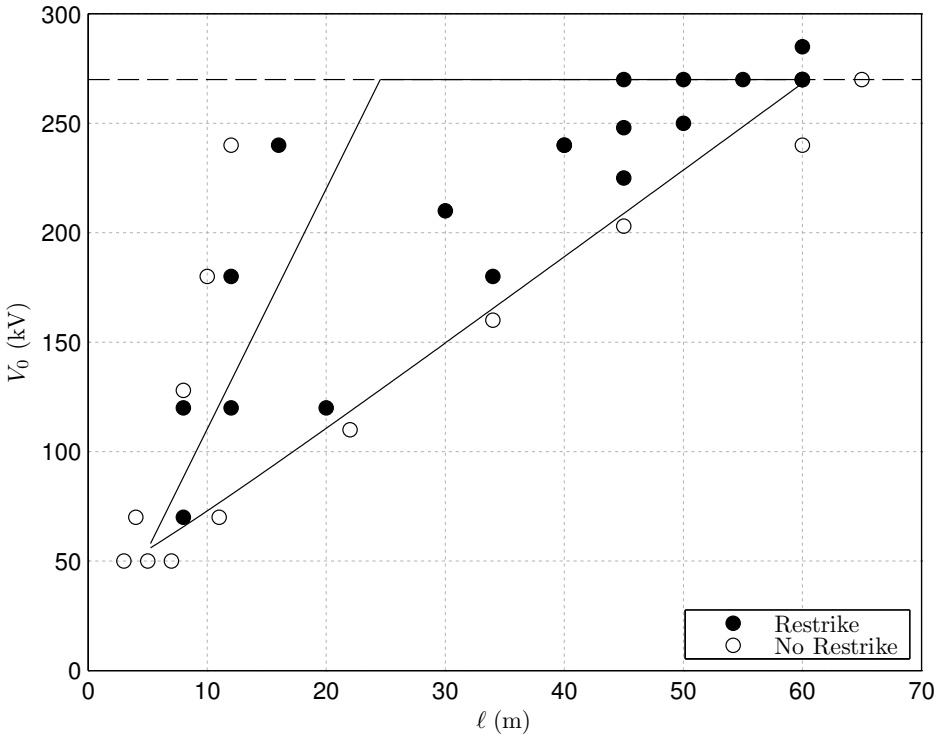

(c) Three-stage configuration.

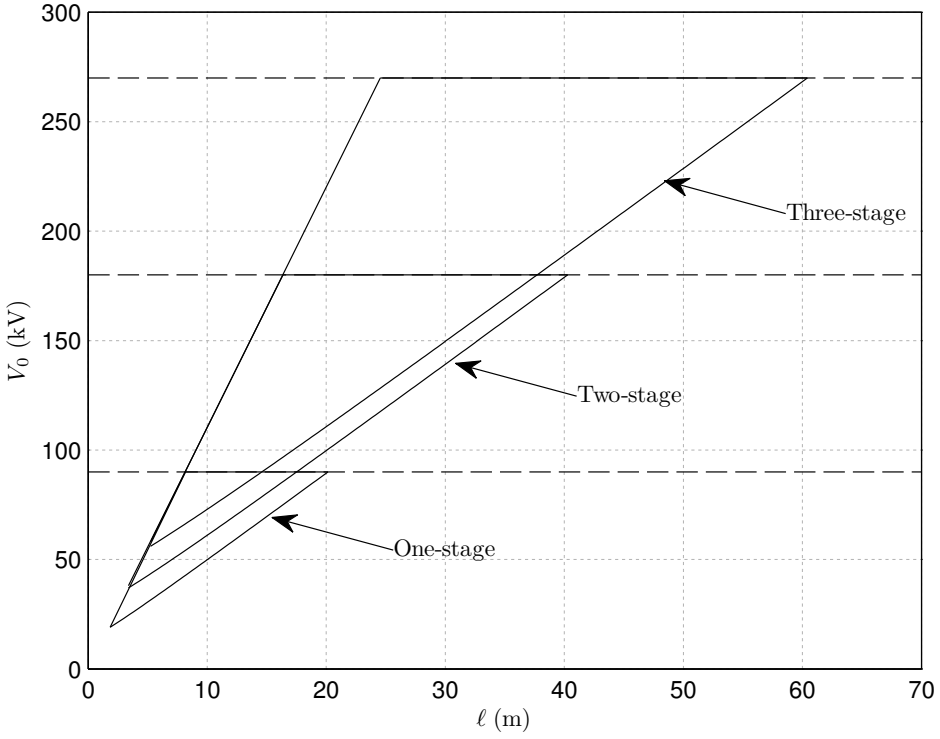

(d) Comparison of all three configurations.

Figure 5.12 Capability diagrams for the Marx generator in its three configurations. The scatter data in (a), (b) and (c) was collated from various relevant experiments. (d) highlights the effect of capacitance on the lower AEF restrike boundary; for any given length, using fewer stages and reducing the capacitance lowers the minimum voltage required to produce restrike.

Chapter 6

PRACTICAL LONG DISTANCE EW EXPERIMENTS

6.1 INTRODUCTION

The restrike prediction model has enabled the reliable creation of long plasma channels, which are arguably the longest arcs of their type to date. However, the practicalities of creating such long arcs are not always straightforward. This chapter describes the practical aspects of long distance EW experiments, both to give the reader an appreciation for the scale of the arcs and to aid future researcher groups who are looking to create their own long arcs.

EW experiments in this research have been performed in several environments: inside the laboratory, in the laboratory's outdoor compound, off the laboratory's earth grid, and completely off-site in a rural setting. The experimental environment that was described in Chapter 3 only covers the first of these; the others have additional operational considerations, largely pertaining to safety. Examples of experiments performed in each of these environments are presented. The use of a thin wire as a return path for the EW current is also presented, because it is an important tool for future applications of long arcs.

6.2 LONG DISTANCE EXPLODING WIRE EXPERIMENTS

6.2.1 Inside the Laboratory

Most of the experimental work in this research was performed inside the laboratory. The laboratory features a local earth grid and lockable doors to control access to the high voltage area. Other advantages of experimenting in the laboratory were that no safety observers were required to keep the public safe, the noise did not disturb others, and inclement weather did not hinder experiments. There was enough floor space to do experiments up to 9 m long in a straight line, and for longer experiments, the EWs were zigzagged across the room (figs. 6.1 and 6.2).

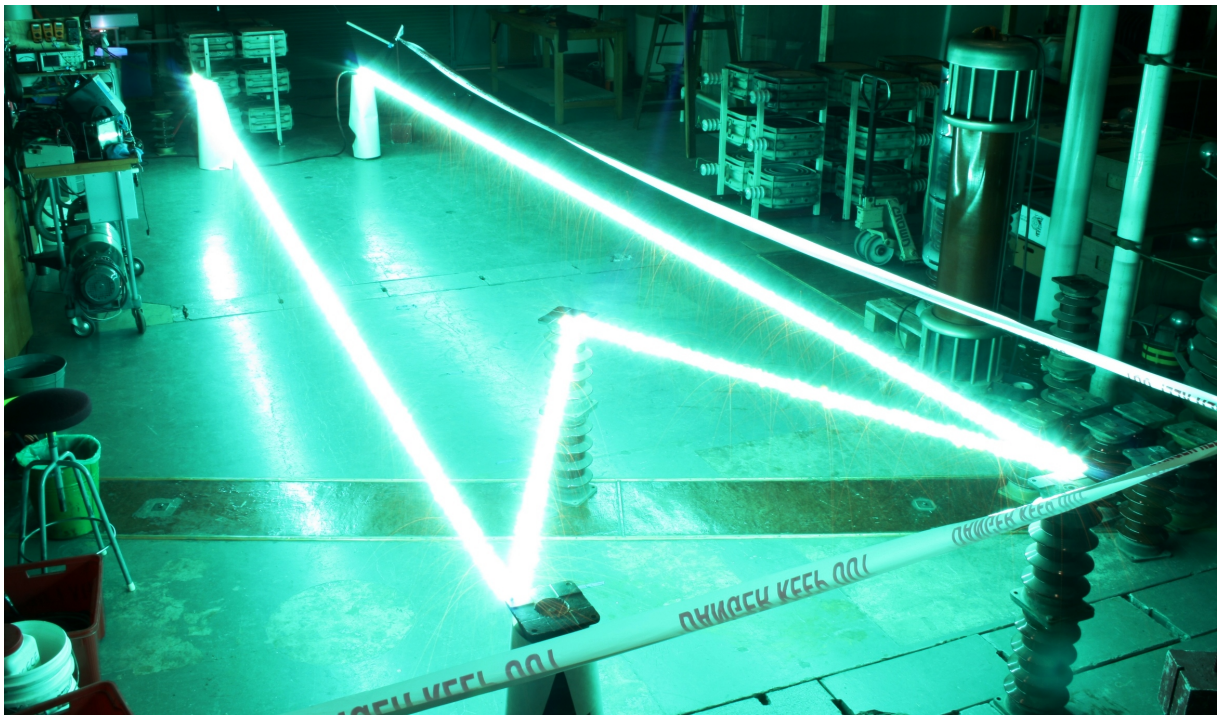

Figure 6.1 A 20 m restrike inside the laboratory, performed while commissioning the one-stage Marx generator. $\ell = 20$ m, $d = 0.2$ mm, $V_0 = 90$ kV, $E_0 = 4.5$ kV/m.

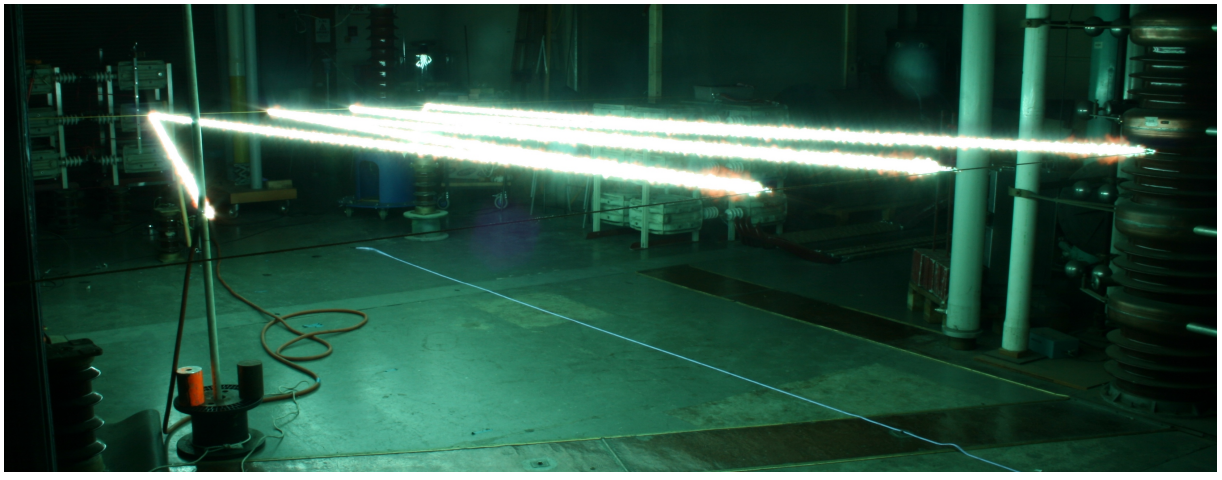

Figure 6.2 A 40 m restrike inside the laboratory, performed while commissioning the two-stage Marx generator. $\ell = 40$ m, $d = 0.2$ mm, $V_0 = 180$ kV, $E_0 = 5$ kV/m.

6.2.2 In the Laboratory Compound

EW experiments in a straight line that were longer than 9 m were performed outside the laboratory. The laboratory had an outdoor compound area, similar in size to the laboratory building, which was also connected to the laboratory's earth grid. The compound was surrounded by a 2 m tall security fence. The wall of the laboratory closest to the Marx generator contained a full-height roller door, allowing access to the compound with sufficient clearance to the high voltage conductors. The output of the Marx generator was connected to a 6 m long aluminium tube 'bus-bar' that was suspended by 2 m tall fibreglass structures, allowing the EW to be connected to the end of the bus-bar outside.

Outdoor experiments required at least one, and sometimes up to three safety observers, who were given radio transmitters to keep in contact with the operators in the Faraday cage. The safety observers ensured that no one was close to the laboratory or its compound during experiments, isolating the hazard of step and touch potentials that could appear during an EPR of the laboratory's earth grid. The University of Canterbury security team was informed before the start of an experimental session, in case someone reported gunshots or explosions on the campus. The New Zealand Police were informed before performing experiments that could be heard in the surrounding neighbourhood, such as vertical experiments that extended above the height of the surrounding buildings. An air horn was used to signal the start of an experiment to prevent unnecessary stress and disturbance to other people working nearby.

The following is an example of one of the more audacious experiments performed in the compound. During a demonstration day, a 40 m crane was volunteered to the University for the purpose of suspending EWs vertically, giving the effect of artificial lightning. The crane was parked outside the compound, but was bonded to the laboratory earth grid using two 95 mm^2 conductors in case there was a fault to the crane. Because there was no earth grid under the crane, an especially significant touch potential hazard had been created, and so the crane was fenced off using a temporary 'danger' tape perimeter. Safe viewing locations were also delineated using danger tape (fig. 6.3). A 1.5 m long fibreglass insulator was suspended from the crane hook, and the EW and a 95 mm^2 return cable was bolted to the end of the insulator. The height between the bottom of the insulator and the ground was measured using a nylon string with pre-marked lengths. To prepare the EW, the crane operator slowly raised the hook until the desired height was reached and then retreated to a safe viewing area. When the safety observers reported that everyone was in the safe viewing areas, the capacitor charging could commence. The turn-around time between experiments was approximately 10 minutes.

The maximum EW length from the bottom of the insulator to the end of the bus-bar was 36 m. The two-stage Marx generator was used as the energy supply at a discharge voltage of 180 kV, resulting in an AEF of 5 kV/m. Although it was not available at the time, the capability

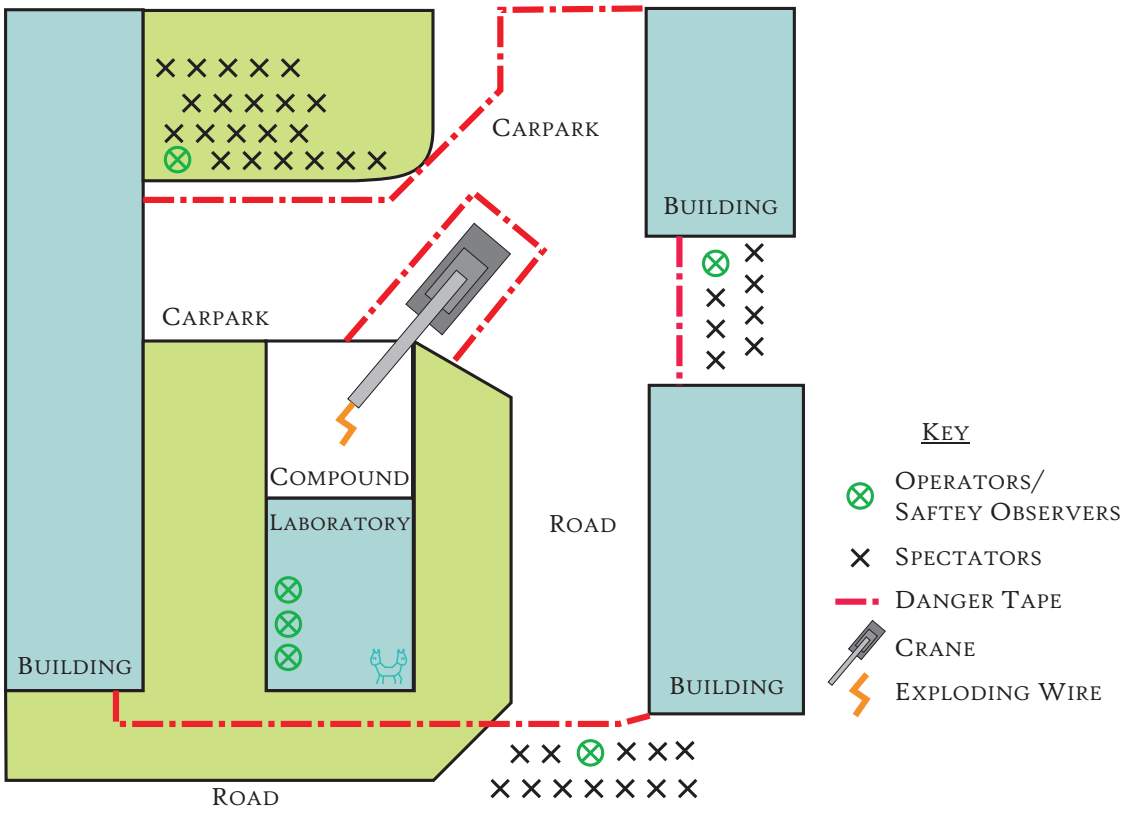

Figure 6.3 The plan view diagram of the layout used for the crane experiments.

diagram in Figure 5.13b shows that this configuration was well within the restrike region; when creating long arcs for demonstrations it is not necessary to operate on the limit of restrike in case experimental variation causes the restrike mechanism to fail. Also, operating at a higher AEF provides more energy to discharge into the arc, resulting in a more spectacular display. The night before the demonstration, some practice experiments were performed (fig. 6.4). On the day of the demonstration, three successful experiments were performed in front of approximately 100 people (fig. 6.5).

6.2.3 Off the Laboratory Earth Grid

Experiments that did not fit into the laboratory's compound could only be performed after-hours, when there was almost no one on campus and the car park was empty. Then, the gates at the end of the compound could be opened, allowing 60 m experiments in a straight line to be performed across the car park. Locating the EW off the laboratory's earth grid created an elevated risk of an EPR, should there be a fault to the ground. Safety observers were again employed to ensure that no spectators or passers-by were close to the earth grid. The car park area also had many points of access, including external doors to adjacent buildings, which were controlled using danger tape.

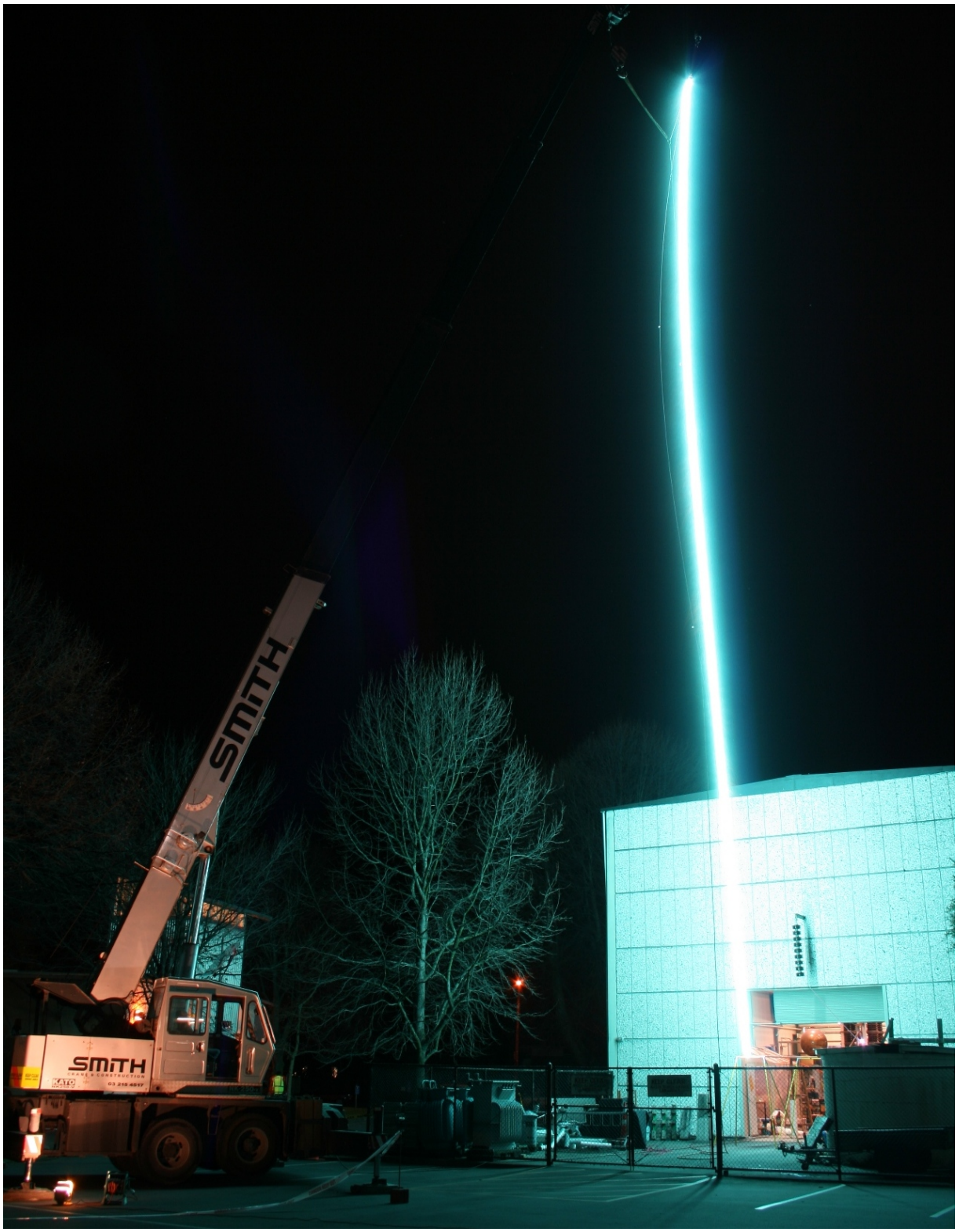

Figure 6.4 A night-time EW experiment performed while preparing for a demonstration. $\ell = 36$ m, $d = 0.2$ mm, $V_0 = 180$ kV, $E_0 = 5$ kV/m.

Figure 6.5 A 36 m vertical restrike produced with an EW suspended from a crane as part of a demonstration. Public observers can be seen in the foreground and also behind the laboratory. A weather observer at the University mistook the experiment for 'dry-day lightning'. $\ell = 36$ m, $d = 0.2$ mm, $V_0 = 180$ kV, $E_0 = 5$ kV/m. Photo credit: Philippa Martin.

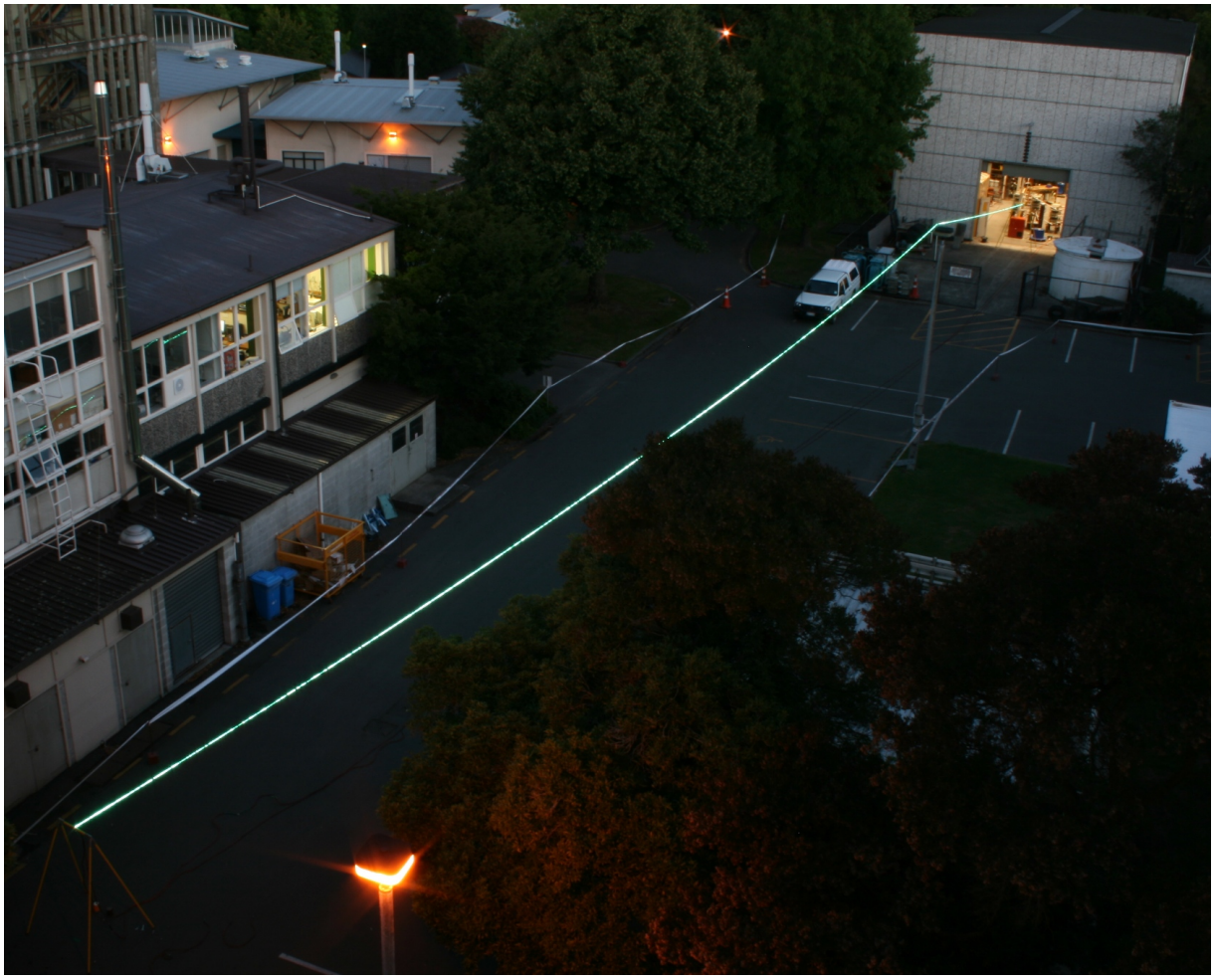

Figure 6.6 A 60 m experiment outside the high voltage laboratory that did not produce restrike. The plasma beads were very close to forming a continuous plasma column. A tree was obscuring the a short section of the wire in the middle of the image. $\ell = 60$ m, $d = 0.2$ mm, $V_0 = 270$ kV, $E_0 = 4.5$ kV/m. Photo credit: Ryan van Herel and Stewart Hardie.

The EW was connected between the end of the bus-bar and a fibreglass support structure at the end of the car park. The wire was also supported by two intermediate insulators built from PVC pipes. Two parallel 95 mm^2 return cables, laid on the ground, provided the return path from the end of the EW. Two 60 m experiments, using $V_0 = 270$ kV ($E_0 = 4.5$ kV/m), did not produce restrike, but photographs of the plasma beads showed that they were very close (fig. 6.6). A 60 m EW with $V_0 = 285$ kV ($E_0 = 4.75$ kV/m) produced restrike (figs. 6.7 and 6.8).

Figure 6.7 A 60 m restrike outside the high voltage laboratory. $\ell = 60$ m, $d = 0.2$ mm, $V_0 = 285$ kV, $E_0 = 4.75$ kV/m. Photo credit: Ryan van Herel and Stewart Hardie.

Figure 6.8 A 60 m restrike outside the high voltage laboratory. $\ell = 60$ m, $d = 0.2$ mm, $V_0 = 285$ kV, $E_0 = 4.75$ kV/m. Photo credit: Kylie Hills.

6.3 THIN RETURN WIRES

A limiting characteristic of the long distance EW experiments presented so far was that thick and heavy return cables were used as a return path for the impulse current. Vertical EW experiments were therefore difficult to perform because the return cables, which weighed approximately 900 g/m, had to be suspended. The multiple-diameter experiments (Section 4.6.2) had previously demonstrated that a thin wire in series, not much thicker than the EW itself, could conduct the impulse current without exploding. A thin return wire, such as 0.63 mm diameter copper wire that weighs just 3 g/m, can be lifted by small vehicles such as weather balloons, rockets or model aircraft. This effectively doubles the possible length of vertical experiments, which would otherwise have to form a 'V' back to the ground.

6.3.1 Capability Diagrams

A set of EW experiments were performed to determine the restrike prediction model constants when a 0.63 mm diameter wire was used as the return conductor for 0.2 m diameter, enamelled copper EWs. The value of k_0 was assumed to be similar to the value used with thick return cables, which was 500 J per Marx generator stage (Section 5.6.4), because the first-phase current waveforms were very similar. The experiments were designed to cover a range of lengths, 4 to 7 m, to increase the accuracy of the linear fit of W_1. To produce a good approximation for k_E, experiments were performed with small incremental reductions in E_0 at each length until restrike was no longer produced. The constants were found to be: $k_1 = 221$ J/m and $k_E = 5.4$ kV/m (fig. 6.9). The capability diagram was then drawn for the 60 kV capacitor bank using a 0.63 mm return conductor, and was confirmed to provide a good fit for the experimental results (fig. 6.10a). Capability diagrams could then be constructed for other energy supplies, such as the one-stage Marx generator (fig. 6.10b).

6.3.2 Off-Site Experiments

A mobile experimental system was created to perform long distance EW experiments away from the laboratory. This was done for several reasons: to prove the feasibility of performing the experiments with a new mobile system; to test weather balloons as a method of supporting EWs; and to test theories on atmospheric electricity.

The one-stage Marx generator circuit was reconstructed onto two small trailers and towed out to a rural site in Port Levy, Canterbury, New Zealand (fig. 6.11). The charging circuit was put on a single-axle trailer and the capacitor banks were put on a double-axle trailer. At the site, a temporary earth grid was constructed using ten sections of 1.2 by 2.4 m steel tread plate,

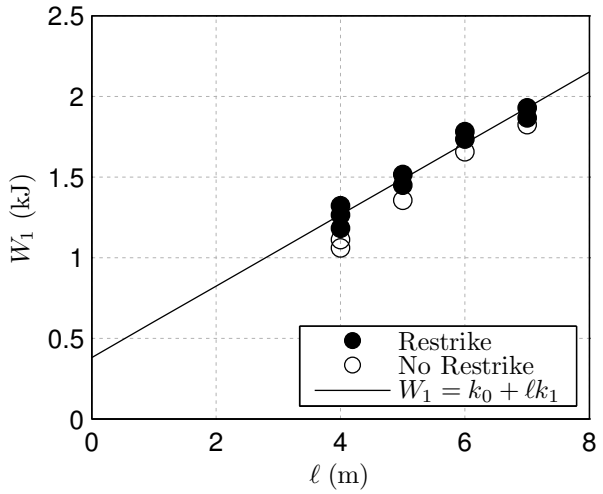

(a) $k_1 = 221$ J/m.

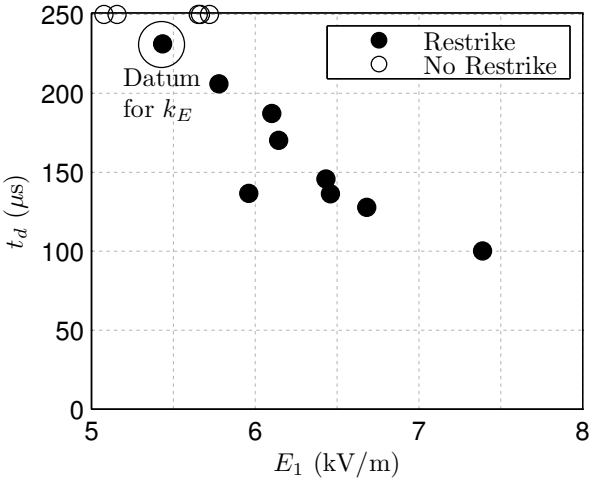

(b) $k_E = 5.4$ kV/m.

Figure 6.9 Experimental results from EWs with 0.63 mm return wires that were used to determine new values for k_1 and k_E. ℓ =4 to 6 m, d =0.2 mm, V_0 =22 to 42 kV, E_0 =5.4 to 7.5 kV/m.

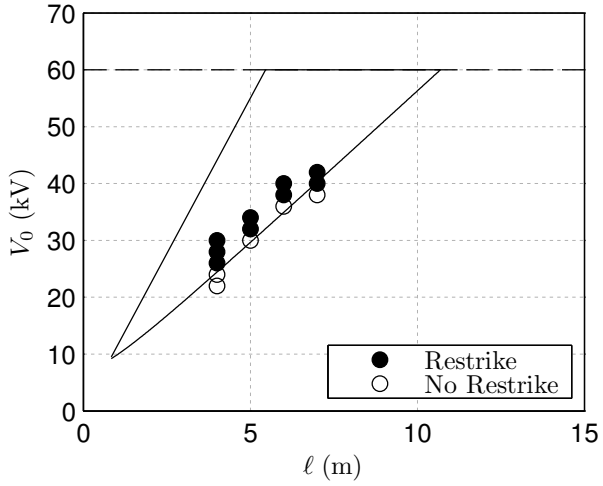

(a) 60 kV capacitor bank.

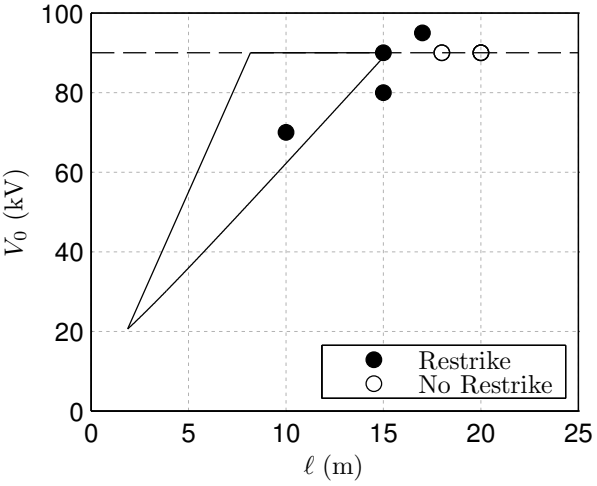

(b) One-stage Marx generator.

Figure 6.10 Capability diagrams for the 60 kV capacitor bank and the one-stage Marx generator for EW experiments using a 0.63 mm return conductor. The scatter data for the 60 kV capacitor bank diagram is from the experiments used to determine the new constants, and the data for the one-stage Marx generator diagram is from the Port Levy experiments.

Figure 6.11 The mobile experimental system at Port Levy, Canterbury, New Zealand.

which were bonded together with twin 95 mm^2 conductors. This was done to mitigate dangerous EPR that would be created if the wire broke and injected current into the ground. The earth grid provided an equipotential zone for operators to leave the control area and approach the capacitors to apply temporary earth sticks. The control area was protected from explosions by a shelter that was constructed from tread plate and polycarbonate, and bonded to the earth grid. In the absence of a grid-connected electricity supply, the charging circuit was energised using a 2 kW petrol generator.

Some horizontal experiments were done to commission the mobile system; a 0.2 mm diameter, 10 m long EW was formed into a 5 m long horizontal 'V' shape, supported by insulated fence posts. Restrike was achieved using 70 kV. Vertical experiments then commenced, using a helium-filled weather balloon to lift the 0.2 mm diameter wire and the 0.63 mm diameter return wire. Restrike was produced using lengths of 15 and 17 m with 90 and 95 kV respectively (fig. 6.12). The results were plotted on the one-stage Marx generator capability diagram in Figure 6.10b. While the fit, which was determined from experiments in the laboratory using the 60 kV capacitor bank, is sufficiently accurate for designing new experiments, it could be improved by recalculating the restrike prediction model constants using a larger data set.

Although the weather on the day of the experiments was mild, there was still a light breeze of 5 to 10 kilometres per hour that caused the weather balloon to move erratically. During the

Figure 6.12 A 15 m restrike prduced by an EW that was suspended from a helium-filled weather balloon. The 0.63 mm diameter return wire was also suspended from the balloon. $\ell = 15$ m, $d = 0.2$ mm, $V_0 = 90$ kV, $E_0 = 6$ kV/m.

capacitor bank charging of one experiment, the movement was enough to break the 0.2 mm wire, which then landed on the charging circuit and caused a short circuit. It was concluded that the weather balloon technique was only appropriate in fair weather with low altitudes, as the wind strength usually increases with altitude. The use of alternative vertical vehicles, such as rockets or model aircraft, may improve the reliability and altitude range of the experimental system.

6.4 CONCLUSIONS

The exploration of the long distance restrike mechanism has necessitated the development of several different experimental environments. These environments have been described in detail to allow future researchers to more easily perform their own experiments. The main conclusion from this chapter is that practical steps can be taken to realise EW experiments virtually anywhere. Experiments inside a high voltage laboratory are the simplest, because the laboratory is likely to have been designed to handle the impulse currents that are associated with high voltage research. Many high voltage laboratories have an outdoor compound, used for testing large equipment or 'wet' tests. It has been shown that such an outdoor compound can provide a suitable area for performing EW experiments and impressive demonstrations of long arcs. Furthermore, with sufficient consideration to safety, EW experiments can be extended off the laboratory's earth grid. In this environment, the major additional considerations are restricting public access, both to protect them from the explosion and to isolate the EPR hazard.

It was also shown that experiments can be performed completely independent of the laboratory. A mobile experimental system was constructed and tested for this purpose. The off-site experimental environment required the creation of a temporary earth grid that allowed operators to move around in an equipotential zone. The off-site environment, which provided extra space and isolated the experiments from the public, also facilitated new vertical experiments, supported by a weather balloon and using a 0.63 mm diameter return wire. Using modified empirical constants for the restrike prediction model, new capability diagrams were drawn for the use of thin return wires.

Chapter 7

FUTURE WORK

7.1 INTRODUCTION

There now exists a reliable method of creating long distance plasma conductors. While there are still improvements to be made to the method, such as validating the model at longer lengths and refining the upper AEF restrike boundary, much of the future research in this area will be in applications of the plasma conductors. It is impossible to predict what the applications may be, and which of these might create significantly useful advancements in technology. Instead, this chapter includes a few interesting applications of plasma conductors that have become apparent during the course of this research.

7.2 RESTRIKE PREDICTION MODEL EXTENSIONS

7.2.1 Longer Arcs

The experiments performed at the University of Canterbury reached the limits of the available equipment. The longest arc that was produced was 60 m long, using a voltage of 270 kV. However, it is expected that with different equipment, much longer arcs could be produced; there is no known theoretical limit to the plasma bead restrike mechanism, only a practical limitation of the voltage rating of the energy supply. Commercial high voltage impulse generators, which are usually used for industry testing of high voltage equipment by applying simulated lightning or switching surges, could be an ideal energy supply for EW experiments.

The restrike prediction model developed in this research allows for the performance of untested energy supplies to be estimated. Equation 5.15 was employed to calculate the maximum length of restrike that could be produced using data-sheet specifications of commercially available high voltage impulse generators (Table 7.1). ℓ_{max} was calculated for circuits both using a thick return cable and using a 0.63 mm diameter return wire. The constants were $k_1 = 203$ J and $k_E = 4.0$ kV/m for the thick return cable circuit and $k_1 = 221$ J and $k_E = 5.4$ kV/m for

Manufacturer	Model	V_0 (kV)	W_0 (kJ)	C (nF)	n	ℓ_{max}[1] (m)	ℓ_{max}[2] (m)
Haefely	SGSA[3]	500	25	200	5	71	58
		800	40	125	8	114	92
	SGΔA[4]	1,200	60	83	12	170	138
		2,000	100	50	20	284	230
		2,600	130	39	26	372	300
	SGVA[5]	4,000	200	25	20	591	477
		6,000	300	17	30	896	722
		8,000	400	25	40	1530	1180
		10,000	500	25	50	2020	1540
High Volt	Series L [6]	1,200	60	83	12	170	138
	Series M[7]	2,400	200	69	24	426	332
	Series G[8]	6,000	900	50	30	1260	953

[1] Using a thick return cable.
[2] Using a 0.63 mm diameter return wire.
[3] [Haefely Test AG b]
[4] [Haefely Test AG a]
[5] [Haefely Test AG c]
[6] [Highvolt Prftechnik Dresden GmbH a]
[7] [Highvolt Prftechnik Dresden GmbH c]
[8] [Highvolt Prftechnik Dresden GmbH b]

Table 7.1 A selection of commercially available impulse generators, their specifications, and the estimated maximum restrike length that they could produce.

the 0.63 mm diameter return wire circuit. The energy supply loss constant was calculated as $k_0 = 500n$, where n is the number of stages. The calculations show that arcs of several hundred metres, or even up to 2 km, are theoretically possible.

7.2.2 Quantifying the Model's Uncertainty

The sample size of data collected in this work was limited, especially with experiments using longer lengths of wire, due to the difficult and time-consuming nature of the experiments. This meant that the statistical probability of restrike could not be analysed. However, it was noted that experiments that lay very close to the upper or lower restrike boundaries did not always perform as expected. To make the restrike prediction model more useful, the uncertainty of the restrike prediction could be investigated. Study of the uncertainty may also lead to further insights about the EW mechanisms.

7.2.3 Understanding the Upper Restrike Boundary

The upper AEF boundary for the reliable production of restrike has been taken to be 11 kV/m. This was an empirically chosen value that was determined from the majority of experiments to

date; there were almost no experiments that did not produce restrike at this AEF. For the one- and two-stage Marx generator configurations, there were almost no experiments that produced restrike with an AEF over 11 kV/m (fig. 5.12). However, the three-stage configuration produced restrike with as high as 15 kV/m.

The mechanism that caused restrike to fail to occur with excessive AEF was only examined briefly in Chapter 4. Further observations are needed to better understand the mechanism, which may be intriguing in itself. Once the mechanism is understood, the upper AEF boundary of restrike can be refined and added to the restrike prediction model.

7.3 TRIGGERING LIGHTNING

The artificial triggering of lightning from thunderclouds has been a research goal for many decades, or even centuries. Triggered lightning has been used for the study of natural lightning, and has potential applications in the protection of infrastructure, such as communications and electricity supply equipment. A comprehensive study of triggered lightning was conducted at the International Center for Lightning Research and Testing (ICLRT) at Camp Blanding, Florida [Rakov *et al.* 2005]. Small rockets were used to extend 0.2 mm diameter, Kevlar-coated copper wires several hundred metres upwards. The rockets were launched during thunderstorms when the electrostatic field at ground level was approximately 6 kV/m. The rapid introduction of the conductor into the cloud-to-ground air gap caused the initiation of a stepped leader from the rocket's tip. The stepped leaders then propagated towards the clouds and sometimes subsequently caused a lightning strike. The lightning hit the rocket's launch tower where extensive instrumentation was poised to record the strikes.

7.3.1 Atmospheric Partial Discharge

Vertical EW experiments, described in Section 6.3, were performed outside at a rural location near Port Levy, Canterbury, New Zealand. Lengths of 0.2 mm diameter wire were extended up to 17 m vertically using a helium-filled weather balloon. The return cable was a 0.63 mm diameter copper wire, which was also suspended from the balloon. The current waveforms recorded during the experiments were considered to be normal except for the appearance of extra 'packets' of charge during the restrike, which were reminiscent of partial discharge (PD) (fig. 7.1). The PD appears as small spikes superimposed onto the current waveforms, each of which have peaks of approximately 200 A and carry a charge of between 0.37 and 0.82 mC. On the 17 m waveform, two PD spikes appeared (Q_2 and Q_3), separated by 200 μs. PD appears on the vertical experiments but does not appear on the horizontal experiment. The charge is much larger than what could have been attributed to PD occurring in the insulation of the energy

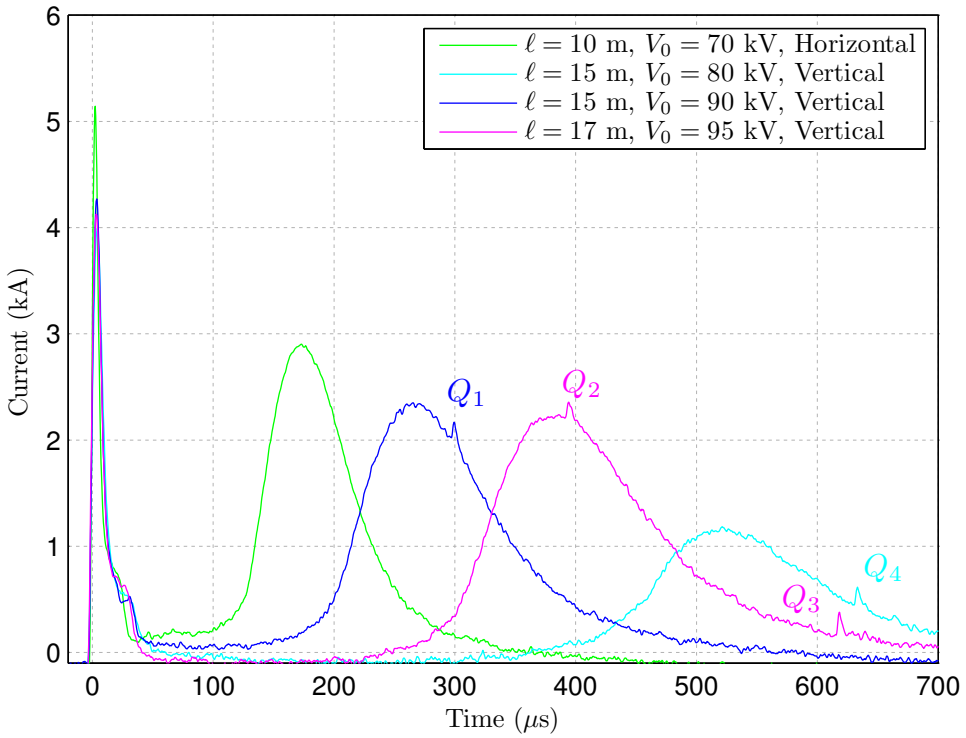

Figure 7.1 Current waveforms from outdoor experiments at Port Levy. The positions of the PD charge packets are indicated. $Q_1 = 0.37$ mC, $Q_2 = 0.52$ mC, $Q_3 = 0.82$ mC and $Q_4 = 0.54$ mC.

supply equipment itself; PD in insulation systems is usually in the order of pC to nC. PD has never been detected in any other EW experiments, and there was no other plausible source for the charge packets coming from within the equipment itself. However, the experiments need to be repeated to confirm that the currents were not an instrumentation anomaly and do actually flow in the EW circuit.

A possible explanation for the charge packets is that the vertical plasma conductors initiated a type of PD in the atmosphere. In the study of lightning, such discharges are referred to as 'stepped leaders', and are the precursor of lightning. Stepped leaders have been determined to carry charge in the order of milli-Coulombs, have peaks of several hundred Amps, and delays between steps of up to hundreds of microseconds [Uman 2000]. All of these quantities are in the same order of magnitude as the PDs detected on the current waveforms, implying that the PDs could be stepped leaders launching off the tip of the EW. The PD currents could flow in a circuit from the stepped leaders, through the capacitance between the air and the earth, through the earth connection of the EW circuit, and up the EW and return wire (fig. 7.2). The currents could be measured in future experimentation using a current transformer on the earth connection of the EW circuit, thus confirming the nature and origin of the PD currents.

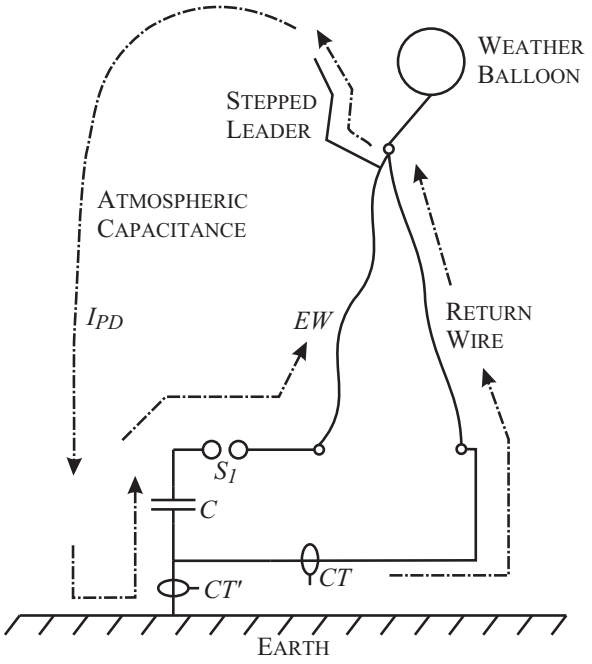

Figure 7.2 The circuit in which PD currents could flow, induced by the formation of stepped leaders. The PD currents should be detected by CT'.

7.3.2 An Atmospheric Triggered Spark Gap

An air gap with an applied electric field can be induced to break down by introducing a triggering spark. The triggering spark is a rapidly introduced protrusion of space charge , which effectively transforms the sphere-to-sphere gap into a point-to-sphere gap [Kuffel and Bera 1968]. The intensified electric field at the point may then cause the inception of a streamer, which will propagate towards the opposite sphere. This breakdown mechanism was central to the operation of the TSG used in this research, which provided controllable and reliable triggering of the EW circuit. The rocket-triggered lightning at ICLRT operates in a similar manner; the rapid introduction of the wire into the atmospheric air gap effectively transforms the relatively smooth ground electrode into a point. The polarity of the main gap and the triggering spark is crucial to the efficacy of the system. The best results are achieved when the triggering spark is on the positive sphere and the triggering spark is of positive polarity (fig. 7.3).

Conductors that protrude into the atmospheric electric field, such as towers or other tall structures, cause the generation of a blanketing layer of positive space charge that acts to reduce the local electric field [Becerra *et al.* 2007]. The likelihood of upward streamer inception is subsequently reduced. The time constant of the space charge accumulation is approximately 10 s [Uman 2000], so the rapid introduction of a conductor using a rocket or similar device is much more likely to initiate lightning. However, if the protruding conductor is an EW, the highly ionised plasma may act to quickly modify local space charge, and create an intensification of

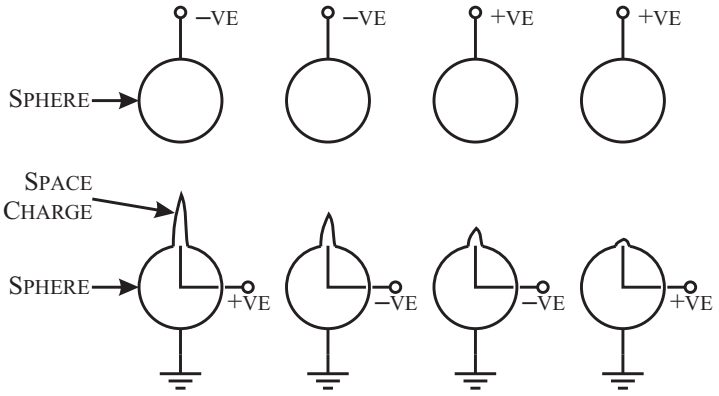

Figure 7.3 Diagrammatic representation of space charge in a triggered spark gap under four polarity permutations [Kuffel and Bera 1968].

electric field, aiding the inception of an upwards streamer. A long plasma conductor, pulled with a rocket towards a thundercloud, could markedly improve the efficacy of the rocket triggered lightning system.

7.3.3 Vertical Carriage of the Wire

A conclusion from the vertical EW experiments performed at Port Levy was that although a helium-filled weather balloon can successfully lift the EW and return wire, even a slight amount of wind causes erratic motion of the balloon and can lead to the wire breaking. There are several alternative vehicles capable of vertically lifting the wires to heights of several hundred metres or more. Two suggestions are rockets and remote-controlled model aircraft. Rockets have the advantage of very rapid introduction of the EW into the atmosphere, and have been shown to be effective with traditional rocket triggered lightning. The main disadvantage of using rockets is that they can be expensive, difficult to launch and require a wire spooling system to quickly pay out the wire without breakage. Model aircraft may be able to introduce the wire in a much more controlled, albeit slower, manner. Some 'quad-rotor' helicopter designs would be especially suitable because they can offer simple and accurate position control (fig. 7.4).

7.4 SUSTAINED PLASMA

The plasma conductors that have been formed in EW experiments to date were short lived. The conductors, created by restrike, only remained ionised and confined as long as sufficient current was flowing through them. The lifespan of the conductors was constrained by the storage limitations of the capacitor banks, which was usually from 100 to 200 μs. Sustaining plasma conductors for several milliseconds, seconds, or even continuously is a feasible research goal for the future, and could be used either for study of the plasma itself or for specific applications.

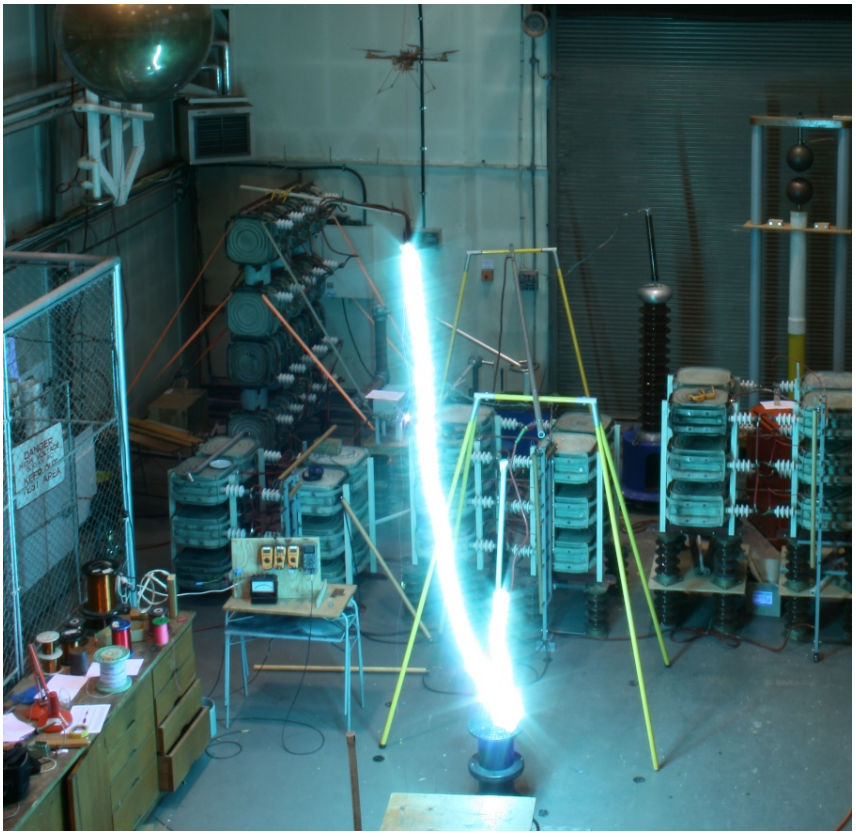

Figure 7.4 An EW and 0.63 mm diameter return wire suspended from a quad-rotor helicopter (pictured at the top of the photograph). This photograph is from a project by Honours student Yanosh Irani, using a quad-rotor helicopter built by PhD candidate John Stowers. $\ell = 4$ m, $d = 0.2$ mm, $V_0 = 30$ kV, $E_0 = 7.5$ kV/m.

There are two key challenges in the pursuit of sustaining a plasma conductor. Firstly, a suitable 'sustaining supply' must be found that can deliver sufficient current, voltage and power to sustain the conductor. To give a rough estimate of the power consumption of an EW arc, the time-varying conductance of the restrike plasma was calculated. It was assumed that the inductive component of the voltage was negligible, so the conductance at time t is

$$G(t) = \frac{i(t)}{v(t)} \tag{7.1}$$

where $v(t)$ and $i(t)$ are the time-varying voltage and current, respectively. An example of the calculated conductance is shown in Figure 7.5. The peak conductance of the plasma, G_p, was highly variable, but appeared to be partially dependent on E_0 (fig. 7.6). Peak conductance values of about 20 mS were common in experiments with AEFs near the lower restrike boundary.

The minimum current that could sustain a plasma arc, I_m was also estimated. In most experiments, the conductance started to decrease significantly once the current dropped below about 1 kA. This can be seen Figure 7.5. It is therefore suggested that 1 kA may be sufficient current to sustain the restrike arc, and so the total power dissipation of the arc was roughly estimated

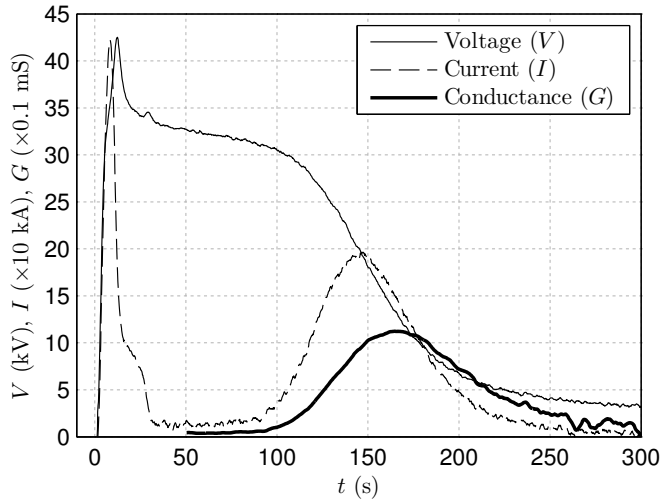

Figure 7.5 An example calculation of the time-varying conductance of an EW restrike plasma. $\ell = 3$ m, $d = 0.2$ mm, $V_0 = 30$ kV, $E_0 = 10$ kV/m.

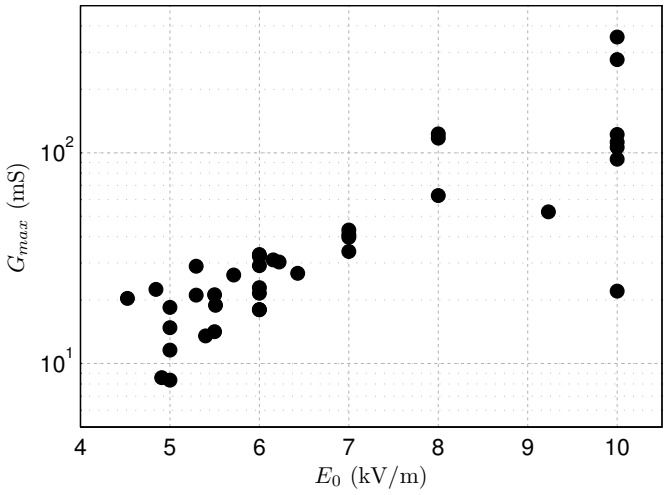

Figure 7.6 A collation of experiments using the Marx generator that produced restrike. The peak plasma conductance is partially dependent on the initial AEF.

to be

$$P = \frac{I_m^2}{G_p} = \frac{1000^2}{0.02} = 50 \text{ MW} \tag{7.2}$$

and the voltage required to maintain the minimum current was estimated as

$$V_m = \frac{I_m}{G_p} = \frac{1000}{0.02} = 50 \text{ kV} \tag{7.3}$$

An energy supply that can continuously output such high power is rare, but where it is available,

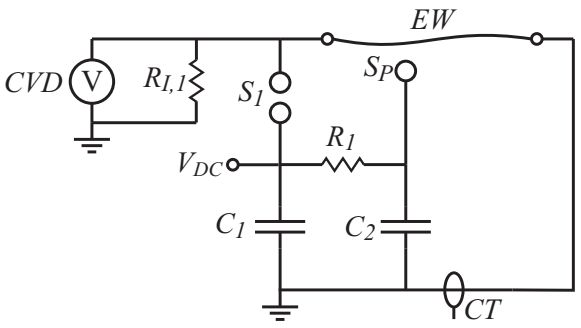

Figure 7.7 A circuit schematic of the prototype plasma switch experiment. The plasma switch is denoted by S_P.

could create some brilliant sustained arcs. A much more viable option for most laboratories is simply to use more capacitor banks to supply the required voltage and power for short bursts. This introduces the second key challenge: connecting the sustaining capacitor banks in coordination with the restrike-initiating capacitor banks. A potential switching mechanism is the 'plasma switch'.

7.4.1 Plasma Switch

The plasma generated during a restrike provides a convenient mechanism for the triggering of an auxiliary spark gap. This idea formed the basis for a prototype 'plasma switch': a triggered spark gap formed between the EW and a sphere. The plasma switch was used to connect a second capacitor bank to the EW in an attempt to sustain the restrike plasma.

The two-stage Marx circuit was reconfigured so that the two capacitor banks could be charged by the same source, but discharged through separate circuits (fig. 7.7). One capacitor bank was connected through the TSG, S_1, and onto the EW as normal. The other capacitor bank was connected to a spherical electrode, which was placed at a set gap length from the EW. The sphere was positioned 100 mm along from the start of the EW. A 6 m long, 0.2 mm diameter EW and 50 kV charge voltage was used for every experiment. The plasma switch was required to withstand the full charging voltage (before the TSG was triggered) without breakdown, yet breakdown at the full charging voltage (when C_1 had discharged) when the EW plasma was present. The plasma switch was also required to withstand the transient voltage conditions created as the TSG switched and during the first phase of the EW.

The shortest gap length that triggered the plasma switch was 55 mm. The switching could be seen on the voltage waveform as an under-damped step, delayed approximately 2000 μs after the first restrike peak (fig. 7.8a). A large current flowed at the time of switching between the two capacitor banks, equalising the voltage to approximately half the charge voltage. The current only flowed through the 100 mm length of EW between the two capacitor banks, indicating

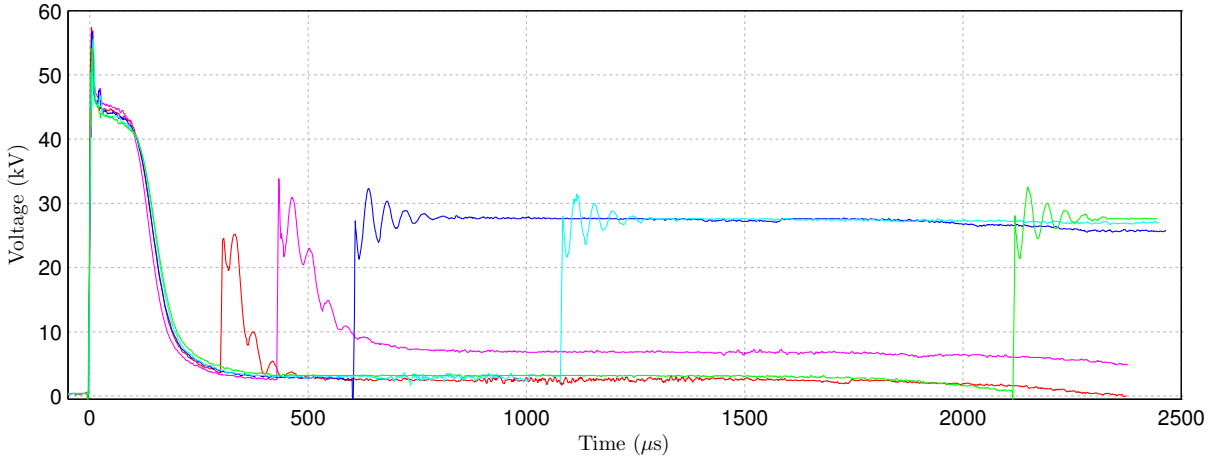

(a) Voltage waveforms.

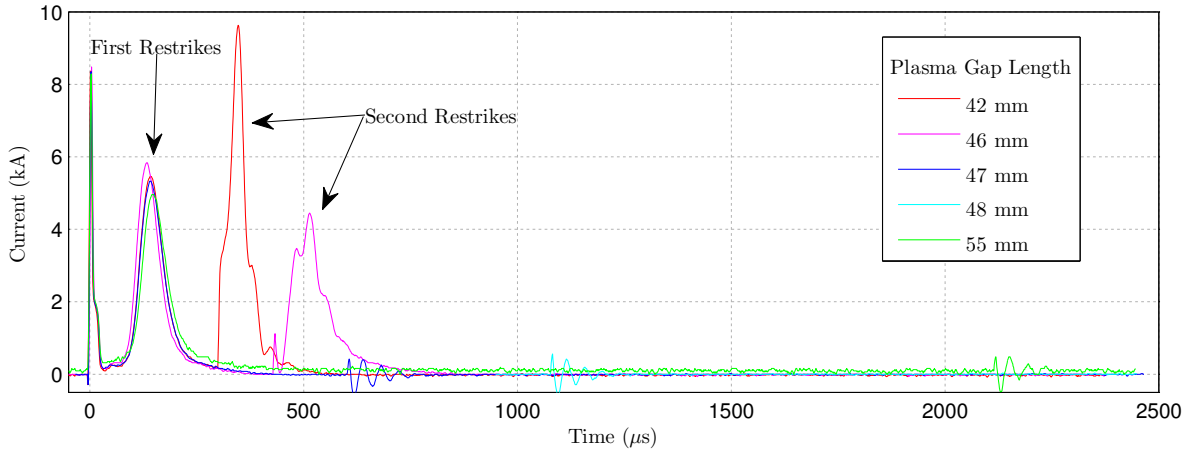

(b) Current waveforms.

Figure 7.8 Voltage and current waveforms from the plasma switch prototype experiments. The legend applies to both figures.

that the EW did not conduct a second restrike. Gap lengths of 48 and 47 mm produced similar results, except the switching delay shortened to 930 and 460 μs respectively. The correlation of switching delay to the gap length hints that the switching mechanism relied on the expansion of the plasma or remnant EW material.

Using a gap length of 46 mm, a second restrike was obtained (fig. 7.9). The current waveform shows that second restrike current flowed through the EW, this time with a 280 μs switching delay (fig. 7.8b). The second restrike reached a peak current of 4.5 kA. A gap length of 42 mm also produced a second restrike, with a switching delay of 153 μs after the first restrike peak. The peak current of 9.6 kA was much higher than the previous experiment, presumably because the shorter delay meant that the plasma was more highly ionised.

The plasma switch was successfully used to switch in a second capacitor bank, proving both that the plasma switch mechanism works and that sustaining the plasma is possible. The switching

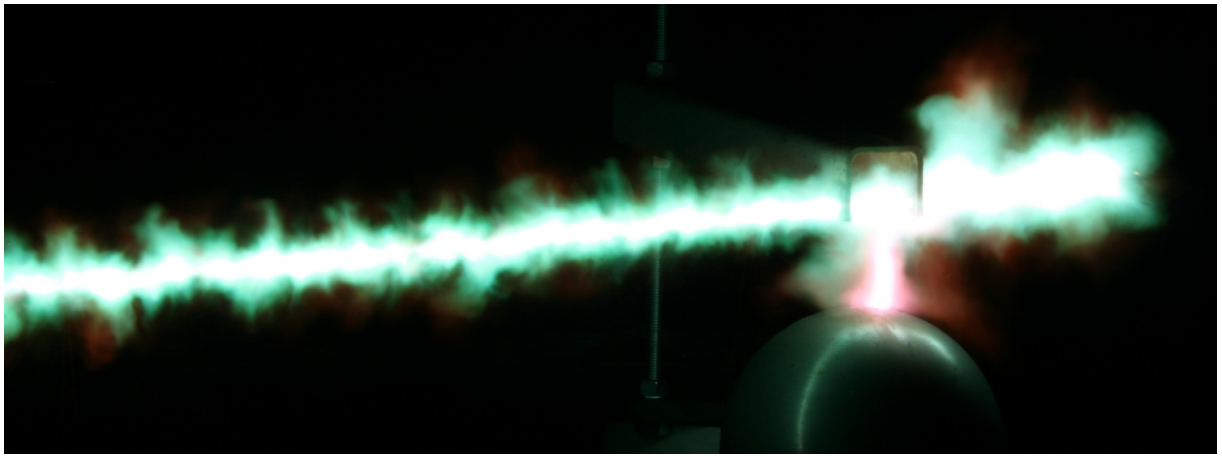

Figure 7.9 A photograph of the plasma switch operating with a gap length of 46 mm.

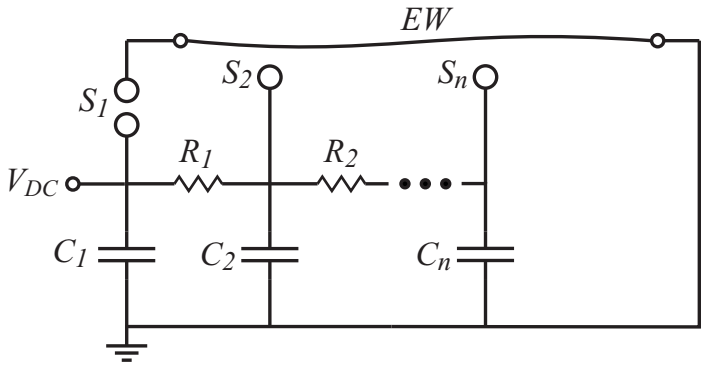

Figure 7.10 A conceptual circuit that could sustain the EW restrike plasma using pulsed power. Each plasma switch, S_2 to S_n, has a set delay to connect capacitors C_2 to C_n sequentially.

delay was controllable by varying the gap length, but if the delay was more than 280 μs, the EW plasma had deionised too much to allow for a second restrike. The controllable switching delay could allow multiple capacitor banks, each with their own plasma switch, to be switched sequentially onto the EW, sustaining the arc using pulsed power (fig. 7.10).

7.5 DIRECTIONAL ARCS

One major advantage of using EWs to create long arcs is that the arcs can be directed to follow arbitrary paths, simply by forming the wire before igniting the experiment. The paths can even loop back on themselves to create shapes that are otherwise impossible when creating arcs using conventional methods. This attribute may be unique to EW and could herald some novel applications of long distance EWs. Two examples of path shapes are coils and knots.

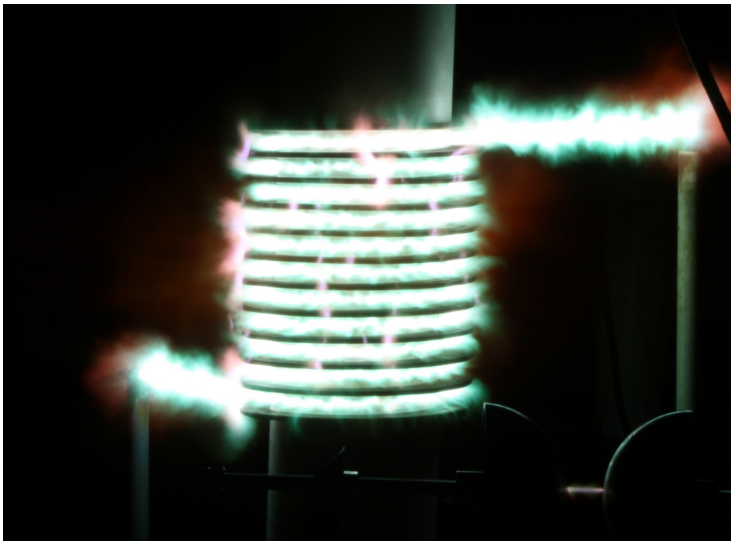

Figure 7.11 A 10-turn prototype plasma transformer[Hammond 2008]. The 75 kV spark gap in the bottom right of the photograph was connected to the secondary of the transformer, and is seen to break down.

7.5.1 Plasma Coils

A working plasma coil was presented in [Hammond 2008], with further descriptions in [Sinton *et al.* 2009a, Sinton *et al.* 2009b]. The plasma coil was one winding of a prototype plasma transformer (fig. 7.11). The EW was a 0.2 mm diameter wire that was wound into a 10 turn helical coil around a PVC former. A PVC helical baffle was used to prevent the turns of the plasma winding shorting together. The plasma winding was magnetically coupled to a concentric, 50-turn non-exploding winding, so that the transformer could be used to generate high voltage impulses. When a 40 kV capacitor discharge was applied to the plasma winding, a peak output voltage of 75 kV was measured across the non-exploding winding, proving that plasma can be used as an electrical machine winding.

7.5.2 Plasma Knots

A long-standing scientific challenge has been to find an explanation for ball lightning [Donoso *et al.* 2006]. Ball lightning is the name given to the plasma-like fireballs that have been reported to appear near lightning strikes. Reported sightings of ball lightning are variable, describing different colours, size, apparent temperature, behaviour and lifetime. Typically, the diameter of the ball is between 10 and 50 cm, lasts about 10 s and appears to output the equivalent of 10 to 150 W of visible light. Although there have been many theories as to what causes ball lightning, it has never been convincingly created in the laboratory.

One theory that purportedly accounts for the creation, stability and behaviour of ball lightning is that the ball is a magnetic knot [Ranada 1998]. A magnetic knot is comprised of a number

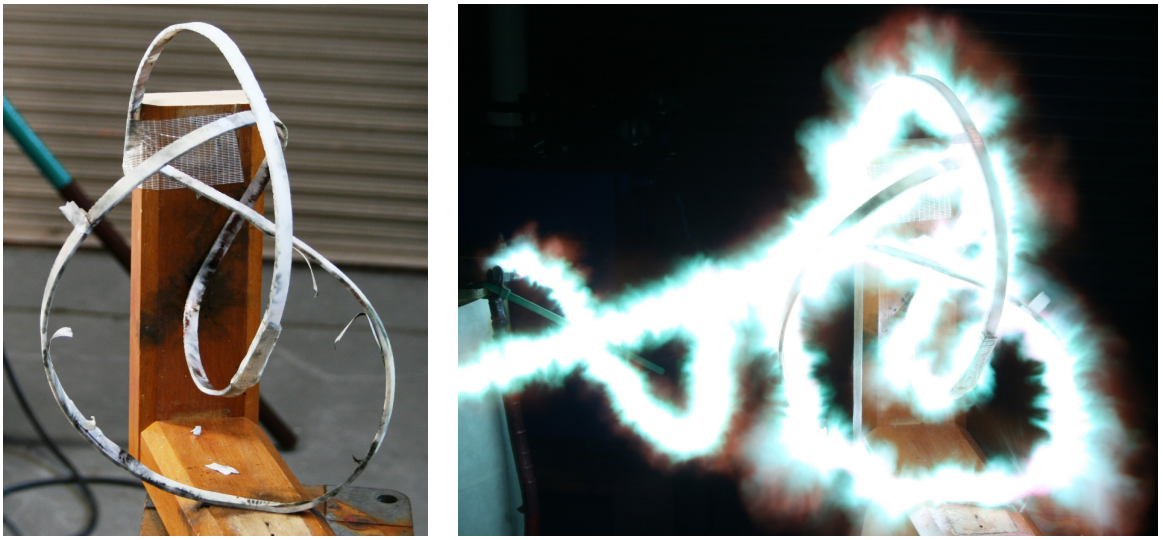

(a) Support apparatus. (b) Restrike.

Figure 7.12 Photographs of the plasma knot support apparatus and a successful plasma knot restrike.

of streamers that have formed closed loops and that have linked magnetic fields. The ball is predicted to be stable, with a predicted lifetime of about 9 s. To attain a power dissipation that matches reports, the streamers must have diameters of 50 to 100 μm and a temperature of approximately 16,000 to 18,000 K. The stored energy in the plasma knot is approximately 20 kJ. The magnetic knots are predicted to form near an ordinary lightning strike where the powerful magnetic and electric fields may cause some streamers to short-circuit.

The theory is untested; Ranada admits that for "obvious reasons" it is not easy to create a plasma knot in the laboratory. However, long distance EW could provide a simple method to form a magnetic knot with linked streamers to test the ball lightning model. The wire could be formed into any knot shape that the researcher desires, so long as appropriate clearances are maintained to avoid unintentional short-circuiting of the plasma knot. Furthermore, the plasma switch concept could be employed to create intentional short-circuiting of streamers. The feasibility of creating a plasma knot was tested by forming the simplest knot with linked magnetic lines, which is the simple 'overhand' knot. A plastic apparatus was constructed to hold the wire in place (fig. 7.12a). A restrike was then obtained using a 3 m length of 0.2 mm diameter wire and 30 kV (fig. 7.12b). No anomalous behaviour was detected, although none was expected because the magnetic linking number of the knot was too low. However, successful production of restrike in a knot shows that this avenue of research is feasible.

7.6 CONCLUSIONS

The restrike prediction model has been used to estimate that other research groups, who have access to a sufficiently large impulse generator, could create plasma arcs up to 2 km long. Even

moderate impulse generators have been predicted to be capable of producing arcs several hundred metres long. It has also been suggested that, should these arcs be created vertically towards a thunderstorm, there is a mechanism that could cause lightning to be artificially triggered. Experiments performed outdoors at Port Levy may have uncovered the first signs of atmospheric breakdown; extra packets of charge that had similar characteristics to stepped leaders were measured. Arcs created with EW also have the unique advantage that they are directional. To illustrate this point, it was shown that arcs can be formed into coils or knots. The plasma knots could be used to form ball lightning and prove a currently standing theory that ball lightning is a magnetic knot with linked streamers. Ultimately, the suggestions for future work that have been presented in this chapter are far from exhaustive, but they can be used as starting points to inspire applications of long, directional plasma conductors.

Chapter 8

CONCLUSIONS

This research was instigated to explore the mechanism that causes arcs to form during long distance EW experiments and to create a model that reliably predicts the arcs' occurrence. A review of the literature identified several studies that had observed the formation of plasma beads during the EW process. However, none of them used wires longer than 1 m, and the longest restrike that had been previously reported was just 3 m long. The AEF quantity was introduced as a means of classifying the experimental outcome, and it became the defining quantity that separates the long distance EW restike mechanism from more common restrike mechanisms. The AEF at which restrike occurs is much lower using the plasma bead restrike mechanism, allowing much longer arcs to be created for a given voltage capability of the energy supply.

An experimental environment was developed, which consisted of equipment, instrumentation, safety systems and operating procedures. The equipment included a three-stage Marx generator that was designed for the purpose of performing EW experiments up to 60 m long, and a triggered spark gap that proved to be reliable for experiments that used a charge voltage of up to 90 kV. The experimental environment was made safe by using a hazard identification system and taking steps to eliminate, isolate or minimise the identified hazards.

Long distance EWs using a variety of AEFs were observed in detail. The heating and fragmentation processes were observed at low AEFs. Fragmentation appeared to be caused by sausage instabilities forming when the wire was in the liquid state. The fragmentation sites were the likely cause of the plasma beads, which were observed to occur when the AEF was nearing the lower restrike boundary. Through photographic methods, the plasma beads were observed to expand and coalesce, eventually forming a restrike channel. At AEFs above the upper restrike boundary, the restrike mechanism failed to occur, presumably because the wire was vaporised before it could produce plasma beads.

A restrike prediction model was then developed, starting with analysis of previous results obtained at the University of Canterbury. The analysis concluded that the AEF was an important quantity in the prediction of restrike, although independently it could not form a complete model. Further experimentation confirmed the existence of an AEF region of restrike, but could

not find useful trends when wire diameter was included. A transient modelling study reached its limit when realistic representation of the complex fragmentation phase became infeasible. A simple restrike prediction model was formulated, which simply used empirical analysis of the existing data to show that restrike was likely to occur between 4.5 and 11 kV/m using 0.2 mm diameter wires. This model was then extended by identifying the importance of the AEF at the time of plasma bead formation, which needed to be at least 4.0 kV/m, and the linear dependence on first phase energy dissipation to the wire length, which was 203 J/m for 0.2 mm diameter enamelled copper wire. The constant loss in the energy supply was determined to be 500 J per stage. Capability diagrams were then constructed using the lower and upper AEF restrike boundaries and the energy supply voltage rating. These diagrams can be used to predict the occurrence of restrike given the wire length and voltage.

Full descriptions of long distance EW experiments up to 60 m long were then presented. The length of the experiments meant that many were difficult to fit inside the laboratory, so they were also performed outside. Additional safety and operation considerations were needed as the experiments moved out into the laboratory compound, then outside the compound, and eventually off-site completely. The off-site experiments allowed a new system of suspending the EW vertically from a weather balloon to be tested. A thin, lightweight return wire was found to conduct the EW without damage, allowing the weather balloon to also lift the return wire and effectively doubling the possible length of vertical experiments.

This research has enabled the reliable creation of long arcs using EWs. Future work in this area may focus on applications of long arcs. Several topics for future work were suggested, starting with some improvements to the restrike prediction model including testing the model with arcs up to 2 km long. Long arcs created vertically were then suggested to be a mechanism for the artificial triggering of lightning. Experiments were presented that had captured what appeared to be atmospheric charge packets or possibly stepped leaders, providing evidence that lightning triggering may be possible. The unique ability of EW arcs to be shaped into arbitrary paths was then explored, with suggested applications of plasma coils and plasma knots, the later of which may aid in proving a theory that ball lightning is a knot of magnetically linked streamers.

REFERENCES

Baksht, R., Pokryvailo, A., Yankelevich, Y. and Ziv, I. (2004), 'Explosion of thin aluminum foils in air', *Journal of Applied Physics*, Vol. 96, No. 11, Dec, pp. 6061–6065.

Becerra, M., Cooray, V., Soula, S. and Chauzy, S. (2007), 'Effect of the space charge layer created by corona at ground level on the inception of upward lightning leaders from tall towers', *J. Geophys. Res.*, Vol. 112, No. D12, Jun, pp. D12205–.

Bennett, F.D. (1958), 'Cylindrical shock waves from exploding wires', *Physics of Fluids*, Vol. 1, No. 4, pp. 347–352.

Bhat, B.K. and Jordan, I.B. (1971), 'Explosion of bare and insulated copper wires', *Journal of Applied Physics*, Vol. 42, No. 2, p. 809.

Burkhalter, P.G., Dozier, C.M. and Nagel, D.J. (1977), 'X-ray spectra from exploded-wire plasmas', *Phys. Rev. A*, Vol. 15, No. 2, Feb, pp. 700–717.

Carpenter, K. and Graneau, P. (1984), 'On the nonexistence of "Ampere tension" in electric conductors', *Magnetics, IEEE Transactions on*, Vol. 20, No. 6, Nov, pp. 2159 – 2160.

Chace, W.G. and Moore, H.K. (1959), 'A brief survey of exploding wire research', In *Exploding Wires*, New York: Plenum Press, Inc., pp. 7–16.

Dannenberg, R. and Silva, A. (1969), 'Exploding wire initiation and electrical operation of a 40-kV system for arc-heated drivers up to 10 feet long', *NASA TN D-5126*.

Dattner, A., Lehnert, B. and Lundquist, S. (1959), *A liquid conductor model of instabilities in a pinched discharge*, Technical Report, AB Atomenergi, Stockholm; Royal Inst. of Tech., Stockholm; Swedish State Power Board, Stockholm, Oct.

DiMarco, J.N. and Burkhardt, L.C. (1970), 'Characteristics of a magnetic energy storage system using exploding foils', *Journal of Applied Physics*, Vol. 41, No. 9, Aug, pp. 3894 –3899.

Donoso, J., Trueba, J. and Ranada, A. (2006), 'The riddle of ball lightning: a review', *TheScientificWorldJournal*, Vol. 6, pp. 254–278.

Dyos, G. and Farrell, T. (1992), 'Electrical resistivity handbook'.

Gallet, G., Leroy, G., Lacey, R. and Kromer, I. (1975), 'General expression for positive switching impulse strength valid up to extra long air gaps', *Power Apparatus and Systems, IEEE Transactions on*, Vol. 94, No. 6, Nov, pp. 1989 – 1993.

Graneau, P. (1987a), 'Wire explosions', *Physics Letters A*, Vol. 120, No. 2, pp. 77 – 79.

Graneau, P. (1987b), 'Railgun recoil and relativity', *Journal of Physics D: Applied Physics*, Vol. 20, No. 3, p. 391.

Grinenko, A., Sayapin, A., Gurovich, V.T., Efimov, S., Felsteiner, J. and Krasik, Y.E. (2005), 'Underwater electrical explosion of a Cu wire', *Journal of Applied Physics*, Vol. 97, No. 2, p. 023303.

Grinenko, A., Efimov, S., Fedotov, A., Krasik, Y.E. and Schnitzer, I. (2006), 'Efficiency of the shock wave generation caused by underwater electrical wire explosion', *Journal of Applied Physics*, Vol. 100, No. 11, p. 113509.

Haefely Test AG *Impulse voltage test system SGΔA*, Basel, Switzerland.

Haefely Test AG *Impulse voltage test system SGSA*, Basel, Switzerland.

Haefely Test AG *Impulse voltage test system SGVA*, Basel, Switzerland.

Hammond, C. (2008), 'A plasma primary high voltage transformer'. Department of Electrical and Computer Engineering, University of Canterbury, New Zealand.

Highvolt Prftechnik Dresden GmbH *Impulse Voltage Generators; 100 kV up to 1200 kV - Series L*, Dresden, Germany.

Highvolt Prftechnik Dresden GmbH *Impulse Voltage Generators; 1000 kV up to 6000 kV - Series G*, Dresden, Germany.

Highvolt Prftechnik Dresden GmbH *Impulse Voltage Generators; 500 kV up to 2400 kV - Series M*, Dresden, Germany.

Ivezic, T. (1991), 'Electric fields from steady currents and unexplained electromagnetic experiments', *Physical Review A*, Vol. 44, August, pp. 2682–2685.

Kuffel, E. and Bera, M. (1968), 'Breakdown in triggered spark gaps in air', *Power Apparatus and Systems, IEEE Transactions on*, Vol. PAS-87, No. 7, july, pp. 1628 –1635.

Kuffel, E., Zaengl, W. and Kuffel, J. (2000), *High voltage engineering: fundamentals*, Newnes, second ed.

Lisitsyn, I., Muraki, T. and Akiyama, H. (1997), 'Wire induced flashover as a source of shock waves for destruction of solid materials', Vol. 1, Jun-Jul, pp. 208 –213.

Lukyanov, A. and Molokov, S. (2001), 'Flexural vibrations induced in thin metal wires carrying high currents', *Journal of Physics D: Applied Physics*, Vol. 34, No. 10, p. 1543.

Lundquist, S. and Vlastos, A.E. (1970), 'Temperature of the restrike channels of exploding wires', *Journal of Applied Physics*, Vol. 41, No. 12, November, pp. 4830 –4835.

Matzen, M.K. (1997), 'Z pinches as intense x-ray sources for high-energy density physics applications', *Physics of Plasmas*, Vol. 4, No. 5, pp. 1519–1527.

Molokov, S. and Allen, J.E. (1997), 'The fragmentation of wires carrying electric current', *Journal of Physics D: Applied Physics*, Vol. 30, No. 22, p. 3131.

Mulholland, D. (2004), 'Explosion of 10m of copper wire'. Department of Electrical and Computer Engineering, University of Canterbury, New Zealand.

Nagaoka, H., Futagami, T. and Machida, T. (1926), 'Electric explosion of wires and threads', *Institute of Physical and Chemical Research*, Vol. 2, Jul, pp. 328–331.

(2001), *New Zealand Electrical Code of Practice for Electrical Safe Distances*.

Novac, B., Smith, I., Downs, P., Marston, P. and Fahey, D. (2005), 'Cockpit canopy shattering using exploding wire techniques', In *Pulsed Power Conference, 2005 IEEE*, June, pp. 848 –851.

Pendleton, W.K. and Guenther, A.H. (1965), 'Investigation of a laser triggered spark gap', *Review of Scientific Instruments*, Vol. 36, No. 11, nov, pp. 1546 –1550.

Rakov, V.A., Uman, M. and Rambo, K. (2005), 'A review of ten years of triggered-lightning experiments at camp blanding, florida', *Atmospheric Research*, Vol. 76, No. 1-4, pp. 503 – 517.

Ranada, A. (1998), 'A model of ball lightning as a magnetic knot with linked streamers', *JGR. Journal of geophysical research. B*, Vol. 103, pp. 23–.

Robson, A.E. and Sethian, J.D. (1992), 'Railgun recoil, Ampere tension, and the laws of electrodynamics', *American Journal of Physics*, Vol. 60, No. 12, pp. 1111–1117.

Rosa, E.B. (1908), 'The self and mutual inductances of linear conductors', *Bulletin of the Bureau of Standards*, Vol. Vol. 4, No. 2, pp. 301–344.

Sarkisov, G.S., Rosenthal, S.E., Struve, K.W. and McDaniel, D.H. (2005), 'Corona-free electrical explosion of polyimide-coated tungsten wire in vacuum', *Phys. Rev. Lett.*, Vol. 94, No. 3, Jan, p. 035004.

Shelkovenko, T.A., Pikuz, S.A., Mingaleev, A.R. and Hammer, D.A. (1999), 'Studies of plasma formation from exploding wires and multiwire arrays using x-ray backlighting', *Review of Scientific Instruments*, Vol. 70, No. 1, Jan, pp. 667 –670.

Shimomura, N., Nagata, M., Teramoto, Y. and Akiyama, H. (2000), 'Unstable behavior in exploding wire array', *Japanese Journal of Applied Physics Part 1-Regular Papers Short Notes & Review Papers*, Vol. 39, No. 10, pp. 6051–6054.

Sinars, D.B., Shelkovenko, T.A., Pikuz, S.A., Hu, M., Romanova, V.M., Chandler, K.M., Greenly, J.B., Hammer, D.A. and Kusse, B.R. (2000), 'The effect of insulating coatings on exploding wire plasma formation', *Physics of Plasmas*, Vol. 7, No. 2, pp. 429–432.

Sinton, R., Hammond, C., Enright, W. and Bodger, P. (2009a), 'Generating high voltages with a plasma coil transformer', In *Techcon Asia Pacific*, Sydney, Australia, pp. 211–219.

Sinton, R., van Herel, R., Enright, W. and Bodger, P. (2009b), 'Plasma conductors and windings', *Australasian Transmission and Distribution Magazine*, Vol. 5, Oct/Nov, pp. 22–23.

Smith, D. (2005), 'Long distance directional ionisation paths in air'. Department of Electrical and Computer Engineering, University of Canterbury, New Zealand.

Smith, D. (2008), *The creation of long distance directional plasma discharges via the exploding wire technique*, Master's thesis, Electrical and Computer Engineering, University of Canterbury, Christchurch, New Zealand.

Smith, D., Enright, W. and Bodger, P. (2007), 'A test circuit for long distance directional plasma discharge using the exploding wire technique', In *15th International Symposium on High Voltage Engineering (ISH)*, Ljubljana, Slovenia.

Standards Australia International Limited (2005), *AS60052: Voltage measurement by means of standard air gaps*, Standards Australia, Sydney.

Taylor, M. (2002a), *Plasma propellant interactions in an electrothermal-chemical gun*, PhD thesis, Cranford University.

Taylor, M.J. (2002b), 'Formation of plasma around wire fragments created by electrically exploded copper wire', *Journal of Physics D-Applied Physics*, Vol. 35, No. 7, pp. 700–709.

Taylor, M. (2003), 'Current diversion around a fragmenting wire during the voltage spike associated with exploding wires', In *Proc. of Inter. Conf. on Electric Fuses and their Applications, Gdansk (PL)*, pp. 1–9.

Taylor, M. (2004), 'Interruption of the explosion of plasma initiator wires', In *Electromagnetic Launch Technology, 2004. 2004 12th Symposium on*, May, pp. 312 – 317.

Ternan, J. (1986), 'Stresses in rapidly heated wires', *Physics Letters A*, Vol. 115, April, pp. 230–232.

Uman, M.A. (2000), *The Lightning Discharge*, General Publishing Company, Ltd.

Vlastos, A.E. (1973a), 'Dwell times of thin exploding wires', *Journal of Applied Physics*, Vol. 44, No. 5, Feb, pp. 2193–2196.

Vlastos, A.E. (1973b), 'Instabilities of electrically exploded wires', *Journal of Applied Physics*, Vol. 44, No. 4, April, pp. 1616 –1621.

Wesley, P., Young, H. and Freedman, R. (2008), 'Sears and zemansky's university physics'.

Whitehead, J.B. (1920), 'The high voltage corona in air', *Proceedings of the American Philosophical Society*, Vol. 59, No. 4, pp. pp. 245–260.